jpl

954709

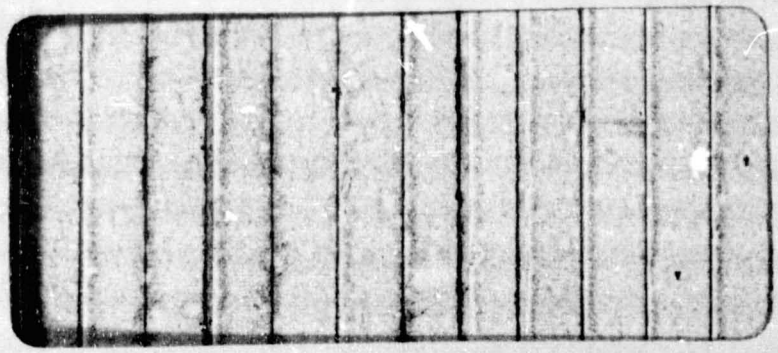

JET PROPULSION LABORATORY
CALIFORNIA INSTITUTE OF TECHNOLOGY
PASADENA, CALIFORNIA

HELIOGYRO PRELIMINARY DESIGN
PHASE II FINAL REPORT

MS404-5 19 January 1978

THE MACNEAL-SCHWENDLER CORPORATION

HELIOGYRO PRELIMINARY DESIGN
PHASE II FINAL REPORT

MS404-5

19 January 1978

MS404-5

HELIOGYRO PRELIMINARY DESIGN

PHASE II FINAL REPORT

for

Jet Propulsion Laboratory
Pasadena, California

Under Contract 954709

19 January 1978

THE MACNEAL-SCHWENDLER CORPORATION
7442 North Figueroa Street
Los Angeles, California 90041

HELIOGYRO PRELIMINARY DESIGN

PHASE II FINAL REPORT

INTRODUCTION

This report summarizes the work performed under Mod. 5 of Contract 954709 for the Jet Propulsion Laboratory. The work included several aspects of the preliminary design of a Heliogyro Solar Sail Module for the Halley Rendezvous Mission. Mr. William Ruff was the Technical Project Manager at JPL. The MacNeal-Schwendler Corporation (MSC) was the prime contractor and their work was directed by MSC's president, Dr. Richard H. MacNeal. Astro Research Corporation (Astro) was a principle subcontractor and their work was directed by Astro's president, Dr. John M. Hedgepeth.

The project, which began in February 1977, was based on the results of a short conceptual design study (contract 954680) conducted during December 1976 and January 1977 by MSC and Astro. The objective was to develop a Baseline Design of a Heliogyro Solar Sail Module on a short schedule, to be considered for the Halley Rendezvous Mission in competition with a Square Solar Sail Module and, later, in competition with a Solar Electric Propulsion System. The main features of the Heliogyro Baseline Design, including the work done at JPL as well as that done at MSC and Astro, are reported in the "Solar Sail Technology Readiness Report," JPL Report 720-1, 18 July 1977. The main part of the work done by MSC and Astro is reported in MSC's report number MS404-1, "Heliogyro Preliminary Design, Final Report," August 24, 1977.

The present Phase II Final Report covers work done since that date on the following six topics:

1. Design and analysis of a stowable circular lattice batten for the Heliogyro blade.
2. Design and analysis of a biaxially tensioned blade panel.
3. Definition of a research program for micrometeoroid damage to tendons.
4. A conceptual design for a flight test model of the Heliogyro.
5. Definition of modifications to the NASTRAN computer program required to provide improved analysis of the Heliogyro.
6. A User's Manual covering applications of NASTRAN to the Heliogyro.

Separate memoranda and technical notes on these topics constitute the body of the Phase II Final Report.

INDEX TO MEMORANDA AND TECHNICAL NOTES

Number	Date	Author(s)	Title
ARC-TN-1041	10 January 1978	J. M. Hedgepeth	Stowable Circular Lattice Batten for Heliogyro
ARC-TN-1053	19 November 1977	L. A. Finley	Biaxially Tensioned Panel Design for Heliogyro Blades
RHM-21	9 August 1977	R. H. MacNeal	A Research Program for Micrometeoroid Damage to Tendons
MS404-2	25 October 1977	R. H. MacNeal M. A. Gockel	Proposed Modifications of NASTRAN to Improve Heliogyro Analysis
MS404-3	28 October 1977	R. H. MacNeal	Conceptual Design of a Flight Test Model of the Heliogyro
MS404-4	30 November 1977	E. D. Bellinger	Heliogyro User's Manual

Revised

STOWABLE CIRCULAR LATTICE BATTEN FOR HELIOGYRO

ARC-TN-1041

by

John M. Hedgepeth

10 January 1978

Prepared for MacNeal-Schwendler Corporation
under Contract No. 404-001 by
Astro Research Corporation
Carpinteria, California

INTRODUCTION

The Heliogyro concept was created in the mid 1960's by Astro Research Corporation (Astro) and MacNeal-Schwendler Corporation (MSC) under the support of NASA Headquarters. References 1 and 2 summarize most of the results of that work.

Astro has a subcontract with MSC to support JPL in applying the Heliogyro concept to the Halley Comet Solar Sailing Mission. William Ruff is the Technical Project Manager at JPL. The work at MSC is being led by Richard H. MacNeal - Program Manager, and at Astro under the direction of Karl Knapp - Program Manager. John M. Hedgepeth is Astro's Senior Scientist.

There are 12 blades in the Heliogyro design, and each blade is envisioned to be 8 meters in width and 7,500 meters in length. The blades are expected to be composed primarily of a thin membrane constructed of material such as Kapton film with an aluminum reflective coating on one side and an infrared emissive coating on the other. An overall view of the baseline Heliogyro is shown in Figure 1.

This report is one of a series dealing with the design and fabrication concepts of Heliogyro blades. In particular, this report details the Heliogyro stowable circular lattice batten.

DESIGN

The Heliogyro blade requires chordwise battens at about 75-meter intervals to hold the leading- and trailing-edge tension members apart. These battens must be

1. capable of resisting a design limit compressive load of approximately 6 newtons and temperatures of 600 kelvin,
2. tightly stowable on the blade reel, and
3. self-deploying when the blade is unrolled.

In addition, the batten should be of lattice construction so that the thermal gradients through the cross section are small and so that the reradiation from the batten will not produce hot spots in the blade reflecting membrane.

The batten design that meets these requirements is shown in Figure 2. It is constructed of thin graphite/polyimide rods in a circular, cylindrical lattice. There are six square longerons that support the compressive load, and six 30-degree helical half-round spirals, three in each direction, that provide support to the longerons to avoid local buckling. The longeron-spiral and spiral-spiral intersections are staggered to aid fabrication (by avoiding the criss-cross pileup) and minimize the local unsupported length of the longeron.

The batten is fabricated in two halves and hinged together on assembly. The hinges allow full compaction when stowed and expansion to a circle when unrolled from the stowage reel.

Two important principles are included in the design:

1. Each half-batten is fabricated on a mandrel with a smaller diameter than that of the finished batten.

2. The "hinges" are composed of interlacing fingers with no hinge pin required.

These two principles allow the batten, when fully deployed, to behave structurally as if there were no hinge and the spirals were continuous. Furthermore, they permit fabrication without the necessity of complicated joints. The tendency of each half-batten to reach a diameter smaller than the batten diameter causes a preload on the hinges, permitting moment carry through. It also produces a force which actually holds the two halves together, resisting possible spreading forces.

These principles are not new. They have been discovered and developed previously by Astro Research Corporation for solid tubular booms such as the Tablock BI-STEM. The application of the principles to a lattice configuration is a new and important development.

Figure 3 shows a sample batten segment fabricated as a part of the development of the design. It is constructed of graphite/epoxy (graphite/polyimide roving was not available) and demonstrates the geometry of the lattice halves and finger hinges.

An accurately constructed model which was used to demonstrate the strength of the batten design for local buckling is shown in Figure 4. This model was fabricated of graphite/epoxy as a complete circle with no hinges. It is 12 cm in diameter and consists of:

longerons . . . . . 0.48-mm square
spirals . . . . . 0.96-cm diameter half-round

The calculated buckling strength of the longerons considered to be simply-supported columns between the intersections is

$$P_{\ell_{theor}} = 24.8 \text{ N}$$

An estimate of the general-instability buckling strength (involving deflection of the spirals) can be obtained by starting with Reference 3 and substituting in the appropriate stiffness of the longerons and spirals. In this process, the axial stiffness of the spirals must be ignored since there is no skin to cause cylinder action (mid-plane stretching) to occur. The theoretical general-instability load thus obtained after some effort is

$$P_{GI} = 20.6 \text{ N}$$

The measured strength is

$$P_{meas} = 22.6 \text{ N}$$

which is very close to the theoretical strengths. The observed buckling mode involved cross-sectional deformation. The results of the test establish an experimental determination of the amount of spiral stiffness required to make the general-instability load approximately equal to the local-buckling strength.

ANALYSIS

Let longerons be square with thickness t_ℓ. Let the helix angle be 30 degrees and the ratio of stiffener area to longeron area be r_A. The buckling loads are then

Euler column buckling:
$$P_{EU} = \frac{3\pi^2 ER^2 t_\ell^2}{L^2} \tag{1}$$

Local longeron buckling:
$$P_\ell = \frac{27}{8} \frac{Et_\ell^4}{R^2} \tag{2}$$

Equation (2) is derived by assuming that the longerons go through the spiral intersections. By staggering the longerons and intersections, we get a potential local buckling load four times this much. Letting $P_\ell/P_{EU} = 1$ actually gives a factor of four on local buckling provided that enough stiffness is incorporated in the spirals to produce stabilization of the intersections and avoid general instability.

Manipulating Eqs. (1) and (2) gives

$$P_{EU} P_\ell = \frac{81}{8} \frac{\pi^2 E^2}{L^2} t_\ell^6 \tag{3}$$

$$t_\ell^2 = \left(\frac{8 P_{EU} P_\ell L^2}{81\pi^2 E^2} \right)^{1/3} \tag{4}$$

$$R^2 = \frac{L^2 P_{EU}}{3\pi^2 E t_\ell^2} \tag{5}$$

$$\frac{R}{L} = \left(\frac{3P_{EU}^2}{8\pi^4 E P_\ell L^2} \right)^{1/6} \tag{6}$$

The volume of material in the longerons and spirals is

$$V = 6L t_\ell^2 (1 + 2r_A)$$

or

$$V = 4(1 + 2r_A)(3\pi^2 E^2)^{-1/3} L^{5/3} (P_\ell P_{EU})^{1/3} \tag{7}$$

Let

$$L = 8 \text{ m}$$

$$E = 124.8 \times 10^9 \text{ N/m}^2$$

$$\rho = 1550 \text{ kg/m}^3$$

Then

$$V = 1.656 \times 10^{-6} (1 + 2r_A)(P_\ell P_{EU})^{1/3} \text{ m}^3 \tag{8}$$

$$t_\ell = 1.858 \times 10^{-4} (P_\ell P_{EU})^{1/6} \text{ m} \tag{9}$$

$$R = 2.24 \times 10^{-2} (P_\ell)^{-1/6} \text{ m} \tag{10}$$

$$\text{Mass} = 0.00257(1 + 2r_A)(P_\ell P_{EU})^{1/3} \text{ kg} \tag{11}$$

where P_ℓ and P_{EU} is expressed in newtons.

For a trial design, set

$$P_{EU} = P_\ell = 12 \text{ N}$$

then

$$R = 3.39 \text{ cm}$$

$$t_\ell = 0.425 \text{ mm}$$

During stowage, the spiral material must elastically deform with a nominal strain of

$$\epsilon = \frac{t_\ell}{2R} \tag{12}$$

The allowable nominal packaging strain is a complicated function of materials and detailed fabrication methods. We assume for preliminary purposes an allowable value of 0.005 for graphite/polyimide. The trial design above gives

$$\frac{t_\ell}{2R} = \frac{0.425}{2 \times 33.9} = 0.00627$$

which is slightly too large.

From Eqs. (9) and (10) we get

$$\frac{t}{2R} = 4.14 \times 10^{-3} (P_\ell)^{1/3} (P_{EU})^{-1/6} \qquad (13)$$

For $t_\ell/2R = 0.005$, and $P_\ell = 12$ N. This gives

$$P_{EU} = 46.7 \text{ N}$$

$$R = 5.33 \text{ cm}$$

$$t_\ell = 0.53 \text{ mm}$$

The strength test described earlier demonstrated that sufficient support is given to the longerons by the spirals if their cross section is half-round with a diameter of $2t_\ell$. For this case

$$r_A = \frac{\pi}{2}$$

and the basic mass of an 8-meter-long batten is 87.6 grams. To this must be added masses to account for the finger hinges and end fittings.

REFERENCES

1. MacNeal, Richard H.: Structural Dynamics of the Heliogyro. NASA CR-1745, 1971.

2. MacNeal, Richard H.; Hedgepeth, John M.; and Schuerch, Hans U.: Heliogyro Solar Sailer Summary Report. NASA CR-1329, 1969.

3. Soong, Tsai-Chen: Buckling of Cylindrical Shells with Eccentric Spiral-Type Stiffeners. AIAA Journal, vol. 7, no. 1, January 1969, pp. 65-72.

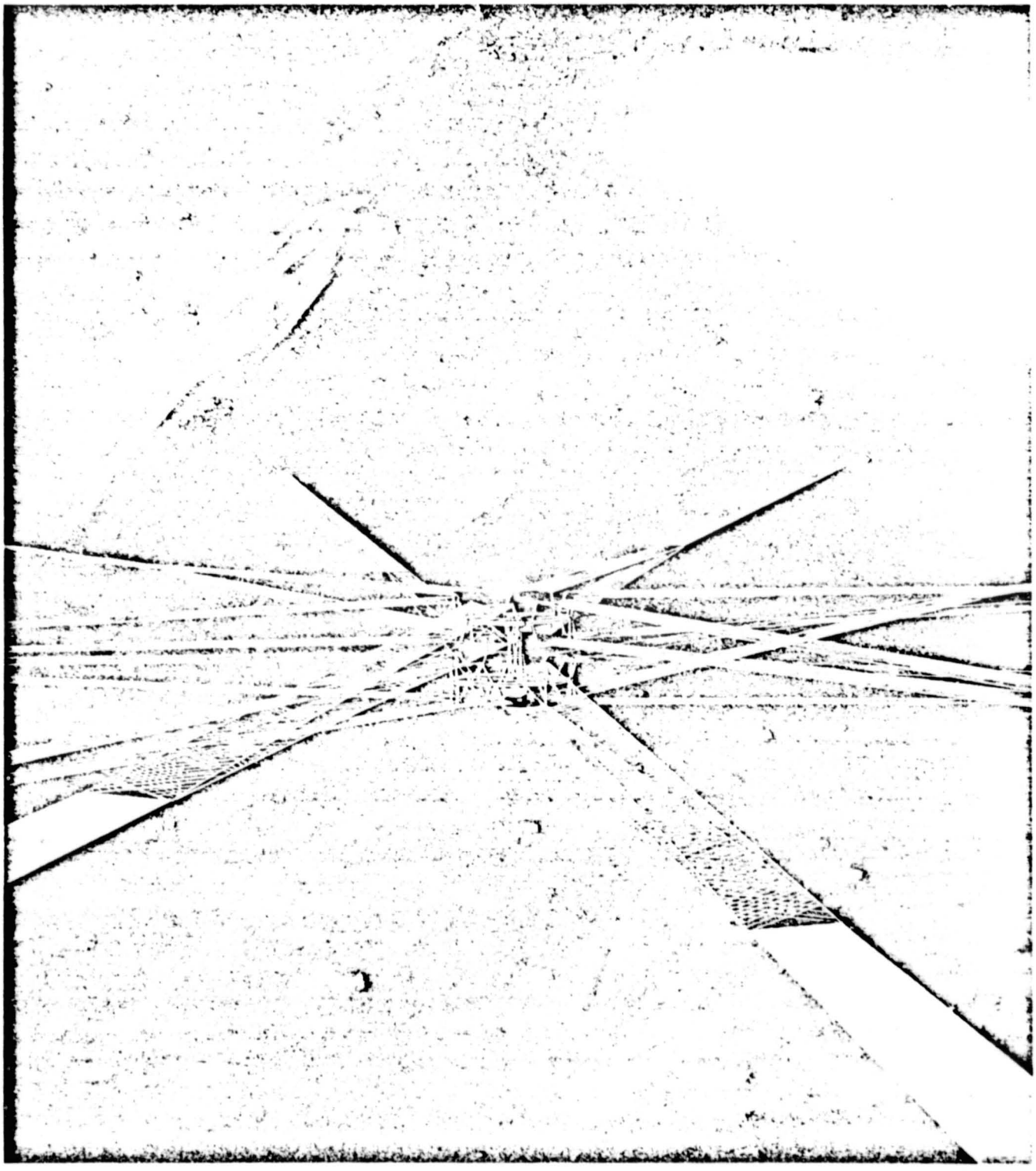

Figure 1. Baseline Twelve-Blade Heliogyro

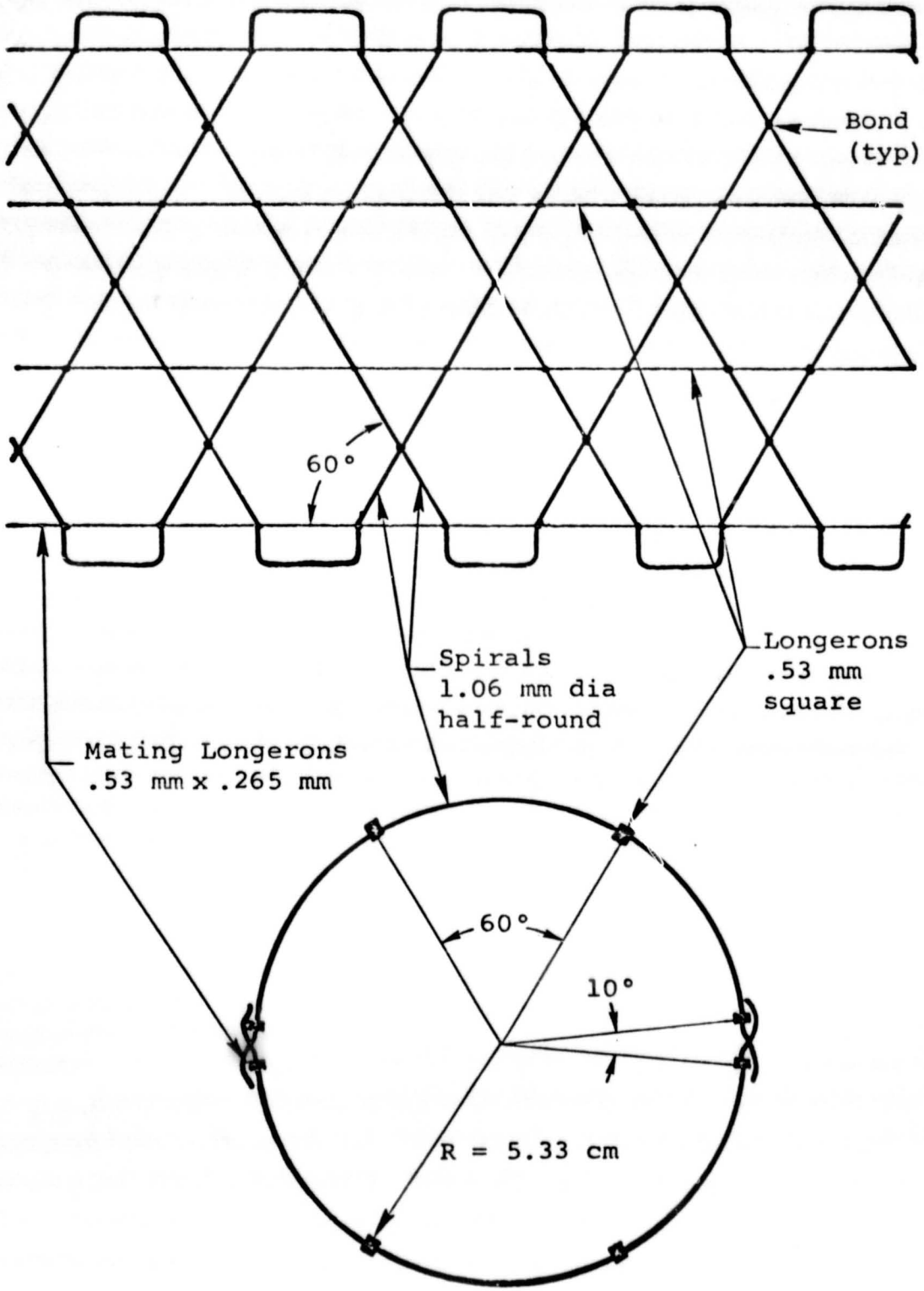

Note: Each half batten molded on 7.11-cm dia mandrel from graphite/polyimide roving.

Figure 2. Sketch of batten with dimensions showing a segment of lattice material (flattened) and a cross section of assembled batten.

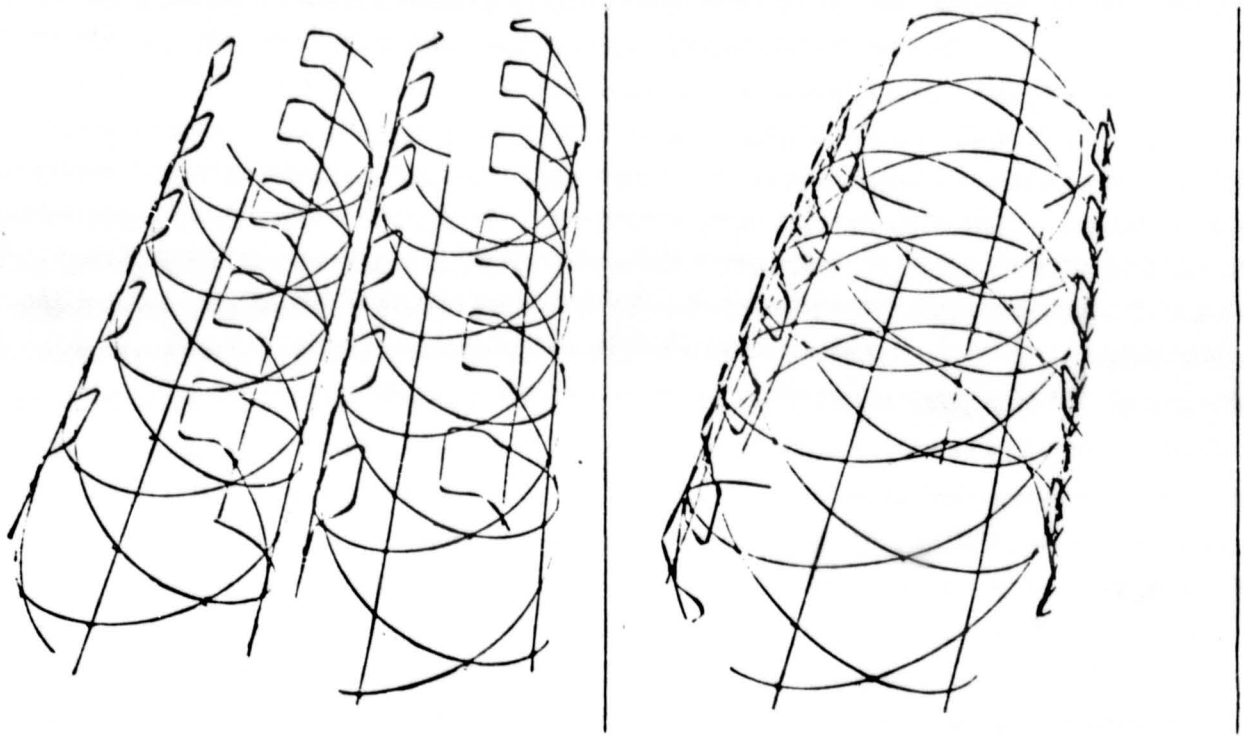

a. batten halves

b. assembled batten segment

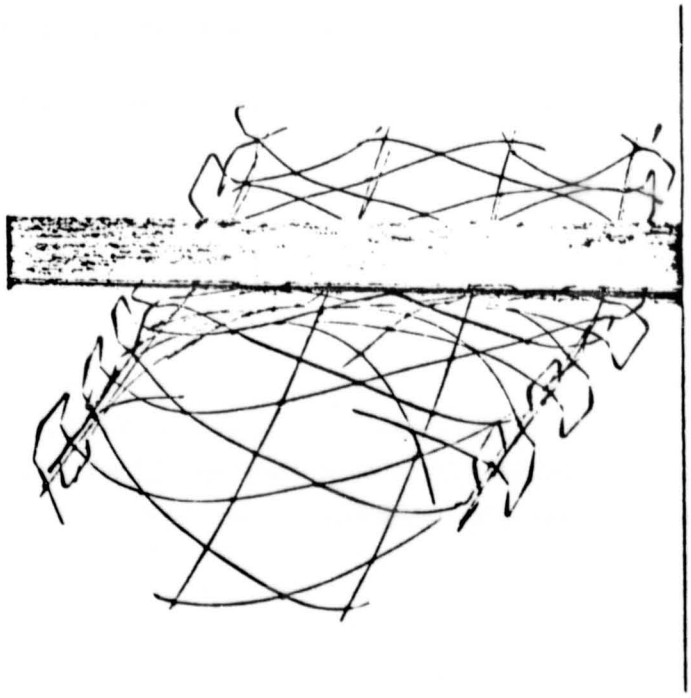

c. flattened batten segment

Figure 3. Demonstration batten segment.

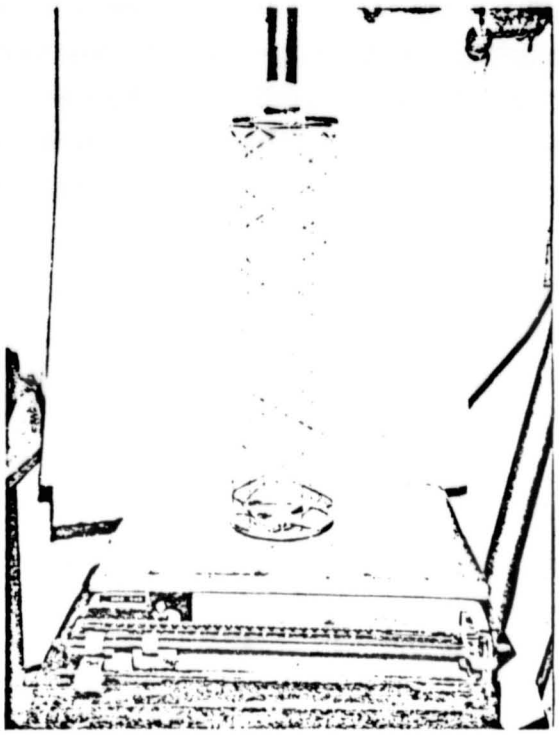

Figure 4. Structural test model.

TABLE OF CONTENTS

BIAXIALLY TENSIONED PANEL DESIGN FOR HELIOGYRO BLADES

ARC-TN-1053

by

Laurence A. Finley

19 November 1977

Prepared for MacNeal-Schwendler Corporation
under Contract No. 404-001 by
Astro Research Corporation
Carpinteria, California

INTRODUCTION

The Heliogyro concept was created in the mid-1960's by Astro Research Corporation (ARC) and MacNeal-Schwendler Corporation (MSC) under support of NASA Headquarters. References 1 and 2 summarize most of the results of that work.

ARC has a subcontract with MSC to support JPL in applying the Heliogyro concept to the Halley Comet Solar Sailing Mission. William Ruff is the Technical Project Manager at JPL. The work at MSC is being led by Richard H. MacNeal, Program Manager. At ARC the work is being led by Karl Knapp, Program Manager. John M. Hedgepeth is ARC's Senior Scientist.

There are 12 blades in the Heliogyro design, and each blade is envisioned to be 8 meters in width and 7500 meters in length. The blades are expected to be composed primarily of a thin membrane constructed of material such as Kapton film with an aluminum reflective coating on one side and an infrared emissive coating on the other. An overall view of the baseline Heliogyro is shown in Figure 1.

This report presents the results of efforts made to eliminate the built-in wrinkles and pretensioned panels in the baseline design. The design was based on the data obtained from scale modeling performed at ARC and incorporates the results of previous analyses concerning wrinkles and membrane tensioning (References 3 and 4).

ABSTRACT

In the baseline Heliogyro design, wrinkles and pretensioned film panels control the dimensional changes in the film which accompany thermal variations. However, wrinkles in the film affect both vehicle performance and dynamic stability. Thus, another method of tensioning and supporting the film panels was sought to allow for the expansion/contraction of the film material without the presence of wrinkles.

A program of model making was initiated, coupled with a review of the previous analysis concerning wrinkles and sail panels. The experience gained in this program suggested a new panel-support design (see Figure 2). This design consists of biaxially-tensioned film panels with parabolic edge members supplying the distributed constant edge loadings.

The support system for each panel extends underneath the adjacent inboard and outboard panels (and vice versa) producing a high sail-to-vehicle area ratio. This interlaced design is biased towards the center of revolution to compensate for the radially varying centrifugal loading of each panel. With suitable variations of panel lengths, edge member tensions, and pivot point locations, this design will be applicable to all radial stations of the 7500-meter Heliogyro blade assembly.

DISCUSSION

The requirement for no wrinkles in the Heliogyro film panels has several far-reaching effects on the design of the attachment method for the film. This can be understood best by considering the reason for the presence of wrinkles in the baseline design. The panels had to be assembled with built-in sag and pretensioned chordwise strain to accomodate displacements resulting from thermal expansion and contraction of the film during a mission. The effects of not compensating for this strain are explained in Reference 4 and consist of the unloading of the edge members during film contraction and the production of chordwise wrinkling during expansion.

Although the baseline design can accommodate the thermal strains of the film panels without significantly changing the stress distribution in the blade assembly, there is an impairment in performance of the Heliogyro from 5 to 10 percent due to the presence of the compensating slack in the film panels. The slack and accompanying wrinkles also have undesirable dynamic characteristics because they may introduce periodic loading patterns near the natural pitching frequency of a blade assembly. The slack in the baseline design was necessary due to the difference in the expansion coefficients of the film membrane and the graphite edge members. For the projected thermal extremes, the graphite polyimide may be considered invariant, while the Kapton will change by ±0.75 percent in the chordwise direction and ±0.69 percent in the spanwise direction. Thus, unless relative motion is allowed between the graphite polyimide edge members and the film, wrinkles are inevitable.

Another separate, though related, effect investigated in the modeling study was the problem of edge curl. If the material forms a closed cylinder at the free edge of a tensioned membrane, actual disintegration of the material may occur in the "solar oven" created by the curl. Incoming radiation is trapped within the dead space enclosed by the curl so that the temperature of the curl exceeds the melting point of the Kapton. If the edge of the film is reinforced with additional material, the curl can be controlled as in the designs which incorporate tension members bonded directly to the Kapton. However, bonding a dissimilar material to the Kapton creates problems of differential expansion. Therefore, a design was sought which supports the panel and eliminates all conditions

where curl and wrinkles might occur. If the material is cut away at a free edge in a parabolic scallop between supports, previous analysis has shown there will be no curl (Reference 4).

Thus, the requirements for the new design were an absence of wrinkles under all thermal conditions while maintaining acceptable stress levels in the film panels. Previous analysis was available describing wrinkles in tensioned membranes, but its application to Heliogyro panels had to be experimentally demonstrated. This is due to factors, such as a high aspect ratio, a varying body loading, and extreme temperature variations, which make a straightforward analysis of the wrinkle properties of the Kapton difficult. The starting point of the modeling program verified the worst case indicated by the previous analysis (Reference 3). This case showed that, whenever one of the principal membrane stresses vanished, wrinkling occurred parallel to the line of principal stress (see Appendix A, Figure A-1(a)). If the chordwise and spanwise stress are nonzero and positive, wrinkling should not occur. Practically, however, we find that if the ratio of one principal stress to another is large, say 50:1, wrinkling is possible.

Using the values N_x for chordwise stress and N_y for spanwise stress, one of the objectives of the test and modeling program was to investigate the value of N_x/N_y at the threshold of wrinkling. This number would be helpful in the Heliogyro design because it would help minimize the stress level in each panel which would, in turn, lengthen film life and reduce long-term creep.

MODELING

A detailed account of the modeling process is found in Appendices A and B. A system of attaching the edge members to the film material was developed which allowed relative motion. Variations of woven, preformed, adjustable, and catenary-type edge members were made, resulting in an applicable system designed for solar sail requirements. (Typical models are shown in Appendix A, Figures A-1 through A-3.)

These preliminary models were made of 0.0001-inch mylar with an aluminum coating similar to the actual sail material. As the models became more representative of a feasible support system, a larger 1- by 2-meter panel was constructed out of 0.00025-inch aluminized mylar. This model had parabolic top and side edge members attached by flexible mylar loops bonded to the panel through which the polyimide edge members were threaded.

The lower edge of the model was loaded by a Whiffletree arrangement which distributed a concentrated central load to the entire lower edge of the panel. By individually changing the loads on the edge catenary members and the bottom edge load, different values of N_x, N_y, and N_x/N_y were obtained. Table B-1 in Appendix B lists the loadings which were studied. Because of the textured nature of the 0.00025-inch mylar and some creases which were inadvertently created in the panel during assembly, all the photographs of the 1- by 2-meter panel show a partially wrinkled surface.

Consequently, these photographs (shown in Appendices A and B) do not adequately reflect the degree of flatness which some loading points represent. A system of photographing the panel was developed which used backdrops, flash lighting, and a reflected grid background (see Appendix B). Even with this special effort to highlight the wrinkle patterns developed (or the lack of them), the film properties of this specific model always adversely affected the clarity of the photographs. Thus, in Figure B-12, Appendix B, there is no overall wrinkle pattern, which indicates a flat panel. However, the four distinct patterns of wrinkles shown in the photograph appeared throughout the testing and were inherent with the material used. Nevertheless, as much use was made of the 1- by 2-meter model in the time permitted.

One particularly interesting pair of photographs, having the same edge member tensions, are shown in Appendix B, Figures B-1

and B-2. The difference in the wrinkle patterns is due to the adjustment of the edge catenary, resulting in a slightly greater horizontal, or chordwise, stress (N_x) applied to the model. The approximate values of N_x may be computed by the expression

$$N_x = T/R$$

where T is the tension of the edge member, and R is the approximate curvature over the arc length. For this case,

$$R = 10 \text{ meters}$$

$$T = 2.56 \text{ N}$$

$$N_x = 0.256 \text{ N/m}$$

The effect of a 1-cm increase in the arc depression at this load could only account for, at most, a 20-percent increase in N_x. Since it did not appear that this alone could be responsible for the presence of so many wrinkles or such a well-developed wrinkle pattern, another factor was assumed to be operative. Further experimentation and repetition of this test point was performed. Although the edge member of the catenary is flexible and conforms to the outline of the catenary in the sail, after it emerges from the sail it must follow the tangential extension of the curve defined in the panel cutout. If it does not follow this extension, a constant distributed load transmitted from the edge member into the panel will not be realized. Thus, once the curve is cut into the panel and the edge member is properly aligned with the tangents at the end points, the only adjustment possible without changing the load distribution is the tension in the edge members.

Another factor which affects this situation is the elastic properties of the panel itself. That is, as N_y increases, the length of the panel changes, much as the full-size panel will change due to thermal variations. For edge members of this design to work under different loads and dimensional variations, some allowance must be made for continuous alignment of the tension members to the panel curve. If the length of a free edge member is short in comparison to the length threaded through the panel, a mechanical means of moving the edge member, relative to the panel, would have to be devised. However, if the point of support for the edge member is distant, relative to the panel, small variations in the location of the end of the panel will not affect the line of action of the edge member due to the small angles involved.

These factors explain the reasoning behind the long stringers and edge members discussed in the suggested alternative design covered in the next section.

In regard to the determination of the threshold ratio of N_x/N_y for wrinkling to occur, this was found to be too complex to be exhaustively examined in a test program of this scope. In general, if this ratio was greater than 0.1, the wrinkles present could be eliminated by adjustment of the edge members. For ratios less than 0.1, the presence of wrinkles was not only a function of N_x/N_y, as the absolute load level of either load also seemed to be a factor. As the loads became higher, the method of adjusting the position of the edge members and the precision of the layout of the edge members became more critical.

In addition, the low aspect ratio of this model did not allow the end effects to distribute themselves over the width of the panel. This could have been partially alleviated by increasing the number of attachment points of the Whiffletree, but time did not permit this. Thus, in Figure B-15 (Appendix B), although $N_x/N_y = 0.02$, it is still difficult to tell if the wrinkle pattern developed is due to the overall loading, or just the higher stress concentrations in the regions of the lower attachment points.

SUGGESTED DESIGN ALTERNATIVE

The results of the modeling indicated that, for a film support system to prevent wrinkles and still maintain a low level of stress, the positions and alignment of the supporting members had to be accurately placed. The alternate design presented by Astro Research satisfies the geometric and kinematic requirements for the support of the edge members (see Figure 2 and the enclosed sketch, SK1868).

The biaxially tensioned panel design, as seen in Figure 2, tensions the film such that no wrinkles will occur under any thermal variation encountered by the Heliogyro. Each panel is supported at each edge by parabolic tension members designed to impart the correct distributed load for that region of the panel. The use of interlocking parabolic end members allows for a minimum expansion gap between sail panels, as the ends of both panels are parallel and rectangular.

The elements of the single-panel support system, shown in Figure 2, are:

Item	Description
A*	Collapsible lattice battens
B*	Outer edge members: tension varies from minimum at the tip to 650 N at the root
C	Inner panel edge members: tensioned at 42 N, 1-mm in diameter, and constructed of polyimide graphite
D*	2-μm film material
E	Polyimide graphite flat ribbon: connects film to parabolic tensioned members
F	Inboard panel end parabola: supports centrifugal load of panel
G	Outboard panel end parabola: maintains minimum tension along outboard end of each panel
H	Location of negator retractor for "G": maintains constant tension for 0.75-m extension (see SK1868, Detail A)
I	Panel edge reinforcement

*Existing member in baseline design.

This arrangement of supporting members produces a minimum edge tension of 0.0125 N/m at each edge of the panel. Because of the slight chordwise contraction of the outer edge of the outboard end parabola, the stress in the center portion of the outer end of each panel will be reduced by approximately 50 percent. However, the stress ratio of N_x/N_y will not be radically affected, as the spanwise stress, N_y, is also at a minimum here.

Similarly, at the inboard edge of each panel, the spanwise tension is the greatest, varying from panel to panel depending on the radial station of the panel. In no case is it less than 0.0125 N/m, and it is a maximum of 0.7 N/m at the tip. Since 0.7 N/m ÷ 0.0125 N/m is approximately 56, a shorter panel length is suggested for the more distant outboard panels.

The expansion and contraction of each panel during temperature changes is taken up in large part by the negator spring which regulates the tension in the outboard parabola. The inboard end of each panel remains stationary relative to the edge members during expansion and contraction of the panel (except for chordwise motion). As the panel expands, the looped edge members allow it to slide, relative to the long, edge catenaries. The chordwise changes in the panel are accomodated by the large-radius, small-angle deviation of the edge catenaries, which are tensioned by a rocker arm scissors mechanism connected to the main edge members (see SK1868, Detail A). The displacements and loads for all temperature extremes have been calculated and appear in Appendix C.

SUMMARY AND CONCLUSIONS

Because of the difficulty of treating the problem of wrinkles from a strictly analytic viewpoint, a series of scale-model film panels were made. Various configurations and methods of attachments were attempted, and ultimately a larger 1- by 2-meter panel was constructed. The relationship between stress levels, precision of application, and precision of loading was more apparent in the larger model. Once a satisfactory method of supporting the sail panel had been obtained, the problem of thermally-induced dimensional variations was examined and a promising solution has been outlined.

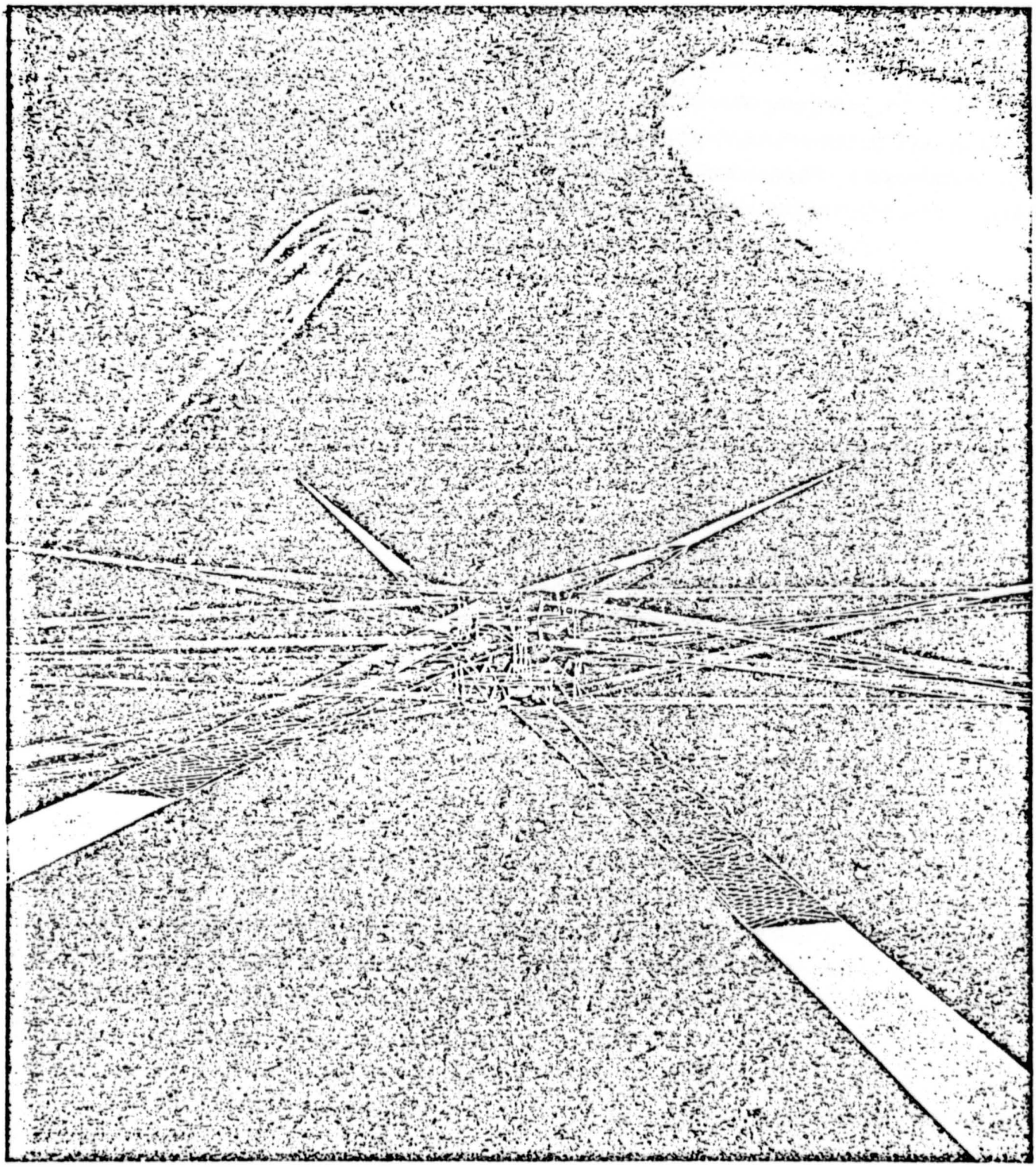

Figure 1. Baseline Twelve-Blade Heliogyro

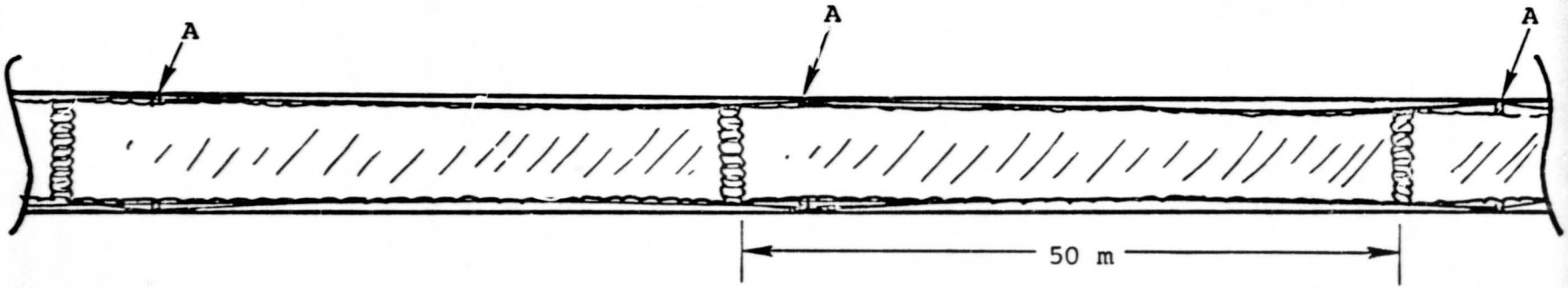

Blade Assembly

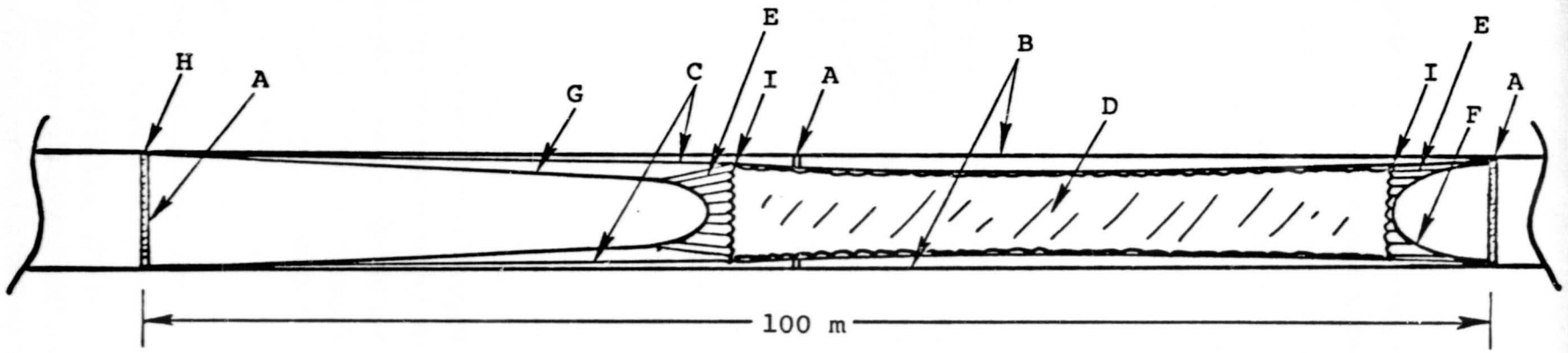

Single-Panel Support System

Figure 2. Biaxially tensioned panel design.

REFERENCES

1. MacNeal, Richard H.: Structural Dynamics of the Heliogyro. NASA CR-1745, 1971.

2. MacNeal, Richard H.; Hedgepeth, John M.; and Schuerch, Hans U.: Heliogyro Solar Sailer Summary Report. NASA CR-1329, 1969.

3. Stein, Manuel; and Hedgepeth, John M.: Analysis of Partly Wrinkled Membranes. NASA TN D-813, 1961.

4. Hedgepeth, John M.: Behavior of Wrinkled Solar Sails for the Heliogyro. ARC-TN-1036, Astro Research Corporation, 1977.

APPENDIX A

CHRONOLOGY OF SMALL MODELS

APPENDIX A

Chronology of modeling small film panels for wrinkle study

1) First model, worst case, for comparison.

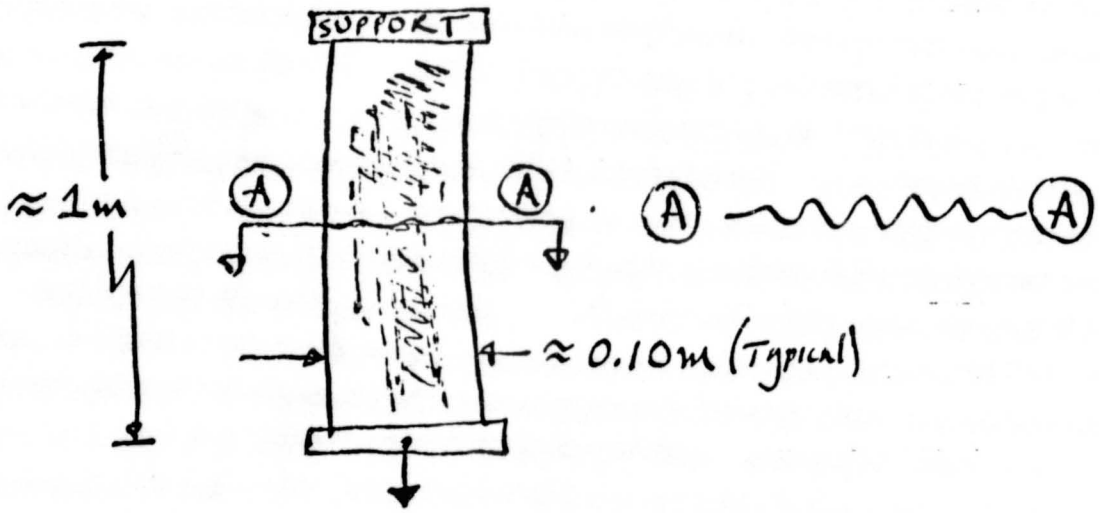

2.) Scalloped ends, slight chordwise tension (See figure A-1)

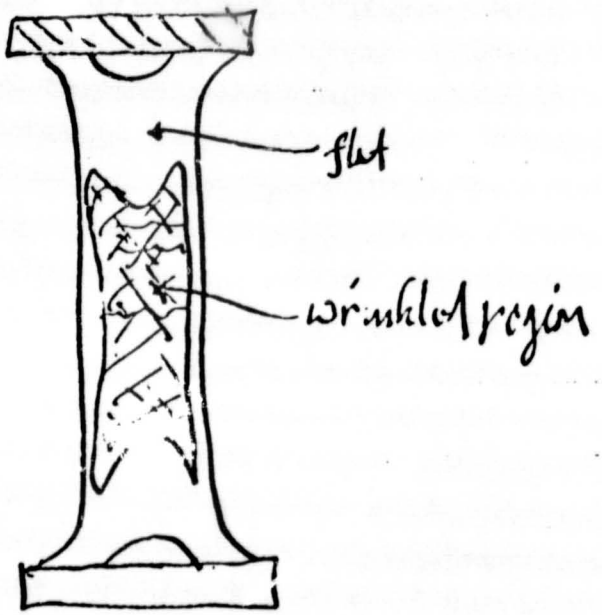

3.) Scalloped edges, strip reinforcements:

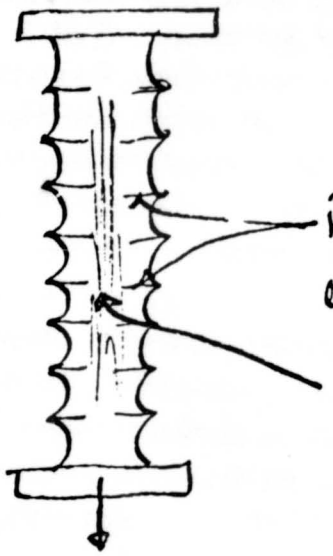

reinforcements not stiff enough to prevent curl

wrinkles in center region as well

4.) interwoven edge members, rectangular panel

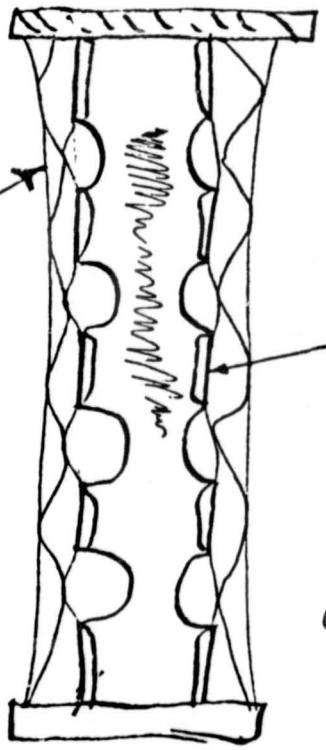

edge member adjusted to form catenary shape

Inner edge member encased by folded over tabs from panel

Produced flat, taut panel, but was overly complex, too much area lost to scallops

5.) Similar to #4, with shallower scallops (eg. lower Δ/L) (See figure A-2)

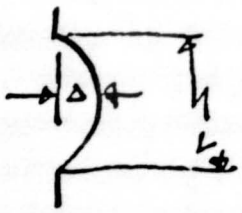

6.) Concept modeled was a restraining member wrapped around edge members to form a restrictive envelope to limit amplitude of wrinkles. Was not successful.

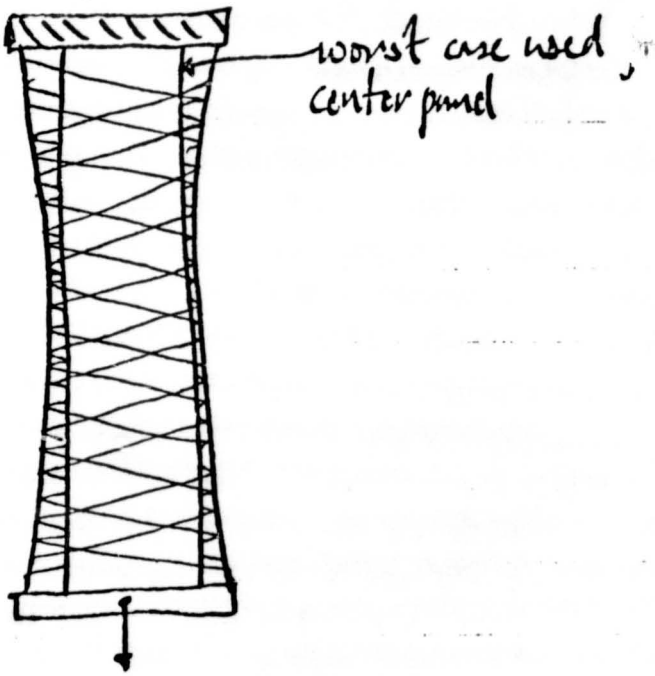

7.) An attempt to improve #6 by using a fine woven mesh above & below the surface of the panel. No obvious improvement was noted, and this concept was dropped.

8.) A concept was tried which proved successful, and seemed practical: (See figure A-3)

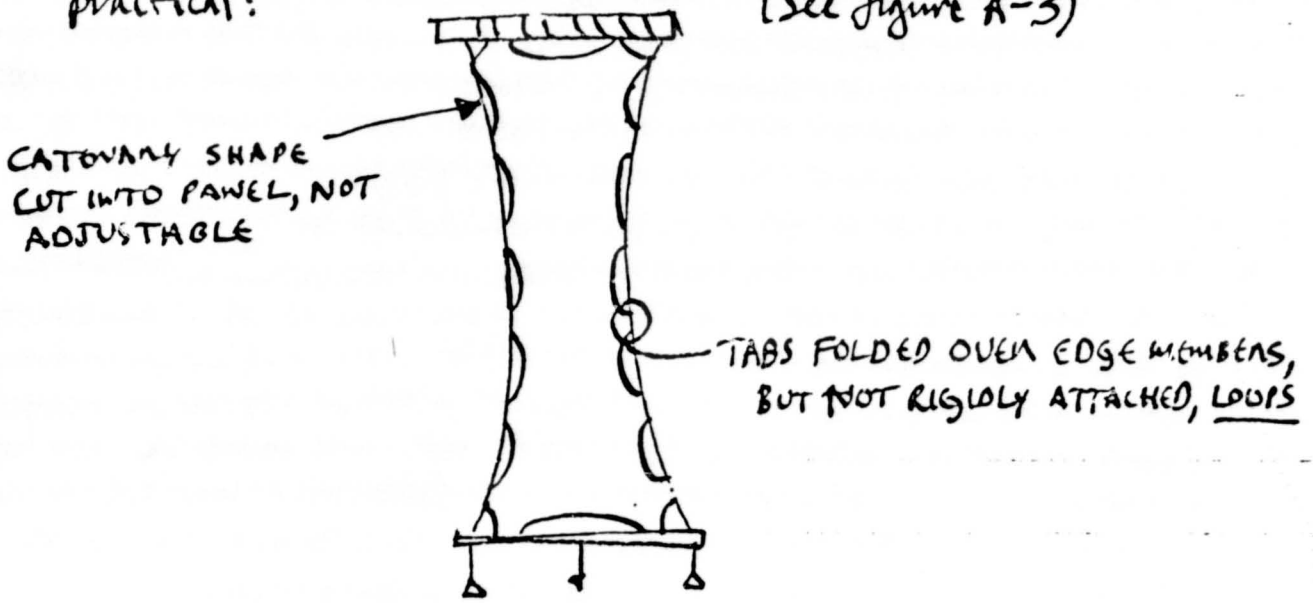

9.) Same as #8 except instead of tabs folded over, metal sliders were bonded to film panel (similar to eyelet on fishing rods)

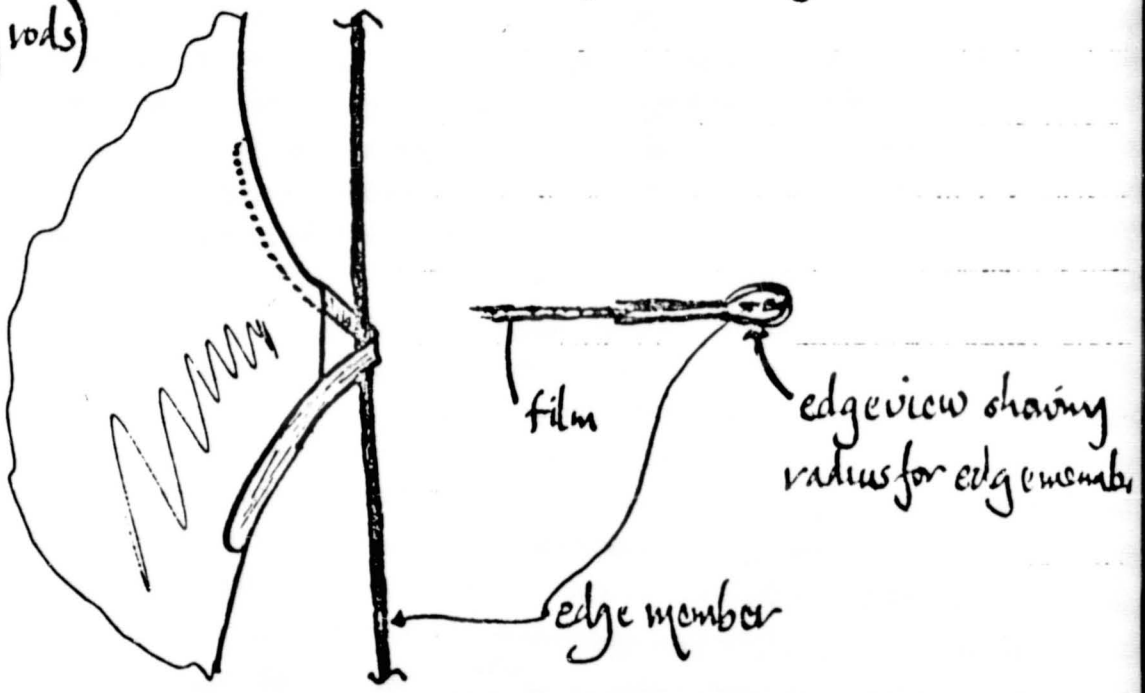

Figure A-1.

Model 2 with $N_x/N_y = 0$
(fully developed wrinkles
at midspan)

Figure A-2.

Model 5 with $N_x/N_y = .011$
(only local "blister"
wrinkles)

Figure A-3.

Model 8 with $N_x/N_y = .03$

APPENDIX B

DATA AND DIMENSIONS FOR 1- BY 2- METER PANEL

APPENDIX B ~ The 1m x 2m Model

1. DESIGN: Two features were included in this model which had not been used on the smaller models. The first was the loops used to attach the film panel to the edge member. They were made of separate pieces of mylar and were the following shape:

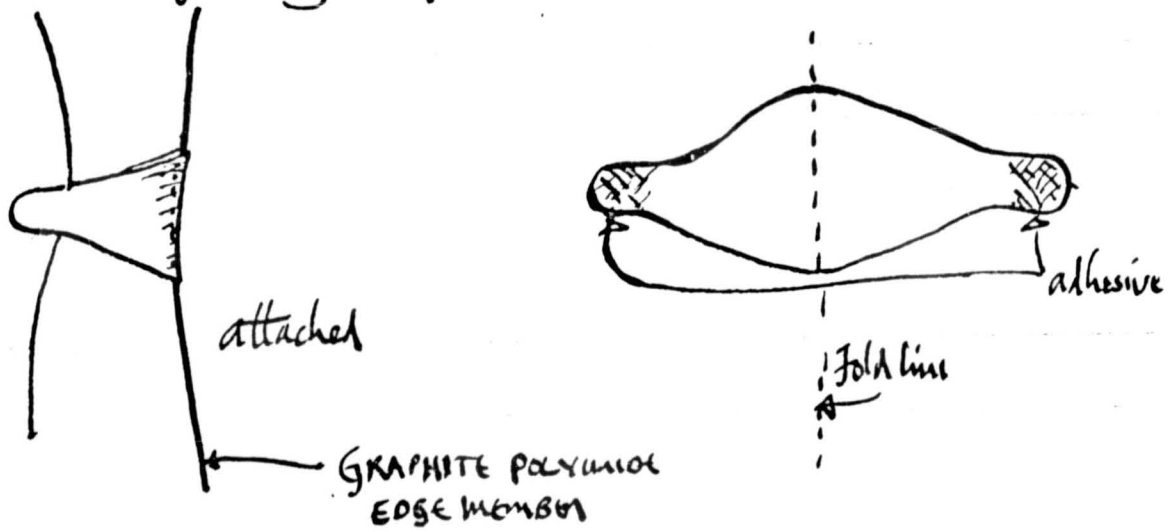

Also, the bottom edge was tensioned with a whiffle-tree arrangement which permitted fine adjustment of the location of the spanwise stress concentrations, and allowed the stress level to be constant across the chord, but capable of being changed by changing the central wt.

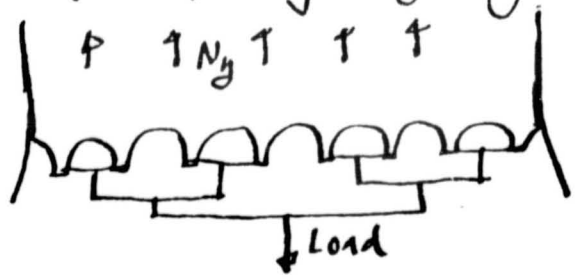

The edge parabolas were laid out on a mylar sheet and the panel was then cut out of an unstressed sheet. The characteristic dimensions were:

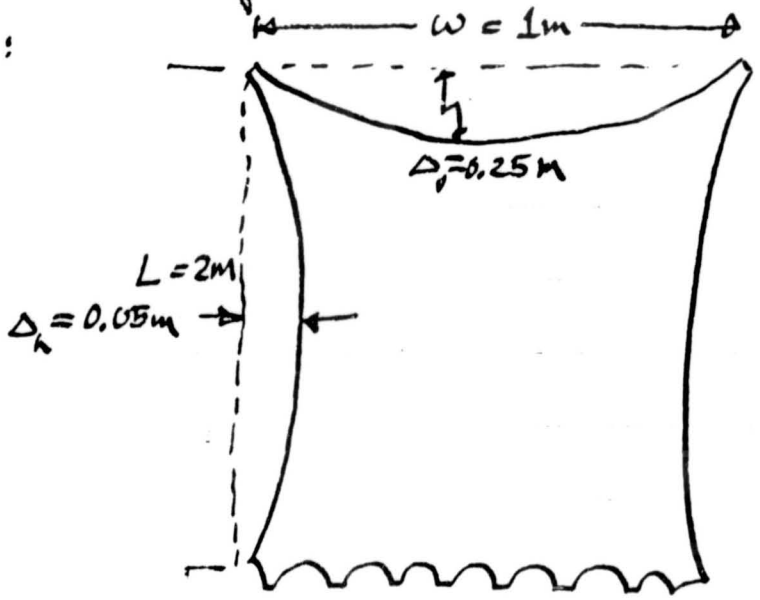

The mylar loops were attached around the top three edges with a pitch of 15cm.

2. Calculation of stress levels

In the tests which followed, the body force on the mylar was neglected. (It was calculated to be 10 gms/m² or approximately 20 gms total for the model.) Since the tare wts of the loading mechanisms were considerably greater than this, it was never more than 20% of the loading on the top edge member.

The expressions used to determine N_x, N_y

$$N_x = (W_{cat} + 61.5\,\text{gms})(9.506 \times 10^{-4})\ N/M$$

$$N_y = (W_y + 50\,\text{gms})(9.506 \times 10^{-3})\ N/M$$

where W_{cat} is the mass of each wt on the spanwise catenary and W_y is the mass of the wt loading the whiffletree

then $N_x/N_y = (W_{cat} + 61.8)/(10(W_y + 50)$

= a dimensionless ratio

The figures 61.8 and 50 represent correction factors for the tare weights of the loading mechanisms. They also represent the minimum N_x and N_y loads obtainable with this model.

3. Test Results — A more complete series of tests was carried out on the 1m x 2m model. The data shown in Table B-1 are the different loadings which were performed. Figures B-1 through B-13 show loadings 1 - 13 respectively. As the testing proceeded considerable effort was also being made to develope system of lighting, background, and reflective patters which would give good definition of the aluminized surface of the panel. (See figure B-14)

Because of the 1 to 2 aspect ratio of this model many of the wrinkles present appear to be end effects which would dissipate in a longer panel. (An earlier test point is shown in figure B-15 which represents the lowest value of N_x/N_y with this model) (No Backdrop was used with this 1 long.)

After loading #1, obvious adjustments were made in the edge members to reduce the wrinkling as much as possible. These adjustments were necessary to compensate for the elastic deformations of the panel, and hence the location and alignment of the edge members. It should be noted that where $N_x/N_y \approx 1$, the panel should appear flat. From Load #1, it can be seen that the surface of the panel is highly textured and wrinkled appearing even though the loads applied should produce a flat panel. These inherent wrinkles and creases were one of the main limitations of this particular model.

TABLE B-1

10-17-77 RECORD SHEET FOR 1X2m PANEL $g = 9.806$ Remarks, etc

LOAD	(1) $(N_x)W_{cat}$	(2) $(N_y)W_y$	(3) (1)+61.5	(4) (2)+50	(5) (3)×g/10⁴	(6) (4)×g/10³	(7) (5)/(6) $= N_x/N_y$	8	9
1	460	0	511.5	50	0.501	0.49	1.02	several photos taken	
2	200	0	261.5	50	0.26	0.49	0.52		
3	200	200	261.5	250	0.26	2.45	0.10		
4	200	200	261.8	250	0.26	2.45	0.10	change sil trp support +2 cm " bottom " +2 cm	
5	200	200	261.8	250	0.26	2.45	0.10	W/vertical stirrups	
6	200	500	261.8	550	0.26	5.39	0.047	Bottom cut +1 cm	
7	200	600	261.8	650	0.26	6.37	0.04		
8	200	100	261.8	150	0.26	1.47	0.17	no change in holes	
9	200	100	261.8	150	0.26	1.47	0.17		
10	200	100	261.5	150	0.26	1.47	0.17		
11	200	600	261.5	650	0.26	6.37	0.040		
12	500	200	561.5	250	0.55	2.45	0.22		
13	500	460	561.5	510	0.55	5.00	0.11	(Double shear added)	
14									
15									
16									
17									
18									
19									
20									
21									
22									
23									
24									
25									
26								ORIGINAL PAGE IS OF POOR QUALITY	
27									
28									
29									
30									
31									

EFFICIENCY, LINE No. 2036

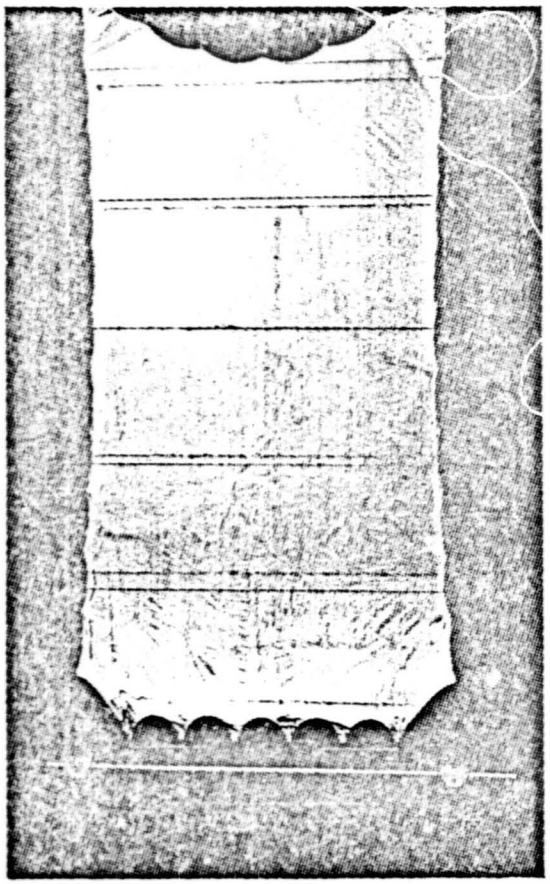

Figure B-1.

Loading #1, $N_x/N_y = 1.02$

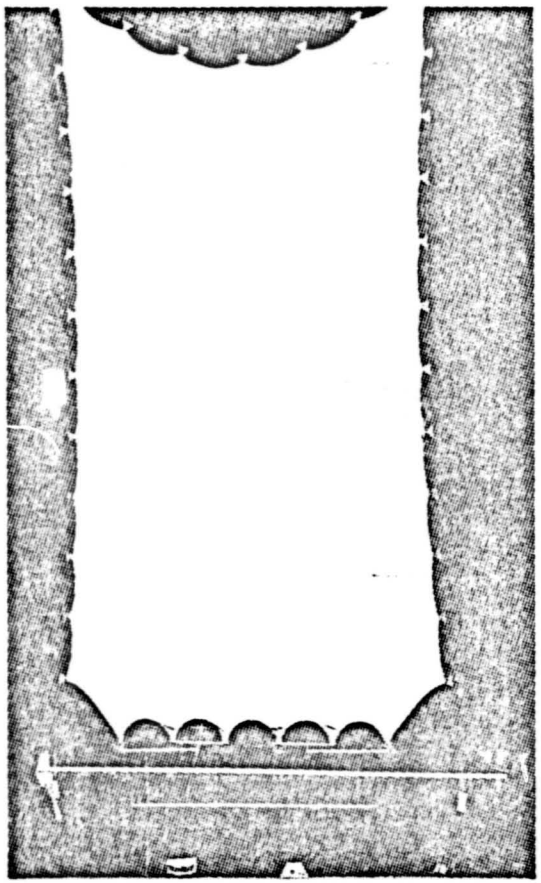

Figure B-2.

Loading #2, $N_x/N_y = 0.52$
(no large wrinkles present)

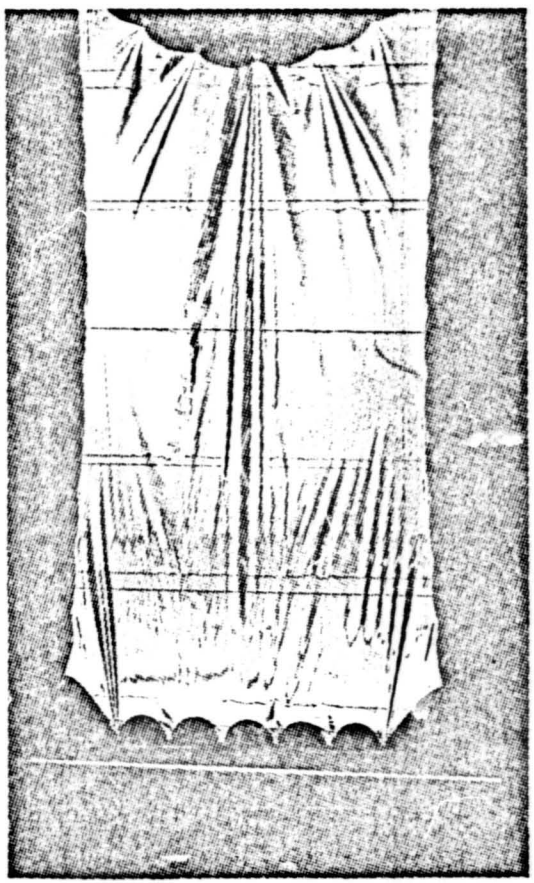

Figure B-3.

Loading #3, $N_x/N_y = 0.1$
(large wrinkles present)

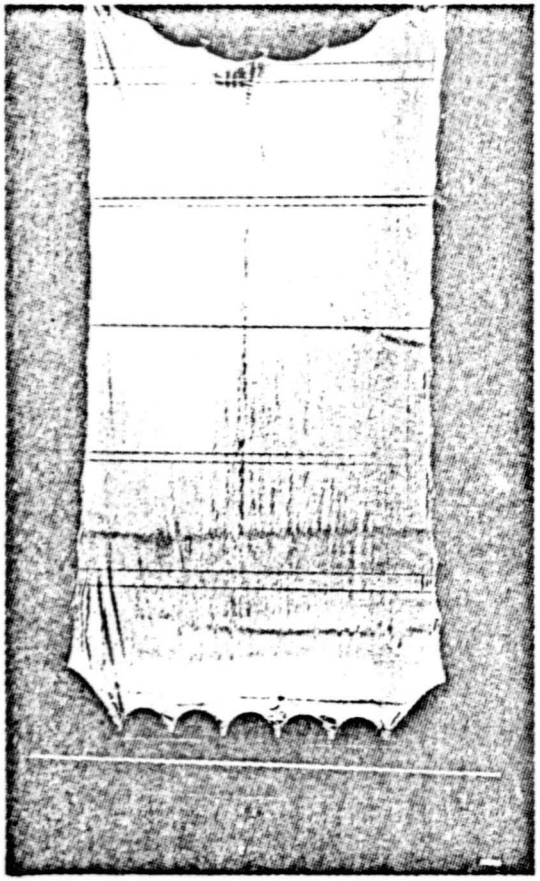

Figure B-4.

Loading #4, $N_x/N_y = 0.1$ (after adjustment of vertical edge members)

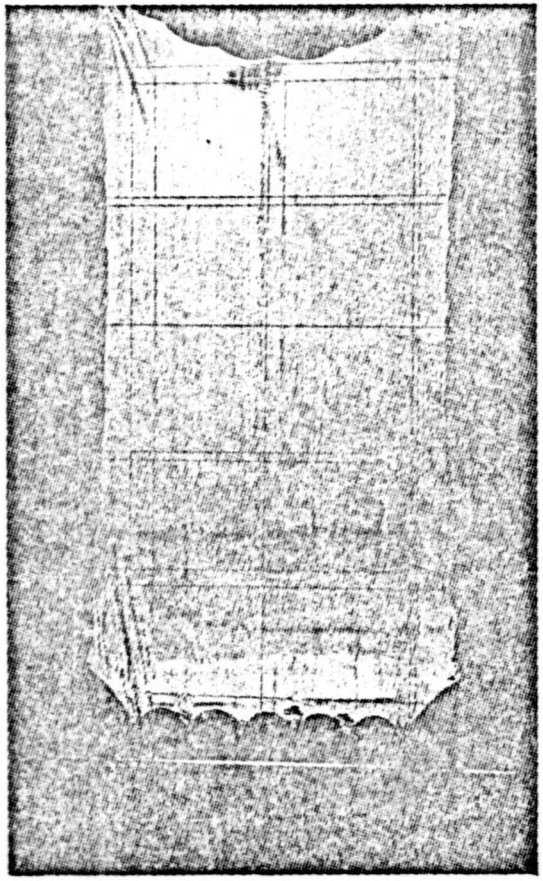

Figure B-5.

Loading #5, $N_x/N_y = 0.10$ (stringers placed in front of panel)

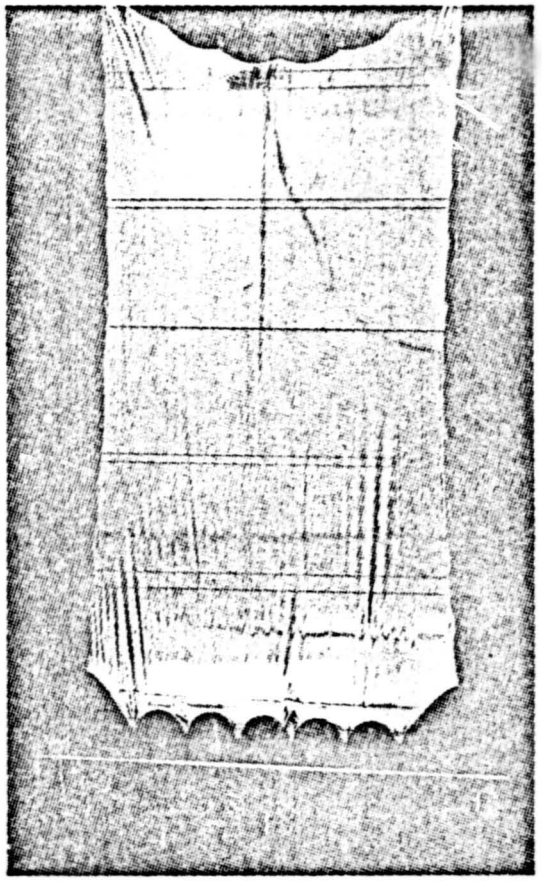

Figure B-6.

Loading #6, $N_x/N_y = 0.047$ (some wrinkles appear at lower corners)

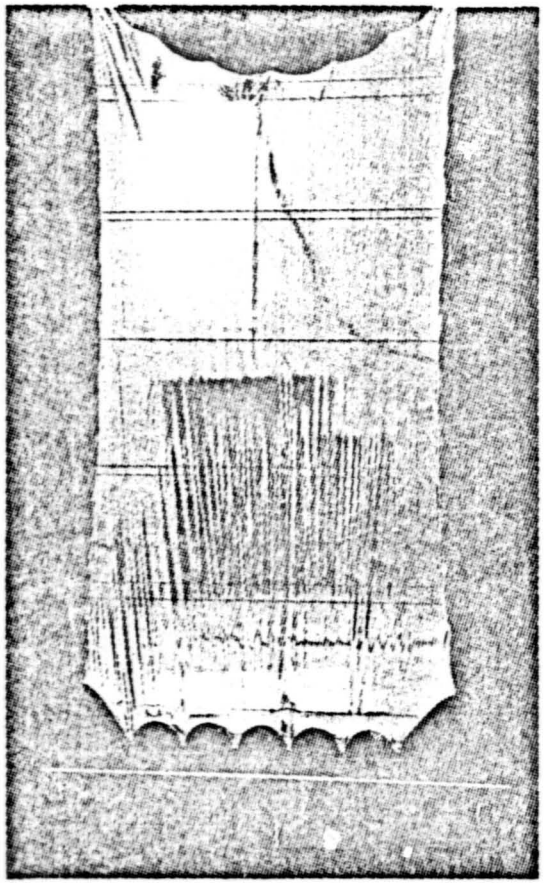

Figure B-7.

Loading #7, $N_x/N_y = 0.040$
(more wrinkles appear
at lower edge)

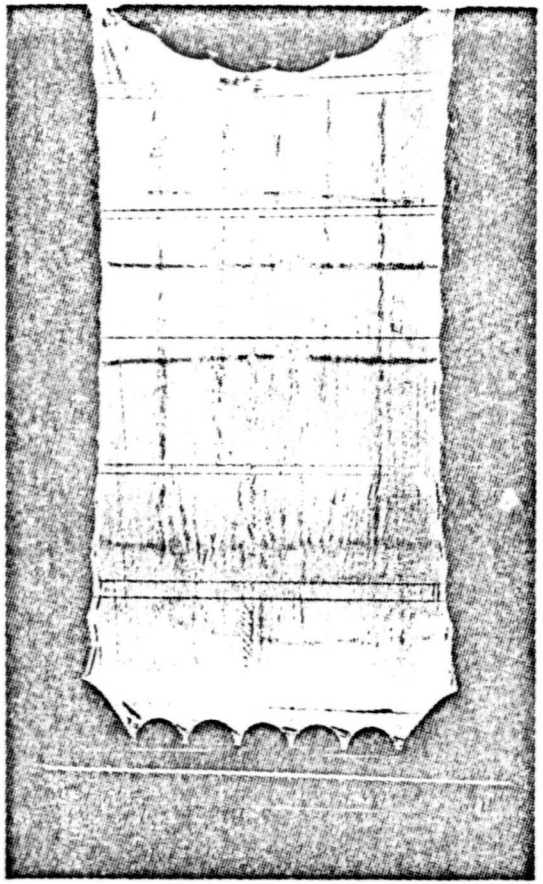

Figure B-8.

Loading #8, $N_x/N_y = 0.17$
(first attempt
at reflective grid)

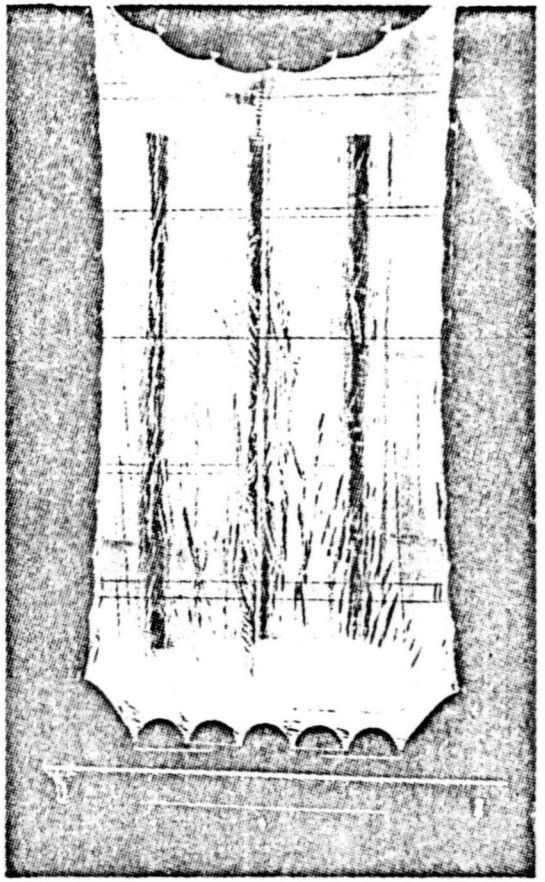

Figure B-9.

Loading #9, $N_x/N_y = 0.17$
(darker grid)

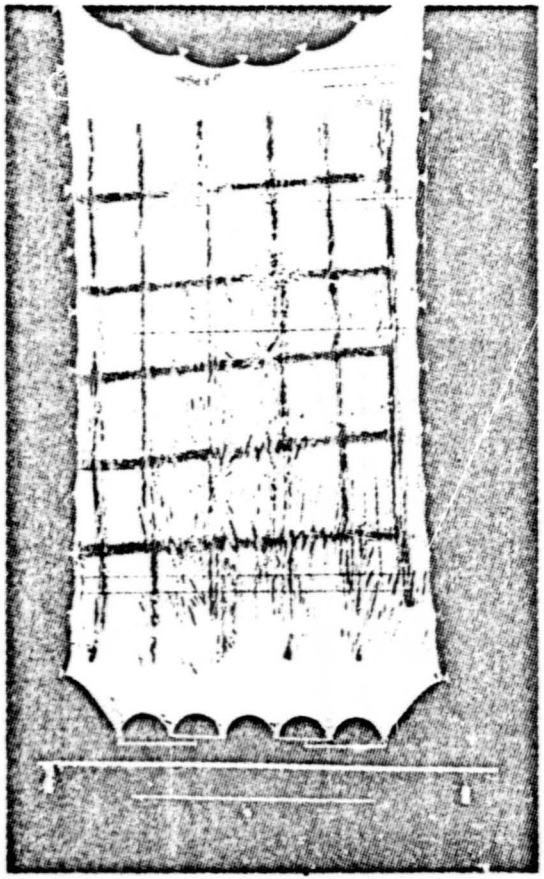

Figure B-10.

Loading #10, $N_x/N_y = 0.17$
(larger grid)

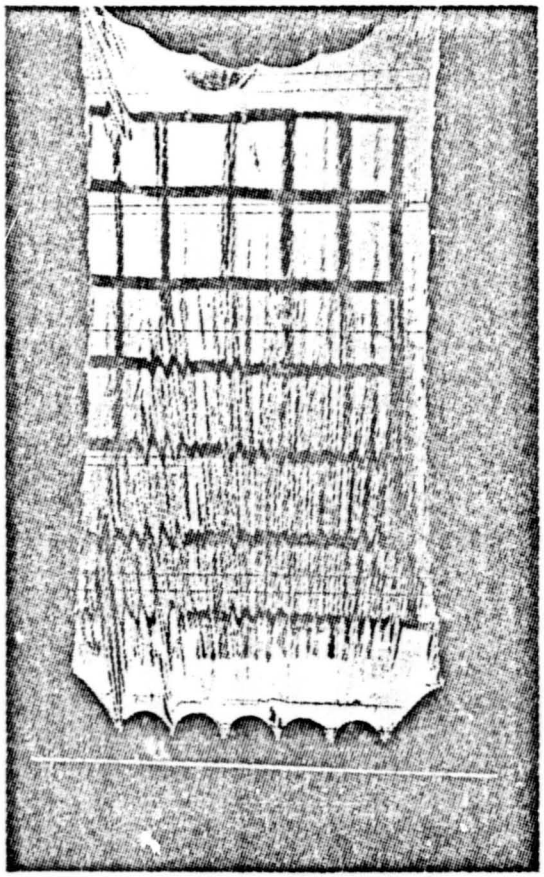

Figure B-11.

Loading #11, $N_x/N_y = 0.04$
(same as Load #7 with
grid added)

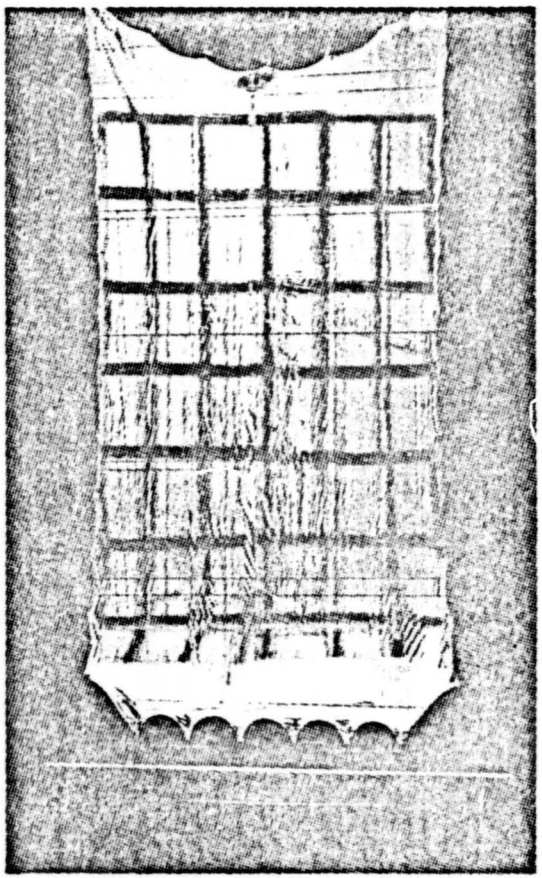

Figure B-12.

Loading #12, $N_x/N_y = 0.22$

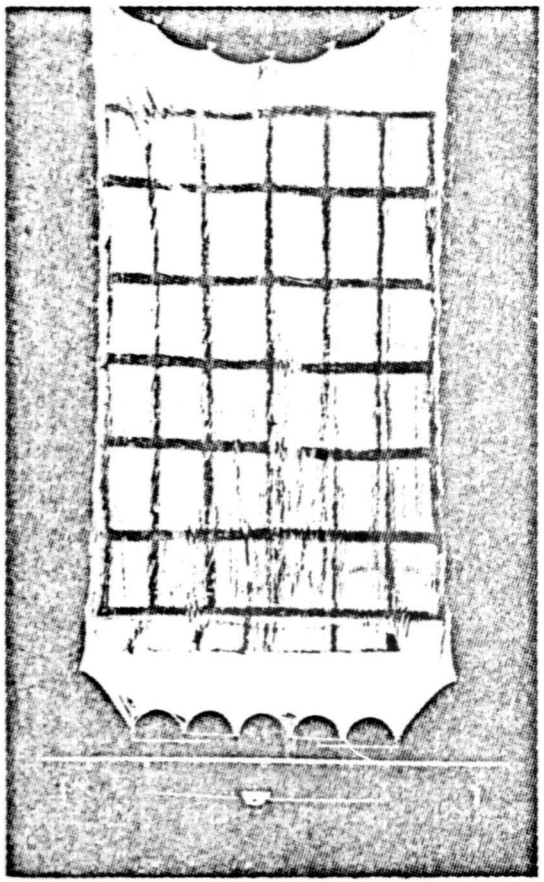

Figure B-13.

Loading #13, $N_x/N_y = 0.11$

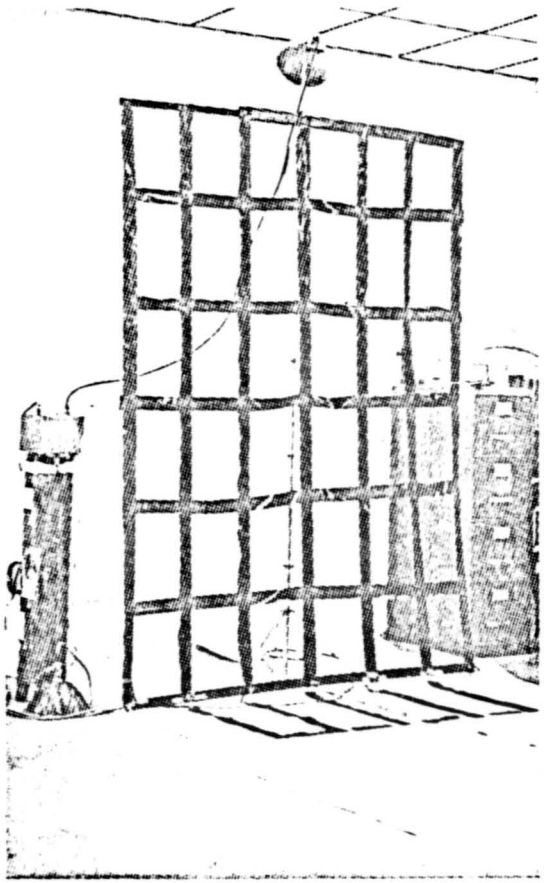

Figure B-14.

Backdrop used in test program

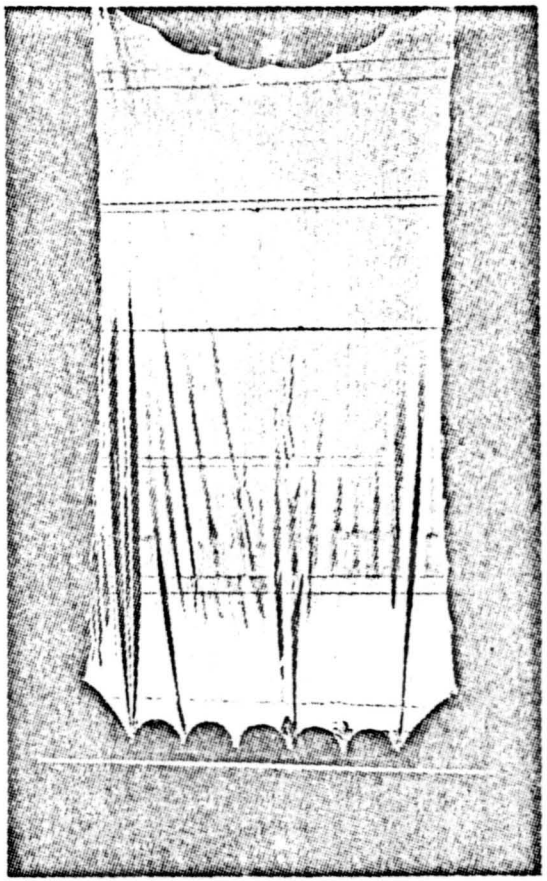

Figure B-15.

$N_x/N_y = 0.024$
(partially wrinkled)

APPENDIX C

CALCULATIONS
RELATING TO THE SUGGESTED ALTERNATE DESIGN

Appendix C - Calculations Relating to the Suggested Alternate Design

Reference: Drawing No. SK 1868

The following calculations deal with the various dimensions and proportions of the support members and edgemember attachments.

The basic long edge parabolas were laid out when the panel was assumed to be fully expanded. The minimum tension allowed was 0.0125 N/Meter of edge member. The long edgemembers are discussed first, then the short parabolas are laid out and finally the cell is allowed to contract and the various loads & displacements are calculated.

Throughout, a maximum extension & contraction of ±.75% in the spanwise direction and ±.69% in the chordwise direction are assumed.

11/5/77 – 4

EDGE PARABOLAS

calculations to determine parabola for leading & trailing edges of panel

∴

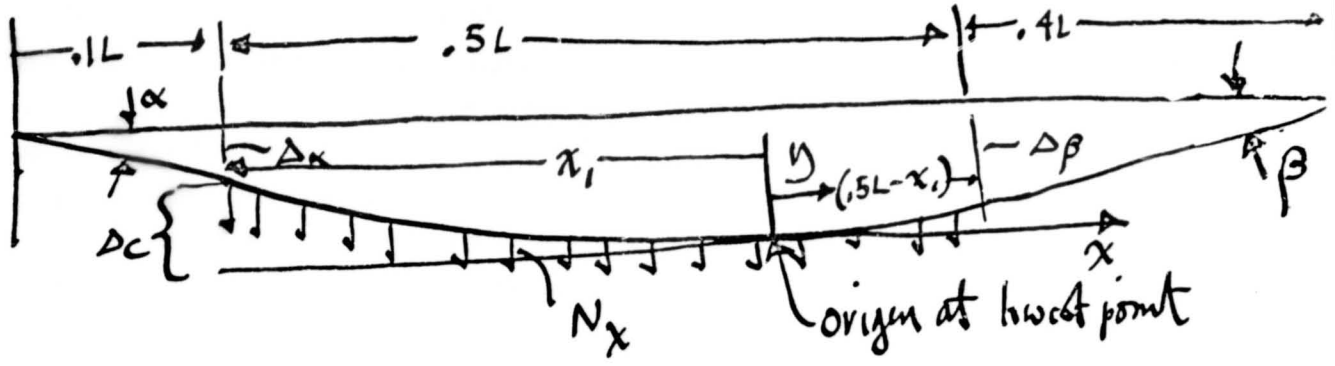

for constant load

$$dy/dx = \frac{N_x x}{T_u} \quad \therefore y = \frac{N_x x^2}{2T_u} + C_1 \quad \text{where } T_u \text{ \& } C_1 \text{ are constants}$$

now at $-x_1$ $dy/dx = -\alpha = \frac{-N_x x_1}{T_u}$ $\therefore T_u = \frac{N_x x_1}{\alpha}$ and $dy/dx = \frac{N_x x}{\frac{N_x x_1}{\alpha}} = \frac{\alpha x}{x}$

and $\underline{y = \frac{\alpha x^2}{2x_1}}$ so that at $x = -x_1$, $y = \Delta_c = \Delta_{catenary}$

$$\therefore \Delta_c = \frac{\alpha (x_1)^2}{2x_1} = \frac{\alpha x_1}{2}$$

But $\Delta_\alpha = (.1L)\alpha$

so total $\underline{\Delta_T} = \Delta_\alpha + \Delta_c = (.1L)\alpha + \alpha\frac{x_1}{2} = \alpha\left(.1L + \frac{x_1}{2}\right)$

now Δ_T has been specified to be $\leq$ 3% of W where $W = 8m$

$\therefore \underline{\Delta_T = .25M}$

$$\therefore \Delta_T = .25M = \alpha\left(.1L + \frac{x_1}{2}\right) \quad \underline{L = 100\ in}$$

$$.25 = \alpha\left(10 + \frac{x_1}{2}\right)$$

for closure Δ_T must also $= y_x = (.5L - x_1) + (\Delta\beta)\beta$

11-5-77-5

IF $y = \frac{\alpha x^2}{2x_1}$ at $x = (.5L - x_1)$ $y = \frac{\alpha (.5L - x_1)^2}{2x_1} = \frac{\alpha}{2x_1}(.25L^2 - 2(.5Lx_1) + x_1^2)$

$= \frac{\alpha}{2x_1}(.25L^2) - (Lx_1) + (x_1^2)$

$y = \frac{1}{8}\frac{\alpha L^2}{x_1} - \frac{\alpha L}{2} + \frac{\alpha x_1}{2}$

$\therefore \Delta_T = \frac{1}{8}\frac{\alpha L^2}{x_1} - \frac{\alpha L}{2} + \frac{\alpha x_1}{2} + (.4L)\beta$

$\therefore \alpha\left[\frac{L^2}{8x_1} - \frac{L}{2} + \frac{x_1}{2}\right] + .4L\beta = .25 = \alpha\left(10 + \frac{x_1}{2}\right)$

unknowns α, β, x_1

other equation is dy/dx at $x = (.5L - x_1) = \beta$:

So $dy/dx = \frac{\alpha x}{x_1}$ dy/dx at $.5L - x_1 = x = \frac{\alpha(.5L - x_1)}{x_1} = \beta$

$\beta = \alpha\left(\frac{.5L}{x_1} - 1\right)$ so that

$$\alpha\left[\frac{L^2}{8x_1} - \frac{L}{2} + \frac{x_1}{2}\right] + .4L\underbrace{\left[\alpha\left(\frac{.5L}{x_1} - 1\right)\right]}_{\beta} = .25 = \alpha\left[10 + \frac{x_1}{2}\right]$$

$$\frac{L^2}{8x_1} - \frac{L}{2} + \frac{x_1}{2} + .2\frac{L^2}{x_1} - .4L = 10 + \frac{x_1}{2}$$

<u>SOLVE for x_1</u>

$$\frac{L^2}{8} - \frac{Lx_1}{2} + \frac{x_1^2}{2} + .2L^2 - .4Lx_1 = 10x_1 + \frac{x_1^2}{2}$$

$$L^2 - 4Lx_1 + \cancel{4x_1^2} + 1.6L^2 - 32Lx_1 = 80x_1 \cancel{+ 4x_1^2}$$

$L^2 + 1.6L^2 - 7.2Lx_1 = 80x_1$ NOW $L = 100M$

11/5/77-6

$2.6L^2 = 7.2LX_1 + 50X_1$

$26{,}000 = 720X_1 + 50X_1$

$X_1 = 26{,}000/800 = \underline{32.5\,m}$

$\therefore .25 = \alpha\left[10 + \frac{32.5}{2}\right] = \alpha\left[26.25\right]$

$\alpha = .25/26.25 = .00952\ \text{rad} = .54° = .51567 = .55°$

and $\beta = .55°\left[\frac{50 - 32.6}{32.5}\right] = .55(.535) = .296° = .30°$

we can determine exact Tension exactly via

$N_x(.5L) = T(\alpha + \beta)$ $\alpha = .00952$ rad $\beta = .00499$

$\therefore (.0125\ N/m)(.5)(100m) = T(.00952 + .00499)$

$T = \frac{(50)(.0125)}{.01451} = 43\ N$

$\underline{\underline{T = 43\,N}}$ (for any panel with this geometry, regardless of Radial station)

and, the geometry

$\Delta\alpha = 10m \cdot \alpha = 10m \cdot .00952$

$= .0952\ m = \underline{9.52\,cm}$

$\Delta\beta = 10m \cdot .00499 = .1996 = \underline{20\,cm}$

Long edge member deflection during panel contraction

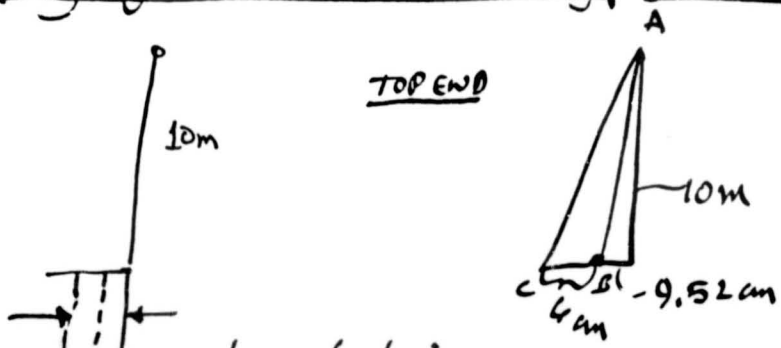

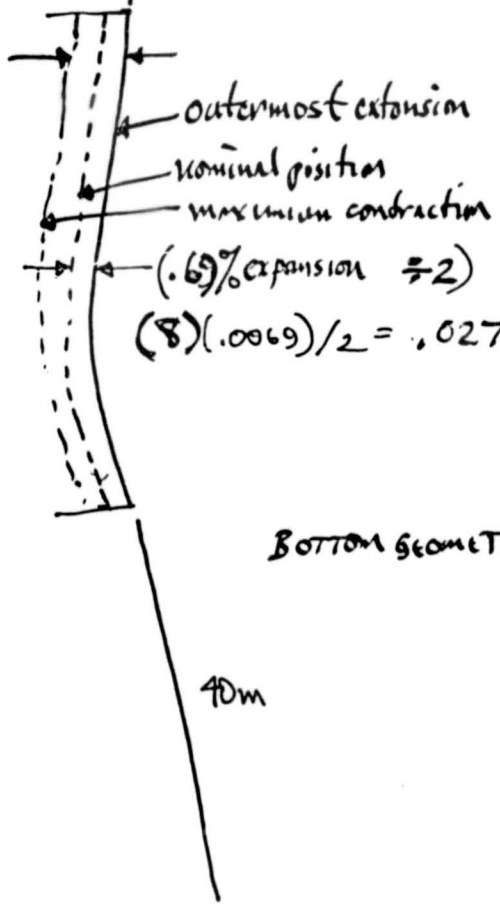

accounts for further contraction from nominal

(8)(.0069)/2 = .027m = 2.7cm = 3cm x2 = 6mm

Δ_L = .00034 m

$\therefore \Delta_{L_{TOP}} + \Delta_{L_{BOTTOM}}$ = .00075 + .00034 = .00109 m

= 1mm change in length

Now, what loads are put into the top & Bottom of the John panels for this contraction? At top edge of panel:

EDGE MEMBER ATTACHMENT POINTS:

If N_x is to be equal to 0.0125 N/m everywhere along the panel, if the attachment points are 1 meter apart, the tension in each loop will be a total of $(1\,m) \times 0.0125\,(N/m) = \underline{0.0125\,N}$.

Now, if the stress level of .35 MN/m^2 is to be regarded as the maximum allowable stress x (2 safety factor) what is the minimum amount of Kapton sail material (linear edge distance) which may carry this load?

Thus $A = P/\sigma$; $t \cdot L = A$ so $L = P/t\sigma = \dfrac{0.0125\,N}{\frac{.35 \times 10^6\,N}{m^2} \cdot 2 \times 10^{-6}\,m}$

$L = .0179\,m = 1.79 \hat{=} \underline{1.80\,cm}$ (with a factor of 2 for safety.)

Now, so as not to concentrate the stress at any one point, webbed loops were designed which spread the tension over a wider area of the sail. These are envisioned to be clear mylar applications formed by folding over the polyimide edge member and bonding to either side of the sail panel. (These loops might also be made of polyimide graphite ribbons fashioned in the same manner)

(Next, consider increased load on top attachment pt)

Geometry at top edge, full extension

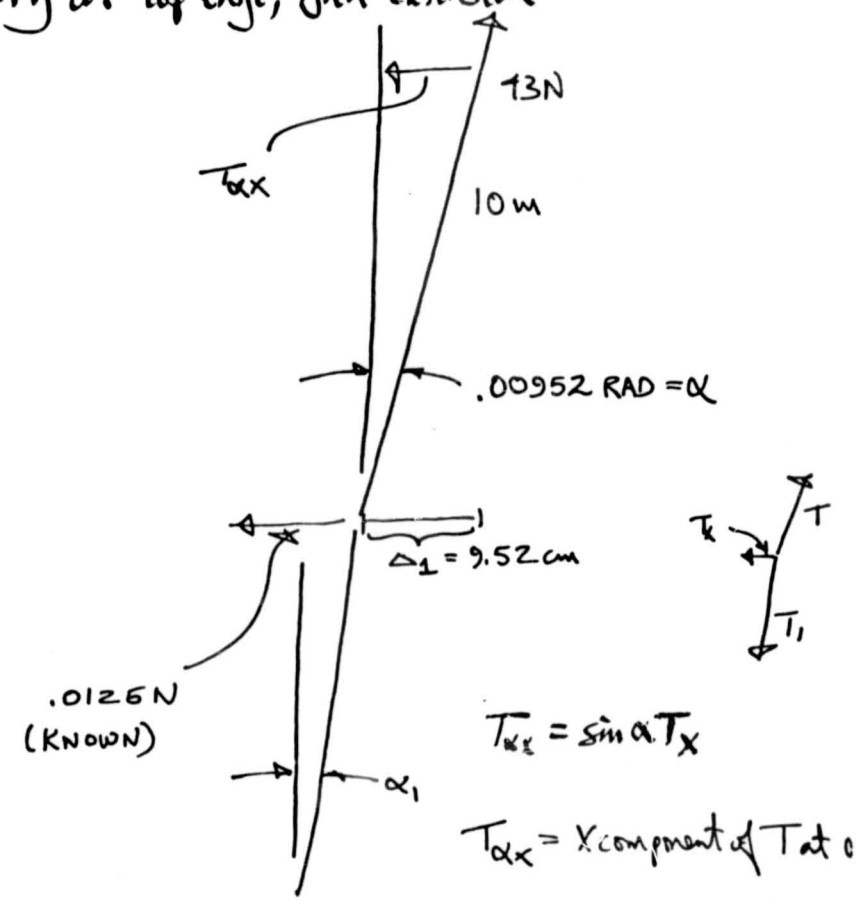

$T_{\alpha x} = \sin\alpha \, T_x$

$T_{\alpha x}$ = X component of T at end

$= (.00952)(43) = .409N$

$\therefore .409N - .0125N = T_{\alpha_1 x} \quad T_{\alpha_1 x} = .396$

$.396 = 43\alpha_1 \quad \alpha_1 = .00923$

When panel contraction occurs, top inside corner members move <u>6cm in</u>

$\therefore$

$\Delta_2 = \Delta_1 + 6cm = 9.52cm + 6cm = \underline{15.52cm}$

$\therefore$ horz component $= T_{\alpha x} = \sin\alpha\,(T)\left(\frac{\Delta + \Delta_1}{10}\right)(43)$

$= \frac{15.52cm}{10m}(43) = .667N$

$\therefore$ X component of α, Tension is the same $= -.409N$

$\Delta T_x = .258N$

∴ At the top edge of the panel, the maximum chordwise tension = .25N

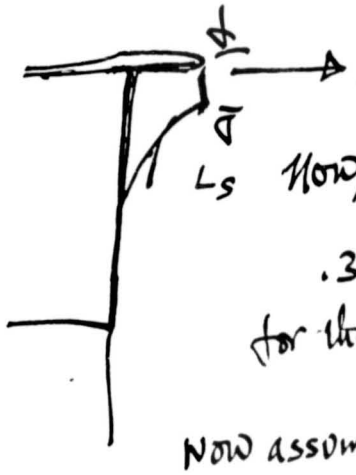

Now, Kapton has a maximum stress level of

$.35 MN/m^2$

for this, the minimum area = $\frac{.25N}{.35 \times 10^6 N/m^2} = 7.055 \times 10^{-7} m^2$

Now assuming that the slider is Kapton, what thickness must it be?

$T = \frac{1}{2}$ Load ∴ $L_s = 4cm$

∴ $t_s = (\frac{1}{2})(7.055 \times 10^{-7}) / 4cm$

$t_s = .00.001 m = .01 m =$

∴ if slider were .1 mm kapton, safety factor of 10:1 would be achieved.

At lower edge the contracted edge load will be approximately ¼ that of the top end.

(Because radius arc is 4 times as long, hence reinforcement panel is ¼ as much material)

Calculated to be .0634 N additional side load.

END PARABOLAS

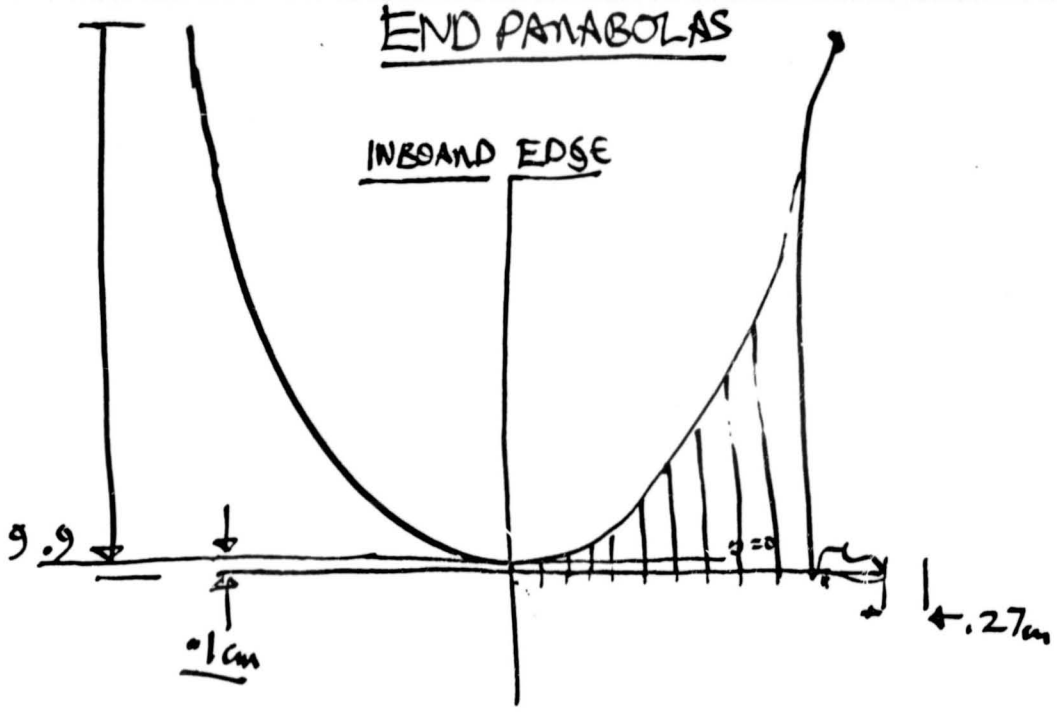

Form $2pq = x^2$

x

$4 - (.27 + .095) = 3.64$

$\Delta x = .364$

	x	y
x_1	.364	.088
x_2	.727	.353
x_3	1.091	.794
x_4	1.454	1.41
x_5	1.82	2.21
x_6	2.182	3.17
x_7	2.55	4.39
x_8	2.91	5.66
x_9	3.27	7.14
x_{10}	3.63	8.80

at $x=0, y=0$

These figures reflect a 100/1 scale for drawing SK 1967 → Actual Dimensions would be in Meters instead of centimeters.

FOR THE LAST STATION:

$x = 3.865 \quad y = 9.9$ $\quad \therefore \quad 2p(9.9) = (3.865)^2$

$p = \frac{(3.865)^2}{(2)(9.9)} = .7486$

$2p = 1.49722$

Now, the layout of the lowest tension parabola (or outboard panel parabola)

Angles used in graphical determination of parabola

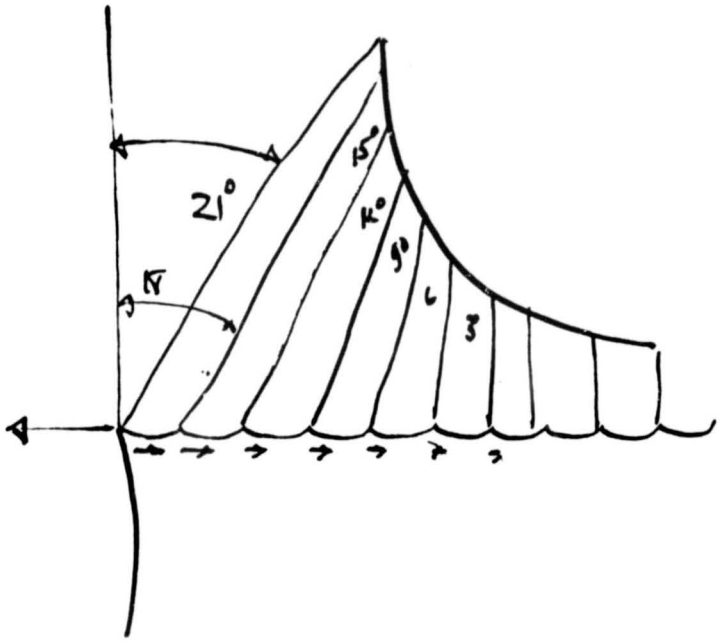

Now, assuming a 0.0125 N/m load desired over the free end, if these stringers are attached every .4m we have an individual vertical load component of $(8)(.0125) \div (21) = .00476\,N = T_i$ = individual components in Spanwise direction. Now, the following summation was made

$$T_C = \sum_{\theta = 21, 18, 15, 12, \ldots 6, 3}^{0} T_i \tan\theta = \underline{.00716\ N}$$ compressive load inward

Last Chordwise tensioner = $N_x = 0.0125\,N$

∴ Looking at outboard end reinforcement at center

$= 0.0125\,N - .00716\,N = \underline{.00534\,N}$

40m equal tension Parabola

GRAPHICAL LAYOUT FOR OUTBOARD PARABOLIC PANEL TENSIONER

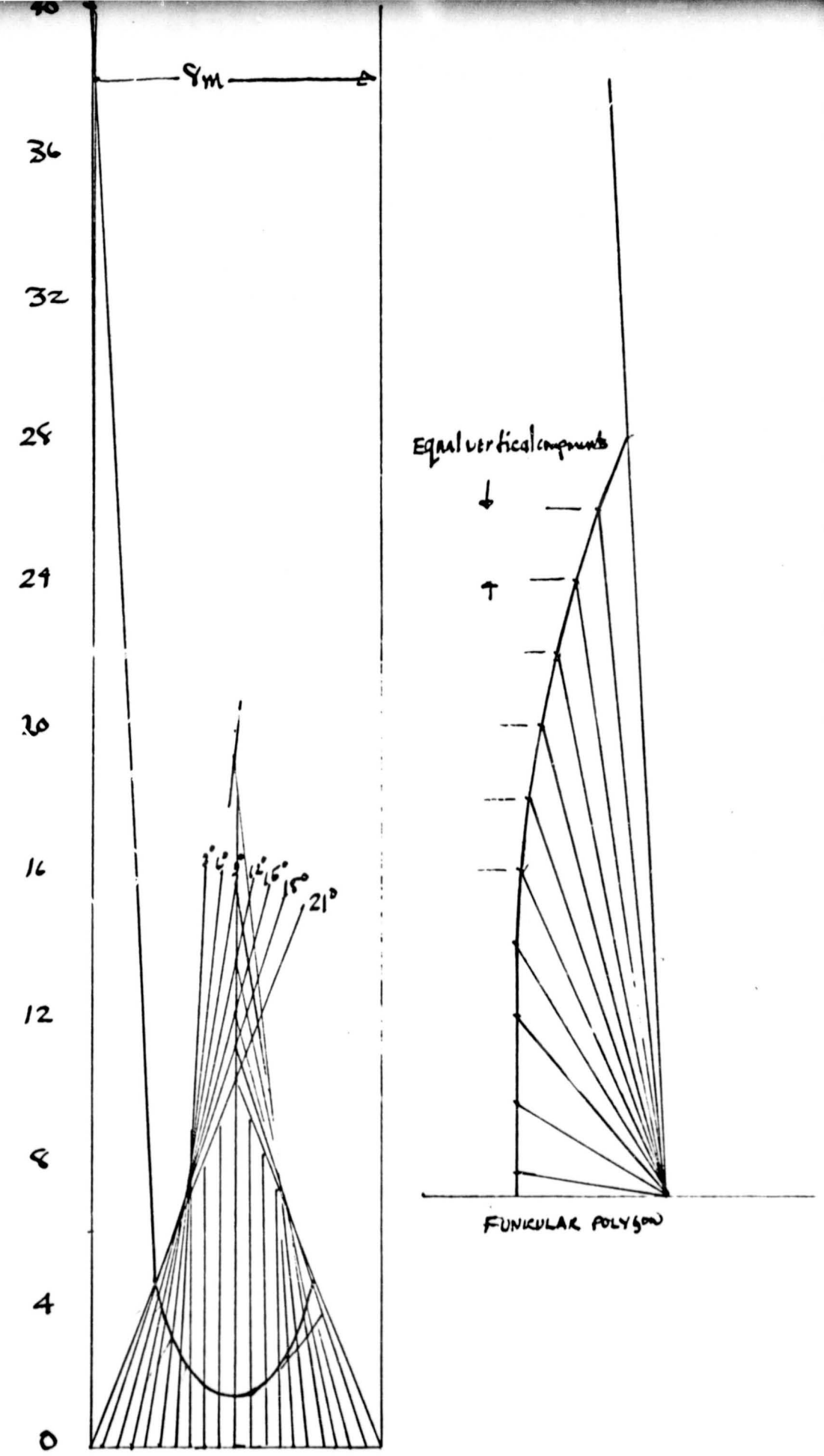

DEPTH OF SCALLOPS ALONG EDGES: No seperate tests were conducted to investigate the problem of curl at unsupported free edge members. Rather, all models were observed for local curl at unsupported free edges and within the test program outlined here, the only instances were in the first worst-case models described in Appendix A. The ratio used in the scallops for the 1m x 2m model were of these outlines:

Spanwise:

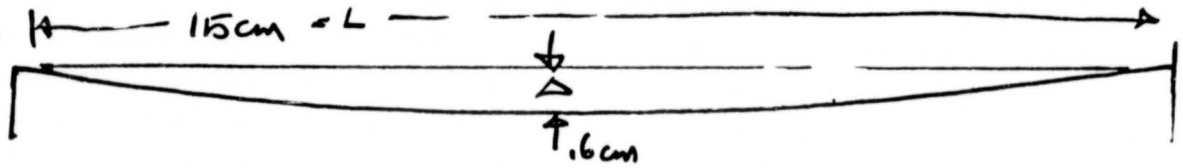

Here the $\frac{\Delta}{L}$ ratio is 0.04. (or 1:25). In the alternative design it was decided to Lower this still further to .02 or 2cm of Δ for 1 m/attachment points. This is true for the long edge attachments : scallops. It was felt that this could be done because N_x/N_y in each panel is not a constant but varies from approximately 1 near each panel tip to a value between 56 and 1 at the root. In figure B-15 the stress ratio was very nearly 56:1, and although wrinkles occured in the body of the panel, no evidence of this was seen at the edge members.

At the inboard edge where the N_y is a maximum the depth of the scallop to the length was increased to .1, $= \Delta/L$ so $\underline{\Delta = 4cm}$, $\underline{L = 40cm}$

PROJECT: EC-404, Heliogyro Preliminary Design

MEMO NO: RHM-21

DATE: August 9, 1977

SUBJECT: A Research Program for Micrometeoroid Damage to Tendons

REFS:
1. R. H. MacNeal, "Meteoroid Damage to Filamentary Structures," NASA CR-869, Sept. 1967.

2. Maiden, C.J., and McMillan, A.R., "Protection Afforded a Spacecraft by a Thin Shield," AIAA J., Vol. 2, No. 11, pp. 1992-1998, Nov. 1964.

3. Bamford, R., "Micrometeoroite Damage to Heliogyro Tendons," J.P.L. Interoffice Memo 354:77:157, June 27, 1977.

4. MacNeal, R.H., "Extrapolation of Hole Size due to Micrometeoroids," MacNeal-Schwendler Corp. Memorandum RHM-19, EC-404, July 20, 1977.

1. INTRODUCTION

A significant weight penalty (of the order of 300 kg) is paid against the micrometeoroid hazard in the baseline design. Estimates of the amount of weight required vary by a factor of four or more, because of uncertainties regarding the damage caused by meteoroids. There are uncertainties regarding the physical distribution (density, velocity and flux) of meteoroids, but even larger uncertainties exist regarding the damage caused to an edge tendon by a meteoroid with given size, density and velocity. It is proposed that, in order to reduce the range of uncertainty, a research effort be undertaken which concentrates on the damage to one-dimensional structures similar to those proposed for the edge tendons of the Heliogyro, using current estimates of the physical distribution of meteoroids.

The study should employ both analytical and experimental methods. Experiments are necessary because the available experimental data was obtained at unrealistically low velocities, and because no data at all is

available for the critical case of low angle (grazing) impact, which is the major source of uncertainty in the meteoroid hazard.

The results of the study will be useful in the future for the design of any large space structure. The most efficient way to carry a small load for a long distance is to use a framework of extremely slender tension and compression members, rather than panels. In the case of large structures for space, the member sizes tend to be in a range where meteoroid damage is an important consideration. Examples: Heliogyro edge tendons and battens, square-sail ties, Astro masts.

2. REVIEW OF CURRENT STATUS

Although a literature search has not been made, it is the opinion of qualified personnel at JPL that no work on micrometeoroid damage to filamentary structures has been published between Ref. 1 (1967) and the present time.

Reference 1 defines a procedure for calculating the probability of failure of a filamentary structure due to micrometeoroids. The procedure is, in part, based on the experimental data that was available at the time and, in part, on assumptions regarding physical behaviour which are unsupported by experimental data. The critical assumptions are in regard to the extrapolation of hole size for normal particle incidence from experimental velocities (2-8 km/sec) to meteoroid velocities (~30 km/sec), and in regard to the damage caused by grazing incidence.

The procedures of Ref. 1 were used at MSC and at Astro in January 1977 to estimate meteoroid damage to the edge tendons of the Heliogyro. The estimates indicated that the probability of failure was less than 1/10th percent for a trifilar edge tendon with 265 kg total weight.

Later, Bamford at JPL discovered numerical errors in the procedure of Ref. 1 for the extrapolation of hole size for normal incidence, and substituted an extrapolation proposed in Ref. 2, which gives much larger holes. He retained the assumptions of Ref. 1 regarding grazing incidence and used a current estimate of meteoroid flux distribution which is more severe than that in Ref. 1. With these modifications to the procedure, he found that the trifilar design has nearly a 100% probability of failure. He then proceeded to develop an edge tendon design with five .001 in. tapes that weighed about twice as much as the trifilar design, and which he found (Ref. 3) to be barely acceptable (4% probability of failure).

Recently, MacNeal (Ref. 4) has proposed another method for extrapolating the hole size for normal incidence which gives much smaller holes than the method used by Bamford, but which also fits the available experimental data. In any case, it may be concluded that we really don't know how to extrapolate the hold size for normal incidence, but that it makes a big difference.

The situation with respect to grazing incidence is even worse. The basic assumption of Ref. 1 was simply to take the hole size for normal incidence and divide it by the sine of the incidence angle, a procedure which, it must be said, is quite reasonable for particles that are very large compared to the thickness of the sheet. Calculation showed, however, that a mathematical singularity (i.e., a 100% probability of failure) exists for an edge-on hit. The singularity was removed by the semi-rational assumption that a particle striking the tape at a small incidence angle will break the tape only if it can also break a solid round wire with the same cross-sectional area. Even so, calculations based on the theory show that most of the damage is done by very small particles at grazing incidence angles.

Justification for the grazing incidence theory of Ref. 1 is slender indeed. Experimental and analytical evidence presented in Ref. 2, show, fairly conclusively, that meteoroids traveling at 30 km/sec will be vaporized when they strike a target, even a very thin one. If this is so, then it could be reasoned that the back end of a high-velocity particle striking a target at low incidence will be vaporized before it reaches the target and that the resulting damage to the tape will be surface scorching which spreads out from the initial point of contact, rather than an elongated hole. In this case, failure of the tape could be computed from the impulsive load caused by stopping the normal momentum component of the particle. Such calculations have not been made.

Again, we don't know much about grazing impact but it makes a big difference. For example, consider the choice of flat tapes vs. curved tapes. If meteoroids simply continue in a straight line and make holes just big enough to pass through, then curved tapes are better than flat tapes because the problem of extremely elongated holes at low incidence is avoided. On the other hand, if the vaporization theory is correct, then curved tapes might be worse than flat tapes because the gas released by the impact will cause higher pressures on the tape. In summary, the current status is that we lack a reliable procedure for calculating meteoroid damage. One is needed because, by current (unreliable) estimates, the weight required to counter the meteoroid threat is significant.

3. PROPOSED RESEARCH PROGRAM

3.1 Experimental Program

Facilities are available which can accelerate small particles to the meteoroid range (30 km/sec). It is proposed that such facilities be used

with targets similar to those proposed for the Heliogyro edge tendons (i.e., thin graphite-polyimide tapes). Many firings will be required to cover the ranges of the relevant parameters. The following parameter ranges are recommended:

1. Particle velocity (10 km/sec to maximum available velocity)
2. Particle mass (10^{-6} grams to 10^{-4} grams)
3. Particle density (two or more values including one that is near 0.5 gm/cm^3. This might be achieved with hollow spheres.)
4. Incidence angles (90°, 20°, 10°, 5°, 2.5°, 1°)
5. Target thickness (.001 inch). Target thickness can be varied instead of particle mass, if particle mass and velocity parameter ranges cannot be met.
6. Target width (1 cm to 3 cm)
7. Target length (10 cm or more)
8. Target materials (graphite polyimide tape, aluminum tape)
9. Tension in target material (zero, 1/3 ultimate stress, 2/3 ultimate stress)
10. Target chordwise curvature (included angle = 0°, 30°, 60°)

Combinations of parameter values should be carefully selected to maximize the value of the knowledge gained for a given cost. This will require that some analytical work precede the experiments.

A Second set of experiments is recommended to validate proposed designs of tendon assemblies, by observing damage when a member is partially or completely cut.

It may also be necessary to study impulsive failures of individual tapes with a separate facility, where the impact is simulated by explosive charges or other means.

3.2 Theoretical Program

A theoretical program is needed to provide empirical formulas that can extend test data to new cases and which can be used to design structures. Research in the following areas is suggested:

a. Nature of the impact. Size and shape of the hole. Phase (solid, gaseous) and angular distribution of the debris. Surface damage when there is no hole. Research in this area involves physics, fluid dynamics and thermodynamics.

b. Failure of tapes due to impulsive loads. Research in this area involves analysis based on structural dynamics principles.

c. Design of redundant systems. How many tapes. How wide. How far between load transfer points. Research in this area involves probability theory and detailed stress analysis.

PROPOSED MODIFICATIONS OF NASTRAN

TO IMPROVE HELIOGYRO ANALYSIS

MS404-2 25 October 1977

MS404-2

PROPOSED MODIFICATIONS OF NASTRAN TO IMPROVE HELIOGYRO ANALYSIS

Prepared by

R. H. MacNeal

and

M. A. Gockel

October 25, 1977

THE MACNEAL-SCHWENDLER CORPORATION
7442 North Figueroa Street
Los Angeles, California 90041

TABLE OF CONTENTS

PROPOSED MODIFICATIONS OF NASTRAN TO IMPROVE HELIOGYRO ANALYSIS

1. INTRODUCTION

The NASTRAN computer program has been used in the Solar Sail design project to perform dynamic analysis of the Heliogyro. The dynamic characteristics of the Heliogyro are similar to those of a conventional helicopter rotor, but the differences are sufficiently great that computer programs designed for conventional rotor analysis (such as the SADSAM program, Ref. 3) cannot be used without extensive modification. Although the NASTRAN computer program has no specific capability for rotor analysis, it is, in general, extremely versatile and easy to modify and has the required capacity. The decision to use NASTRAN for analysis of the Heliogyro has been justified by the results that were achieved, but experience in that effort also indicates the need to improve some aspects of NASTRAN to provide a more usable and less costly analysis procedure. This report outlines the tasks which are considered necessary to carry out the required analysis types (dynamic stability analysis and transient response analysis) in a design environment.

2. IMPROVEMENTS TO THE HESSENBERG METHOD OF COMPLEX EIGENVALUE EXTRACTION

2.1 Background

NASTRAN includes three methods of complex eigenvalue extraction, but the only efficient method for general use is a transformation method called by the keyword "HESS." In this method, the second order equations

of dynamic motion are converted to first order form and are then transformed by Hessenberg reduction to upper Hessenberg form. The QR-method is used to compute the eigenvalues, and inverse iteration is used to compute the eigenvectors.

The present version suffers from the following limitations:

1. All coefficients must remain in memory. In prior Heliogyro work, this led to a limitation of about 40 dynamic degrees of freedom.
2. The logic for limiting the number of eigenvectors to be computed is deficient, requiring that all be computed if any are needed.
3. The solution is sensitive to matrix scaling. The Heliogyro has low natural frequencies (.005 cycles/sec). It was found necessary to scale the equations of motion so that the lowest natural frequency was near 1 cycle/unit time in order to obtain reliable solutions.
4. The mass matrix is inverted, requiring it to be nonsingular. The solution becomes less reliable if it is nearly singular. While this limitation can always be avoided, the resulting modeling techniques become tedious and unnecessarily complicated.

2.2 Technical Approach

The size limitation will be expanded by rewriting the algorithm to release unneeded space in memory. The user will have the ability to define the region in eigenvalue space where eigenvectors are to be determined. Matrix scaling will be done inside the solution process, making it transparent to the user. Two options for allowing singular mass matrices will be investigated.

2.2.1 Relaxing Size Limitations

The upper Hessenberg matrix has nonzero terms on and above the diagonal, and on one subdiagonal. It is proposed that this matrix be transposed, and given another Hessenberg reduction, so that it becomes both upper and lower Hessenberg in form, i.e., tridiagonal. The eigenvalues and eigenvectors of tridiagonal matrices with several thousand degrees of freedom can be solved with all coefficients in memory. Since this is far beyond the requirements of the Heliogyro analysis, the only operation that requires further consideration is the Hessenberg reduction itself. Wilkinson (Ref. 1) has stated that the second Hessenberg reduction has some theoretical shortcomings with respect to numerical stability, but that in practice these become evident on only a small range of pathological problems.

The basic Hessenberg reduction is defined by the equations

$$[A]\ [N] = [N]\ [H] \tag{1}$$

(See Ref. 1, p. 355-412.) [A] is the matrix whose eigensolution is to be found, [N] is a unit lower triangular matrix, and [H] is the upper Hessenberg form of [A].

Reference 1 describes a technique for performing the reduction in memory by overwriting terms of [N] and [H] on [A] as the terms are computed. This results in a storage requirement of $2(N_A^2 + N_A)$ words for single precision, complex matrices where N_A is the number of columns in [A]. Since the present method requires $6N_A^2 + 8N_A$ words, considerable improvement can be made. This would raise the present limit of about 40 degrees of freedom to about 70 degrees of freedom for computers similar

in capacity to the Univac 1108 used in previous Heliogyro work. Seventy degrees of freedom (modal coordinates) is regarded as adequate for Heliogyro work. Higher capacity is available on larger computers.

The present QR iteration for eigenvalues requires storage of [Q], a full unitary matrix, [R], an upper triangular matrix, and [A], which is almost triangular in form. This results in $4(N_A^2 + N_A)$ words for single precision, complex matrices, which would become the new limiting factor. However, as mentioned above, another stage of Hessenberg reduction will be performed on $[A]^T$, so that both it and the [Q] and [R] matrices will retain their tridiagonal form throughout the iteration. Thus, the required storage will be that for the Hessenberg reduction, $2(N_A^2 + N_A)$.

At some future date, consideration will be given to the addition of spill logic to HESS. This will remove the limitation on problem size imposed by available core memory, but the practical limit imposed by cost considerations is at present not much larger than seventy degrees of freedom.

2.2.2 Restricted Eigenvector Calculation

The user will control the number of eigenvectors calculated and output by the method described in remark 8 on the modified EIGC Bulk Data card shown in Figure 1.

2.2.3 Scaling of Coefficient Matrix

The [A] matrix will be equilibrated to avoid scaling problems, using the method described in Ref. 1, pp. 356-357. The basic equation is

Input Data Card EIGC Complex Eigenvalue Extraction Data

Description: Defines data needed to perform complex eigenvalue analysis.

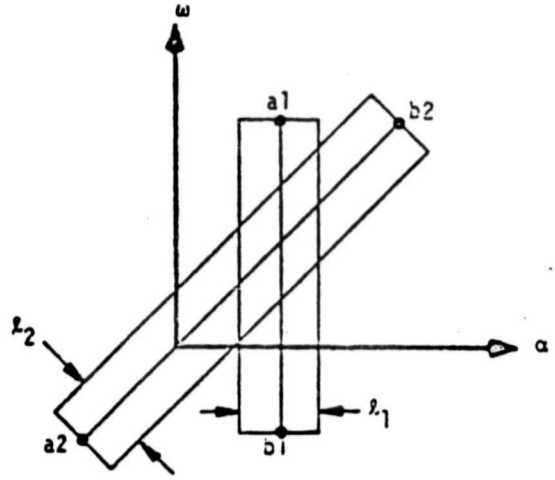

Format and Example:

1	2	3	4	5	6	7	8	9	10
EIGC	SID	METHØD	NØRM	G	C	E			+abc
EIGC	14	HESS	PØINT	27		1.-8			ABC
+abc	α_{a1}	ω_{a1}	α_{b1}	ω_{b1}	ℓ_1	N_{e1}	N_{d1}		+def
+BC	2.0	5.6	2.0	-3.4	2.0	4	4		DEF
+def	α_{a2}	ω_{a2}	α_{b2}	ω_{b2}	ℓ_2	N_{e2}	N_{d2}		
+EF	-5.5	-5.6	5.6	5.6	1.5	6	3		

(etc.)

Field	Contents
SID	Set identification number (unique, Integer > 0).
METHØD	Method of complex eigenvalue extraction, one of the BCD values "INV," "DET," or "HESS."
	INV - Inverse power method
	DET - Determinant method.
	HESS - Upper Hessenberg method
NØRM	Method for normalizing eigenvectors, one of the BCD values "MAX" or "POINT."
	MAX - Normalize to a unit value for the real part and a zero value for the imaginary part the component having the largest magnitude.
	PØINT - Normalize to a unit value for the real part and a zero value for the imaginary part the component defined in fields 5 and 6 - defaults to "MAX" if the magnitude of the defined component is zero. PØINT is not available for modal formulations.

(Continued)

Figure 1. Modified EIGC Bulk Data Card.

EIGC (Cont.)

G	Grid or scalar point identification number (required if and only if NØRM=PØINT) Integer > 0).
C	Component number (required if and only if NØRM=PØINT and G is a geometric grid point) ($0 \leq$ Integer ≤ 6).
E	Convergence criterion (optional) Real ≥ 0.0)
$(\alpha_{aj}, \omega_{aj})$	Two complex points defining a line in the complex plane (Real)
$(\alpha_{bj}, \omega_{bj})$	
ℓ_j	Width of region in complex plane (Real > 0.0)
N_{ej}	Estimated number of roots in each region (Integer > 0)
N_{dj}	Desired number of roots in each region (Default is $3N_{ej}$) (Integer > 0)

Remarks:

1. The preferred method is HESS, provided that sufficient main storage is available. Insufficient storage for HESS will cause the program to switch to INV.
2. Each continuation card defines a rectangular search region for METHØD=INV or DET. Any number of regions may be used and they may overlap. Roots in overlapping regions will not be extracted more than once.
3. Complex eigenvalue extraction data sets must be selected in the Case Control Deck (CMETHØD=SID) to be used by NASTRAN.
4. The units of α, ω are radians per unit time.
5. At least one continuation card is required.
6. For the determinant method with no damping matrix, complex conjugates of the roots found are not printed.
7. See Section 10.4.4.5 of the Theoretical Manual for a discussion of convergence criteria.
8. For the Upper Hessenberg Method, N_{dl} controls the number of vectors computed. All vectors for roots in the area defined by the (α, ω) pairs will be completed and output, if these values are input, regardless of the value of N_{dl}.
9. The required working storage for the Upper Hessenberg Method is given by

$$W = 6N^2 + 8N$$

where N is the order of the stiffness matrix if there is no damping, and twice the order of the stiffness matrix if damping is present.

10. If Method = HESS, the mass matrix must be nonsingular.

Figure 1. Modified EIGC Bulk Data Card (Cont.)

$$[A]_{new} = [D][A]_{old}[D]^{-1} \qquad (2)$$

where $[D]$ is a diagonal matrix.

2.2.4 Allowance for Singular Mass Matrices

Two techniques will be investigated. The easiest to implement involves shifting the eigenvalues of the problem. Instead of inverting the mass matrix [M], the shifted matrix $[p_s^2 M + p_s B + K]$ is inverted. This allows singularities in [M] to be repressed by terms in the other matrices. This technique has proven effective in the modified Givens method in MSC/NASTRAN.

An elegant but more difficult method identifies singular degrees of freedom in [M], and reduces the size of the problem in a manner analogous to static condensation, (see Ref. 2). Although this method may cost more to implement, the reduction of problem size operates favorably on the cubic cost curve typical of transformation methods, by suppressing the uninteresting infinite frequency modes of the system.

3. IMPROVEMENTS TO THE TRANSIENT RESPONSE CALCULATION MODULES

3.1 Background

The transient response modules are the largest consumers of computation time for Heliogyro analysis, and require the following new capabilities in addition to general efficiency enhancements:

1. Improved spill logic: the ability to solve problems too large to fit into memory by placing some portions of the calculations in secondary storage, if necessary.

2. Rotating to nonrotating coordinate transformations ("Resolver"): The method of Lagrange multipliers has proven effective in prototype work at MSC and will be added to the TRD module.

3. Nonlinear, timevarying coefficients: certain structural and photodynamic terms must be updated at every time step. The only practical method to accomplish this is by placing the equations that generate these terms inside the transient response calculation.

4. Data Reduction: the Floquet method of system identification will be implemented to recover the frequency and damping of system modes from the time histories of transient response.

Numerical integration procedures must be carefully designed to treat problems with few dynamic degrees of freedom inexpensively while, at the same time, imposing no absolute limit on the solution of large problems.

The computation of transient response may be divided into two phases:

a. Preparation phase: assembly and reduction of the equation of motion;

b. Numerical integration phase.

The key to a low-cost solution is to do as much work as possible in the Preparation Phase in order to limit the amount of data accessed at each integration step. The reason is that, if the amount of data cannot fit within the available high speed memory, the cost of accessing it will be the dominant element in the total cost. Thus, the problem size for low-cost solutions has a practical limit which depends on the size of the available high speed memory. Careful planning of the data processing procedures is required to ensure that this critical size will be as large as possible.

The NASTRAN procedures for numerical integration need to be reviewed and upgraded. NASTRAN tends to emphasize the solution of problems with very many degrees of freedom rather than low cost solutions of moderate size problems. Our SADSAM program has the opposite emphasis. It produces very low cost rotor analysis (Ref. 3) but problem size is limited by fixed dimension statements. What is really wanted is both capabilities, however incompatible they may appear to be.

With regard to integration algorithms, NASTRAN currently provides a choice of two -- a version of the Newmark Beta method for general use and a semi-analytic recursion method for uncoupled modal equations. We use the same version of the Newmark Beta method for rotor analysis in SADSAM with considerable success.

With regard to the treatment of nonlinear effects, it may be assumed that each nonlinear force or moment is a function of the motions at particular points. The matrix which relates these motions to the reduced dynamic freedoms will be core held, in packed form, during numerical integration. The user may reduce its size either by reducing the number of reduced dynamic freedoms, or by limiting the number of points to which nonlinear forces and moments are applied. The FØRTRAN code which computes nonlinear forces and moments, and the associated tabulated empirical data, will also be core held during numerical integration; so will the integration matrices which are derived from the linear mass, damping and stiffness coefficients for the reduced dynamic freedoms. If all of the data cannot fit in the high speed memory, some of it will be kept in disk storage and transferred to the CPU at each time step. The solution vector, plus other data needed for post-processing, will be transferred to disk storage at each time step.

3.2 Technical Approach

3.2.1 Design Goals for the Transient Analysis Modules

A "standard"-size Heliogyro model is defined here to consist of one blade with a fully or partially fixed hub. The transient response module will be modified to solve this model without spill. A "large"-size Heliogyro model is defined as one with six blades, payload, and control system modeling. The module will be designed to solve this problem routinely, using spill logic if necessary. Upper limits on problem size are tabulated below.

Symbol	Meaning	Max. Size Standard	Large
N_g	Grid points x 6 d.o.f. each	300	2000
N_d	Dynamic variables (not eliminated by constraints or static condensation)	150	1000
N_p	Forcing points	75	500
N_h	Modal variables	15	80
N_t	Time steps	1000	1000

3.2.2 Expansion of Present Modules

Time-dependent loads are presently generated and reduced to modal generalized forces $\{P_h\}$ in the TRLG module. This module is adequate for Heliogyro analysis. So is the numerical integration performed in the TRD1 module.

A modified version of the TRD1 module will be provided for Heliogyro analysis. The basic integration algorithm will be

$$[D]\{u_{i+1}\} = \{P_{i+1}\} + \{N_{i+1}\} + [C]\{u_{i+1}\} + [E]\{u_i\} + \{\bar{N}_{i+1}\} \quad (3)$$

The only term not used in the present algorithm is $\{\bar{N}_{i+1}\}$. [C], [D] and [E] are constant matrices for a given time step size. The $\{u_i\}$ vector represents the modal variables $\{u_h\}$ at the time step i. $\{N_{i+1}\}$ is a nonlinear term (i.e., displacement or velocity dependent) which is available now in NASTRAN but has restricted utility.

The new term $\{\bar{N}_{i+1}\}$ represents nonlinear, time-dependent forces applied directly to grid points. Two types of nonlinear forces that are useful for Heliogyro analysis are described in Refs. 4 and 5. The nonlinear forces are generated by the following equations, performed at every time step:

$$\{u_{d,i+1}\} = [\bar{\phi}_{dh}]\{u_{i+1}\} \tag{4}$$

$$\{P^{n\ell}_{d,i+1}\} = f(t_i, \{u_{d,i}\}, \{u_{d,i+1}\}) \tag{5}$$

$$\{\bar{N}_{i+1}\} = [\bar{\phi}_{dh}]^T\{P^{n\ell}_{d,i+1}\} \tag{6}$$

The $[\bar{\phi}_{dh}]$ matrix is a compressed matrix of eigenvectors whose coefficients for u_d variables without nonlinear forces are set to zero. It is stored in packed form in single precision. The $\{u_d\}$ variables are physical motions at the nonlinear stations. $\{P^{n\ell}_{d,i+1}\}$ represents the resulting nonlinear physical forces, and $\{\bar{N}_{i+1}\}$ is the vector of generalized modal nonlinear forces.

Memory Requirements

Equation Number	Terms	Sizes
(3)	[C], [D], [E]	$3N_h^2$
(3)	$\{u_i\}$, $\{u_{i+1}\}$, $\{P_{i+1}\}$, $\{N_i\}$, $\{\bar{N}_i\}$	$5N_h$

Equation Number	Terms	Sizes
(4)	$\{u_{d,i+1}\}$, $[\bar{\Phi}_{dh}]$	$N_h \times N_p$ (*)
(5)	$\{p^{n\ell}_{d,i+1}\}$	N_p
(6)	$\{\bar{N}_i\}$	N_h

where N_h is the dimension of $\{u_i\}$ and N_p is the number of forcing points.

Total storage requirement: $3N_h^2 + 6N_h + N_p + (N_h \times N_p)$ (*).

	CDC	IBM/Univac
Single precision words for standard problem	1,200	1,600
Single precision words for large problem	60,000	80,000

The high-speed memory requirement for large problems is within the range of possibility on computers available today. For example, on the Univac computer used on past Heliogyro analysis, there are 42,000 words of core used for code, and 85,000 words of open core available for data storage with the TRD1 module. After the data center which operates the computer completes a scheduled hardware upgrade, there will be 127,000 words of open core available for data storage. Spill logic will be provided for the module, but it appears that spill will not be required for Heliogyro analysis.

3.3.3 Resolver Capability

The equations of motion of the blades are most conveniently expressed in rotating coordinates, while those of the control system must relate to a nonrotating reference frame. The time-varying transformation will be modeled by the technique of Lagrange multipliers (see Ref.

(*)Single precision on all computers. Other variables are double precision on IBM and Univac.

6, Section 4.6). All degrees of freedom in the nonrotating coordinate system will be sequenced to be the last n variables. The time-dependent terms will be added to $\{\bar{N}_{i+1}\}$.

3.3.4 Floquet System Identification

The Heliogyro modes have low natural damping, so that determination of system stability by inspection of transient analysis requires inspection of hundreds of rotor revolutions before asymptotic behavior is achieved. Methods to determine closed-form frequency and stability parameters for the system based on the Floquet hypothesis have been described in the literature (see Ref. 7). The basic integration algorithm (Equations 3 through 6) is modified as follows:

> After the system has reached an interesting state, a time of initial observation t_o is established, based on user input (i.e., after y rotor revolutions, or after the variation in response between successive cycles is less than z percent). Equation 4 is solved to find the state at time t_o, named $\{u_{i+2}\}$.

$$[D]\{u_{i+2}\} = \{P\} + [C]\{u_{i+1}\} + [E]\{u_i\} \qquad (7)$$

[P] contains the time-dependent and nonlinear forces.

A matrix of perturbed initial states $[\bar{\phi}_{hh}(t_o,t_o)]$ is determined, i.e.,

$$[\bar{\phi}_{hh}(t_o,t_o)] = \underbrace{\begin{bmatrix} u_{i+2} & u_{i+2} & u_{i+2} \end{bmatrix}}_{h} + [IC] \qquad (8)$$

An obvious choice for the perturbed initial condition matrix, [IC], is a diagonal matrix of small terms. Provisions will be made for

user-selection of this initial condition and several others. The $[\bar{\phi}_{hh}]$ matrix is then integrated using Equation 7 above and the same startup techniques as the present algorithm. At the t_n time step, Equation 7 is of the form

$$[D][\bar{\phi}(t_n,t_o)] = \{P\} + [C][\bar{\phi}(t_{n1},t_o)] + [E][\bar{\phi}(t_{n2},t_o)] \qquad (9)$$

This equation is evaluated at every time step over one rotor cycle. Note that only three additional $N_h \times N_h$ matrices need be stored at one time.

Reference 7 describes the method of computing the frequency and stability parameters of the system from the state transition matrix after one period. This matrix can be computed from

$$[\phi(t_o + T,t_o)] = [\bar{\phi}(t_o + T,t_o) - IC][IC]^{-1} \qquad (10)$$

where T is one rotor period. Small changes to utility routines will be needed to compute logarithms of complex diagonal matrices. The calculations will be performed in a new module.

The use of a reduced set of initial conditions for approximate answers is a subject of current research. For example, $N_h/2$ initial vectors rich in the lowest modes would be expected to produce response dominated by the lowest modes. A least-squares fit can be used to find the reduced $[\phi(t_o + T,t_o)]$ matrix. As the cost of this operation is cubic with N_h, cost and memory size reduction can be quite dramatic, and may even improve the accuracy of determination of the low-frequency modes. Provision will be made to use a variety of initial conditions and smoothing techniques.

Since this is a research topic, an experimental version of NASTRAN will be used as a test bed for developing a production tool. Low cost but inconvenient input and output formats will be used until the practicality of the method has been demonstrated.

3.3.5 Summary of Enhancements for Module TRD1X

New Input Data Blocks

$[\phi_{dh}]$ Eigenvector transformation

UCØNTRØL General data block, input by user on DTI Bulk Data cards

New Output Data Blocks

$[\phi(T)]$ State transition matrix at end of one rotor cycle (optional)

$[\phi(t)]$ State transition matrices at every time step over one rotor cycle, stored in appended form (optional)

EXPØUT General output data block (optional).

Method

1. General input and output data blocks are used for data during module testing, and for unconventional features. Input for system identification research, such as specification of initial conditions, will be done on DTI, UCØNTRØL Bulk Data cards. Special debug output, or output requirements not anticipated, will pass out through the EXPØUT data block. These blocks allow module changes without requiring MPL updates.
2. Inspect the new nonlinear data to determine unloaded rows of $[\phi_{dh}]$. Eliminate these rows and convert to single precision if necessary.

3. Compute the new nonlinear forces and extend the integration algorithm to accommodate them. Upgrade the integration routine to store all needed data in core.

4. Improve user control of output. Allow integration over a time span without any output.

5. Install code for resolver. User inputs will be on DTI Bulk Data cards.

6. Install code for Floquet system identification.

4. DMAP SEQUENCES FOR SOLUTION OF STRUCTURES IN ROTATING COORDINATE SYSTEMS

4.1 Background

Past Heliogyro analysis in NASTRAN was done with ad hoc DMAP alters to the NASTRAN rigid formats. This was effective during exploratory studies, when the significance of many second-order effects had to be determined. It resulted in twenty rigid format ALTER packages, many of which have only subtle differences. This exploratory work has shown which effects must be included in the analysis. This will allow consolidating the technology into the general-purpose DMAP sequences listed below.

A new capability has been developed in MSC/NASTRAN since the prior work was completed. It is a small strain, large deflection statics capability which accounts for geometric nonlinearity, including higher order terms not included in the present differential stiffness capability. Use of this technology and the DMAP sequences listed below will decrease the labor and calendar time needed to assemble Heliogyro models, and will increase the portability of this technology to JPL.

4.2 DMAP Sequence to Compute Linearized Structural Matrices from Geometric Nonlinear Analysis

User Input - Initial geometry, rotation speed, sun load intensity, structural description, blade pitch angles.

Output - Structural matrices for perturbations from the equilibrium position, bulk data cards or their equivalent defining the structure at its equilibrium position, the Coriolis force damping matrix, "tennis racket" effects (moments due to the angle between the rotor plane and the principal axes of inertia), and photodynamic influence coefficients.

4.3 DMAP Sequence to Compute System Stability

User Input - The matrices from the DMAP sequence described in Section 4.2, the hub constraints for hub-fixed modes, collective modes, and cyclic modes, plus models of damping devices and control systems.

Output - Eigensolutions, stability margins, energy absorbed per mode by damping devices. Both modal and direct solution techniques will be available. The Lagrange multiplier technique will be used to implement the complex constraint equations needed for cyclic modes.

4.4 DMAP Sequence for Transient Analysis

User Input - Linearized matrices from the DMAP sequence described in Section 4.2, control perturbations, nonlinear photodynamics, nonlinear Coriolis effects and nonlinear solar illumination pressure forces.

Output - Time histories of motion and internal forces, options for roots of perturbation solutions to the nonlinear transient solution using the Floquet system identification technique.

5. ESTIMATE OF THE REQUIRED EFFORT

The following table presents an estimate of the manhours required to perform the tasks described above. It assumes that the work will be done by senior engineers and programmers who are experienced in NASTRAN development. Computer time is not estimated but experience with this type of development shows that computer cost is about one-half of the manhour cost.

Task	Manhours
1. Rewrite code for the Hessenberg method of Complex Eigenvalue extraction	550
2. Modify the transient response module	360
3. Install the resolver capability	210
4. Install Floquet System Identification	270
5. Write DMAP sequences for Heliogyro Analysis	410
Total	1,800

6. REFERENCES

1. Wilkinson, J. H., The Algebraic Eigenvalue Problem, Oxford Univ. Press, 1965.

2. Dell, A.M., Weil, R.L., Thompson, G.L., "Roots of Matrix Pencils: The Generalized Eigenvalue Problem," Communications of the ACM, Vol. 14, No. 2, pp. 114-117, Feb. 1971.

3. SADSAM User's Manual, MacNeal-Schwendler Corp. Report MSR-10, Dec. 1970.

4. Bellinger, E.D., "Modification of NASTRAN for the Nonlinear Coriolis Force Calculations of a Rotating Blade," MacNeal-Schwendler Corp. Memo EDB-2, Project EC-404, Heliogyro Preliminary Design.

5. Bellinger, E.D., "Modification of NASTRAN for Nonlinear Solar Illumination Pressure Force Calculations on a Heliogyro Blade," MacNeal-Schwendler Corp. Memo EDB-3, Project EC-404, Heliogyro Preliminary Design.

6. MacNeal, R.H., "The Dynamics of Rotating Elastic Bodies," MacNeal-Schwendler Corp. Report MSR-36, August 1973.

7. Gockel, M.A., "Practical Solution of Linear Equations with Periodic Coefficients," AHS Journal, Jan. 1972.

Conceptual Design of a Flight Test Model of the Heliogyro

MS404-3

28 October 1977

MS404-3

CONCEPTUAL DESIGN OF A FLIGHT TEST MODEL OF THE HELIOGYRO

Prepared by

Richard H. MacNeal

28 October 1977

THE MACNEAL-SCHWENDLER CORPORATION
7442 North Figueroa Street
Los Angeles, California 90041

TABLE OF CONTENTS

Conceptual Design of a Flight Test Model of the Heliogyro

1.0 INTRODUCTION

As part of the design review of the Heliogyro Solar Sail proposed for the Halley Rendezvous mission, a need was identified for a flight test program. This report is addressed to the conceptual design of a vehicle capable of providing the required information. The vehicle will also be able to perform useful planetary missions.

2.0 DESIGN CRITERIA FOR A FLIGHT TEST PROGRAM

Although the length of Heliogyro blades exceeds the size of any ground-based facility, the mechanical components involved in deployment are of comparatively modest dimension (8 m), so that deployment tests can be performed in the laboratory. Special care in removing gravitational effects will not be required, because the centrifugal forces during deployment are of the order of 1/2 g. Thus, ground-based deployment tests should be considered to be adequate and reliable.

The only major area in which ground-based tests are not feasible is the area of dynamics and control, which involves complex interactions between photon pressure and centrifugal force. The forces due to photon pressure acting on a very thin film are of the order of .001 g so that a vacuum chamber would be required. The largest scale model that could fit in a vacuum chamber is of the order of 1/1000 scale, which is too small to provide useful information. Thus, only a flight test will be able to verify theoretical dynamic calculations.

In order to provide useful dynamic information, the flight test configuration and the environmental conditions should be reasonably similar to those of the full-scale vehicle. For this reason the following should be avoided:

a. Low altitude flights where atmospheric drag is appreciable compared to photon pressure.

b. A vehicle with fewer than four blades. (This is the smallest number that can provide dynamic similitude with the full-scale vehicle.)

c. Very small vehicles, which will of necessity violate dynamic similarity, for example, by having a central hub which is much heavier than the blades.

The most important dynamic phenomenon requiring verification by flight test is blade flutter. In order to study this phenomenon under realistic conditions, it will be required that the frequency ratios and damping levels of the lower modes be approximately correct. Under these conditions, a scaling parameter which approximately measures the susceptibility to blade flutter is

$$\eta = \frac{1}{T_o}\left(\frac{R}{R_s}\right)^{4/3} \qquad (1)$$

where R = blade radius

R_s = distance to the sun

$T_o = \frac{1}{2} M_b \Omega^2 R$ = the tension at the blade root

M_b = mass of one blade

Ω = spin rate (rad/sec)

C-2

It will be noted that the susceptibility to flutter is increased either by decreasing the spin rate, or by decreasing the distance to the sun. Thus, the severe conditions which exist near the sun can be simulated near the earth by decreasing the spin rate. Furthermore, since the build-up of unstable motions is very slow, flutter margins can be positively and safely identified by first decreasing the spin rate until flutter occurs and then increasing the spin rate before the amplitude of oscillations becomes large.

3.0 DESIGN CONSTRAINTS AND SELECTION OF PARAMETERS

Figure 1 shows a comparison of parameters for the full-scale Halley vehicle and for a proposed flight test model. The parameters identified by asterisks (*) were selected on principles other than dynamic similitude or design optimization, and may be considered to be design constraints. These parameters include the identity of the launch vehicle, the reflective area, the film material, the closest approach to the sun, and the mission duration. The Ariane launch vehicle was chosen because of its availability and capacity. The selected values of reflective area, closest approach to the sun, and mission duration are based on the idea that the vehicle be capable of useful missions at the completion of the flight test program. The film material was selected to be the same as that for the full-scale vehicle.

The blade chord (or more precisely, the deployment reel length) is a free parameter which was varied parametrically. The data shown in Table 1 correspond to a blade chord of 4.1 meters. Results for other blade chord lengths are discussed in Section 5.

The remaining parameters in Table 1 were derived by scaling the full-scale Halley vehicle, using principles of dynamic similitude. Details of the scaling procedure are explained in the Appendix to this report.

4.0 DESCRIPTION OF THE 4.1 METER FLIGHT TEST MODEL

Figure 1 shows the 4.1 meter flight test model in its stowed configuration, and Figure 2 shows one blade in its deployed configuration. The vehicle has six blades which deploy in a single plane. The arrangement of the mechanical components, and also the deployment sequence, is identical to that of the full-scale vehicle, except that the central support column remains attached to the launch vehicle. Spaces are provided between the deployment reels to permit bracing of the central support column, if necessary to limit deflections during launch.

The mass distribution of the 4.1 meter flight test vehicle is compared with that of the full-scale vehicle in Table 2. It will be noted that the mass fraction for structure is significantly smaller than that for the full-scale vehicle, in accordance with the square-cube law for the growth of structural weight with size. The mass fraction for electrical components is significantly larger, due mainly to the fixed size of many of the components in the control system. Detailed mass distributions for the flight test model and for the full-scale vehicle are shown in Table 3. On balance, the mass per unit reflective area is slightly less for the flight test vehicle than for the full-scale vehicle.

The total mass of the flight test vehicle (323.3 Kg) is small enough to permit large payloads when the Ariane is used as the booster. Figure 3 shows the range of characteristic accelerations (acceleration due to

normal incidence of radiation pressure at 1 A.U.) that are available for a range of payload mass within the lift capability of the Ariane.

5.0 PARAMETRIC VARIATION OF BLADE CHORD

The blade chord (deployment reel length) was varied from a minimum of 2.9 meters to a maximum of 4.4 meters. The upper value is the largest that will fit within the Ariane's payload envelope. The lower value corresponds to a point where total mass is rising rapidly (see Figure 4). Detailed mass distributions for deployment reel lengths of 2.9, 3.4, 4.1, and 4.4 meters are tabulated in Table 3. Although the 4.4 meter chord produces the least mass, the 4.1 meter chord produces only a slightly larger mass and has significantly larger clearances with respect to the Ariane shroud.

The large structural mass of the model with a 2.9 meter chord is mainly due to the higher blade root tension required to compensate for the increased blade radius, while satisfying the flutter criterion, Equation 1.

6.0 CONCLUDING REMARKS

The Heliogyro model described in this report is capable of meeting the objectives of a useful flight test for the design of a full-scale vehicle of the size proposed for the Halley mission, and also for performing useful planetary missions, both within the constraints imposed by the Ariane launch vehicle. Smaller models, which might produce useful flight test data, but which would not utilize the full capacity of the Ariane, have not been examined in detail. It is estimated, from an earlier unreported study, that the minimum size vehicle which would be

useful as a flight test model has approximately 5000 m^2 of refle tive area and a chord of one meter. This vehicle could easily be boosted to the minimum required circular orbit (1200 Km) by the Scout launch vehicle.

Table 1

Comparison of Parameters for the Full-Scale
Halley Vehicle and the 4.1 Meter Flight Test Model

Parameter	Full-Scale Halley Vehicle	4.1 Meter Flight Test Model
Launch Vehicle*	Space Shuttle+I.U.S.	Ariane (3-stage)
Reflective Area*	624,800 m^2	60,000 m^2
Film Material*	.08 mil Kapton	.08 mil Kapton
Number of Blades	12	6
Deployment Reel Length	8.0 m	4.1 m
Blade Radius	7500 m	2838 m
Blade Aspect Ratio	937.5	692.2
Closest Approach to Sun*	.25 AU	.30 AU
Mission Duration*	4 yrs	5 yrs
Rotational Speed	.027 rad/sec	.0514 rad/sec
Blade Root Tension	750 N.	161 N.
Relative Maneuver Time	1.0	.823
Flap Hinge Offset/ Blade Radius	.005	.00587
Maximum Flapping Moment	1222 Nm	56 Nm
Design Torque for Pitch Motor	5 Nm	0.4 Nm
Mass of Sail Module	3837 Kg	323 Kg
Sail Module Mass/Area	6.14 gm/m^2	5.39 gm/m^2

*Design Constraints

Table 2

Comparative Mass Distributions for the Full-Scale Halley Vehicle and the 4.1 Meter Flight Test Model

Item	Full-Scale Halley Vehicle		4.1 m Flight Test Model	
	Kg	%	Kg	%
Film + Coating + Seams	2123	55.3	208.4	64.5
Structure	1436	37.4	77.0	23.8
Hardware and Mechanisms	205	5.4	19.8	6.1
Electrical Components	73	1.9	18.1	5.6
Total	3837	100.0	323.3	100.0

Table 3

Detailed Mass Distributions

Deployment Reel Length	← Flight Test Models →				Full-Scale
	2.9 m	3.4 m	4.1 m	4.4 m	8.0 m
	← Mass (Kg) →				
BLADES					
Bare Film (.08 mil Kapton)	173.22	173.22	173.22	173.22	1764
Coatings	21.48	21.48	21.48	21.48	219
Seams	13.74	13.74	13.74	13.74	140
Edge Tendons	54.82	40.56	28.93	25.56	514
Battens	8.87	8.87	8.87	8.87	90
Tip Weights	3.00	3.60	4.44	4.80	20
Hardware	6.93	6.93	6.93	6.93	71
Total	282.06	268.40	257.61	254.60	2818
RETENTION SYSTEM					
Flap Hinge Stays	10.10	6.83	2.57	1.94	61
Deployment Reels	14.00	11.00	10.70	10.55	145
Yokes	11.10	6.67	8.15	9.47	217
Booms	8.06	4.43	5.33	5.93	102
Dampers	.23	.34	.27	.22	11
Pitch Axis Structure	9.17	8.12	7.06	6.70	110
Total	52.66	37.39	34.08	34.81	646
OTHER COMPONENTS					
Center Truss	5.39	5.39	5.39	5.39	197
Pitch Motors	6.92	6.91	6.84	6.81	48
Pitch Bearings	1.58	1.40	1.22	1.16	19
Deployment Mechanisms	6.93	6.93	6.93	6.93	84
Control System	10.00	10.00	10.00	10.00	15
Electrical Wiring	1.25	1.25	1.25	1.25	10
Total	32.07	31.88	31.63	31.54	373
Total For Sail Module	366.79	337.67	323.32	320.95	3837

FIGURE 1 FOUR METER HELIOGYRO, STOWED CONFIGURATION

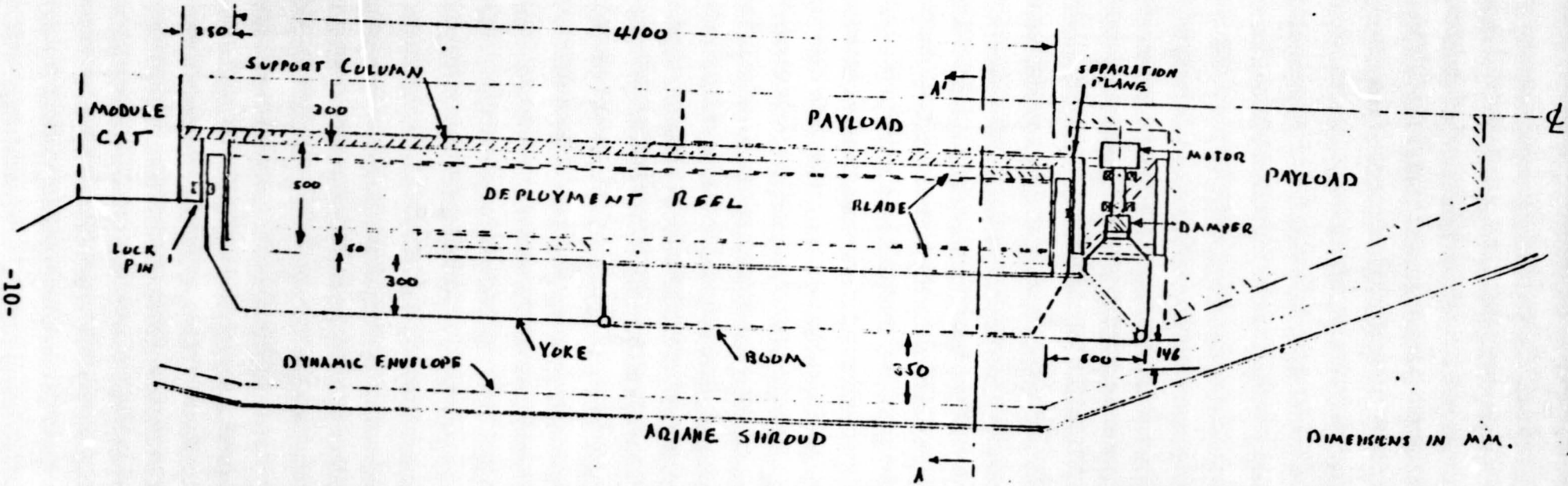

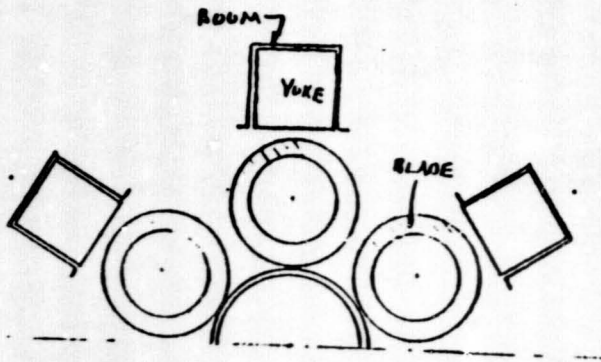

SECTION A-A'

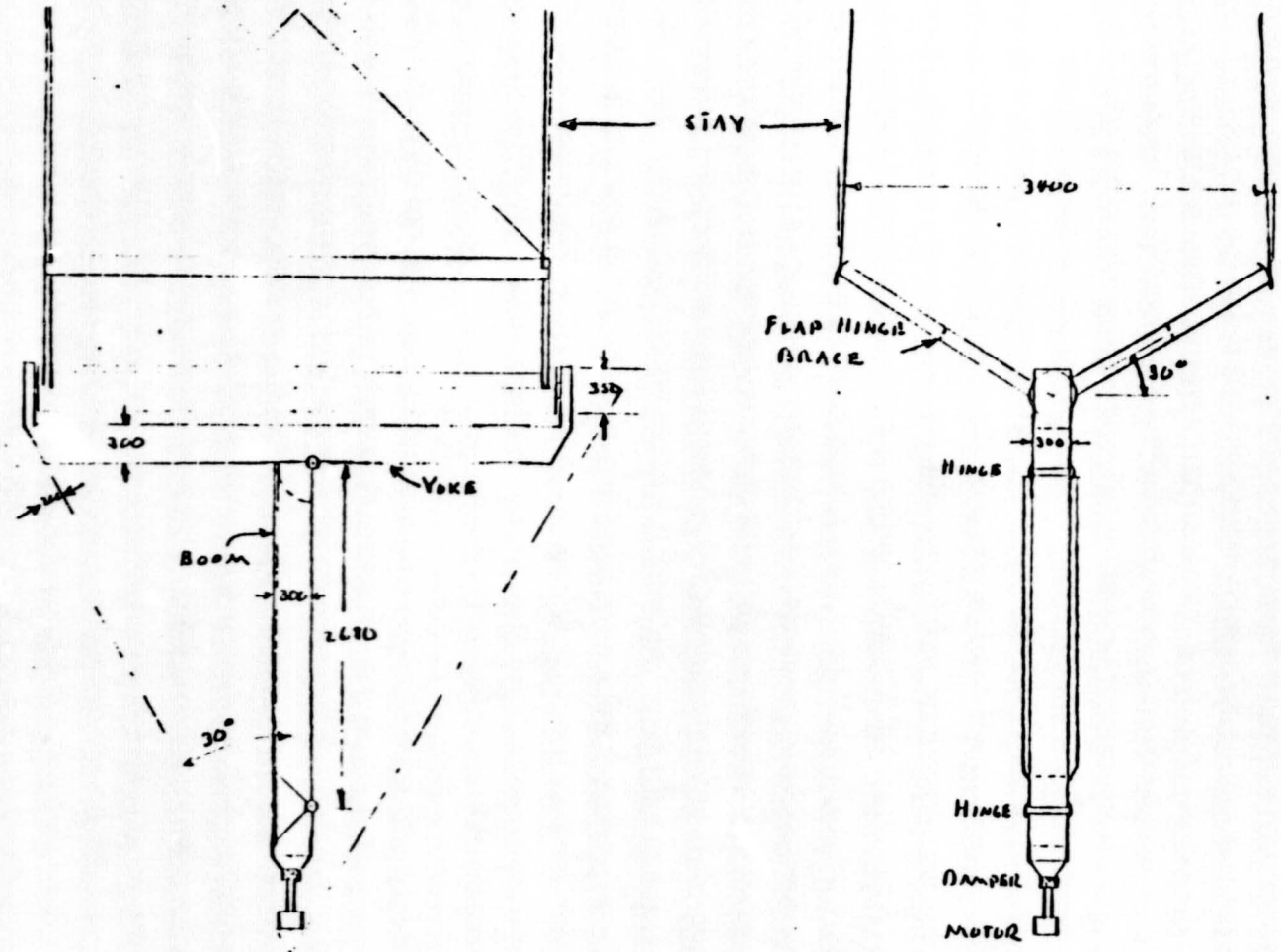

FIGURE 2

FOUR METER HELIOGYRO BLADE

DEPLOYED CONFIGURATION

DIMENSIONS IN MM.

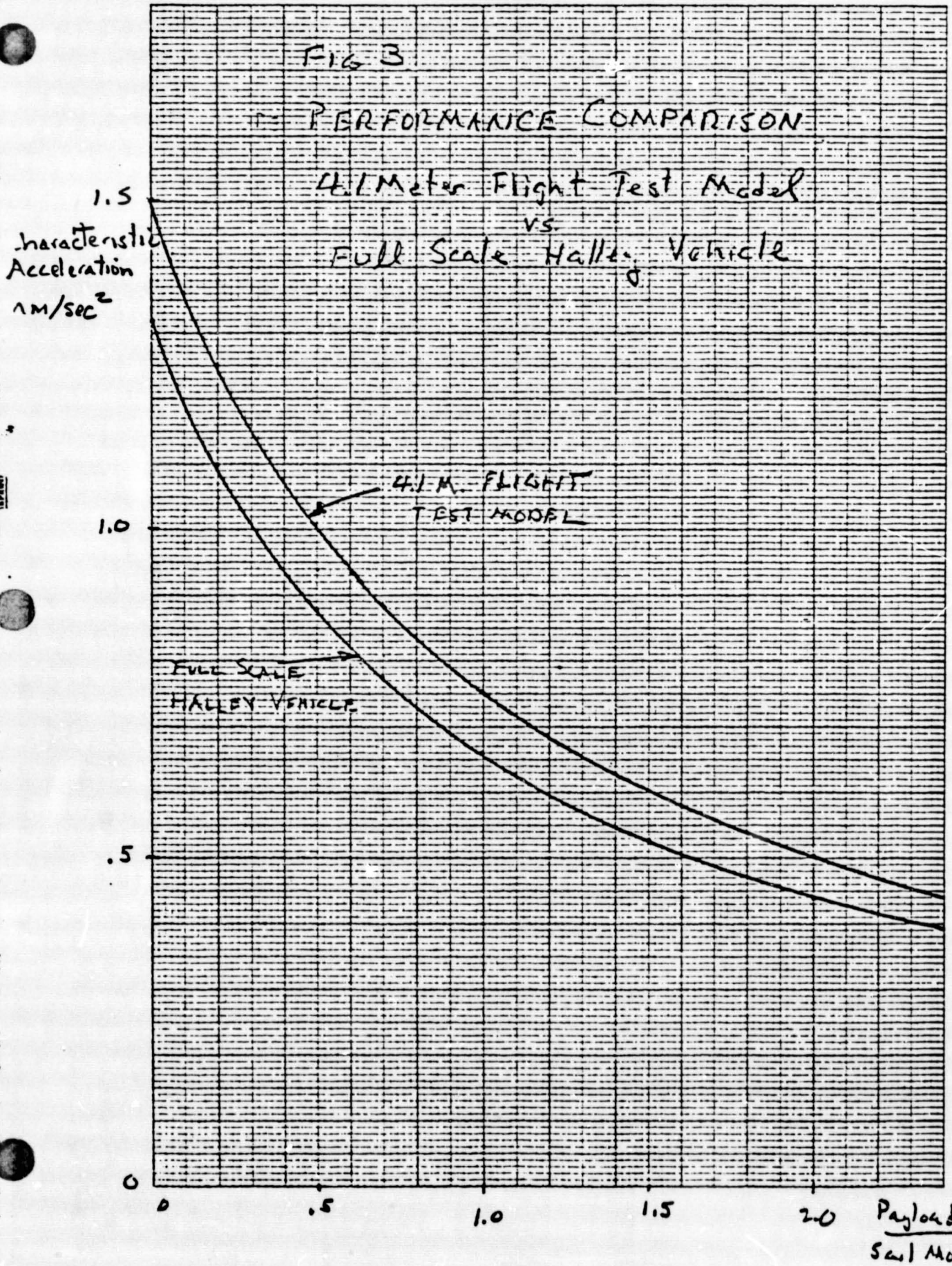

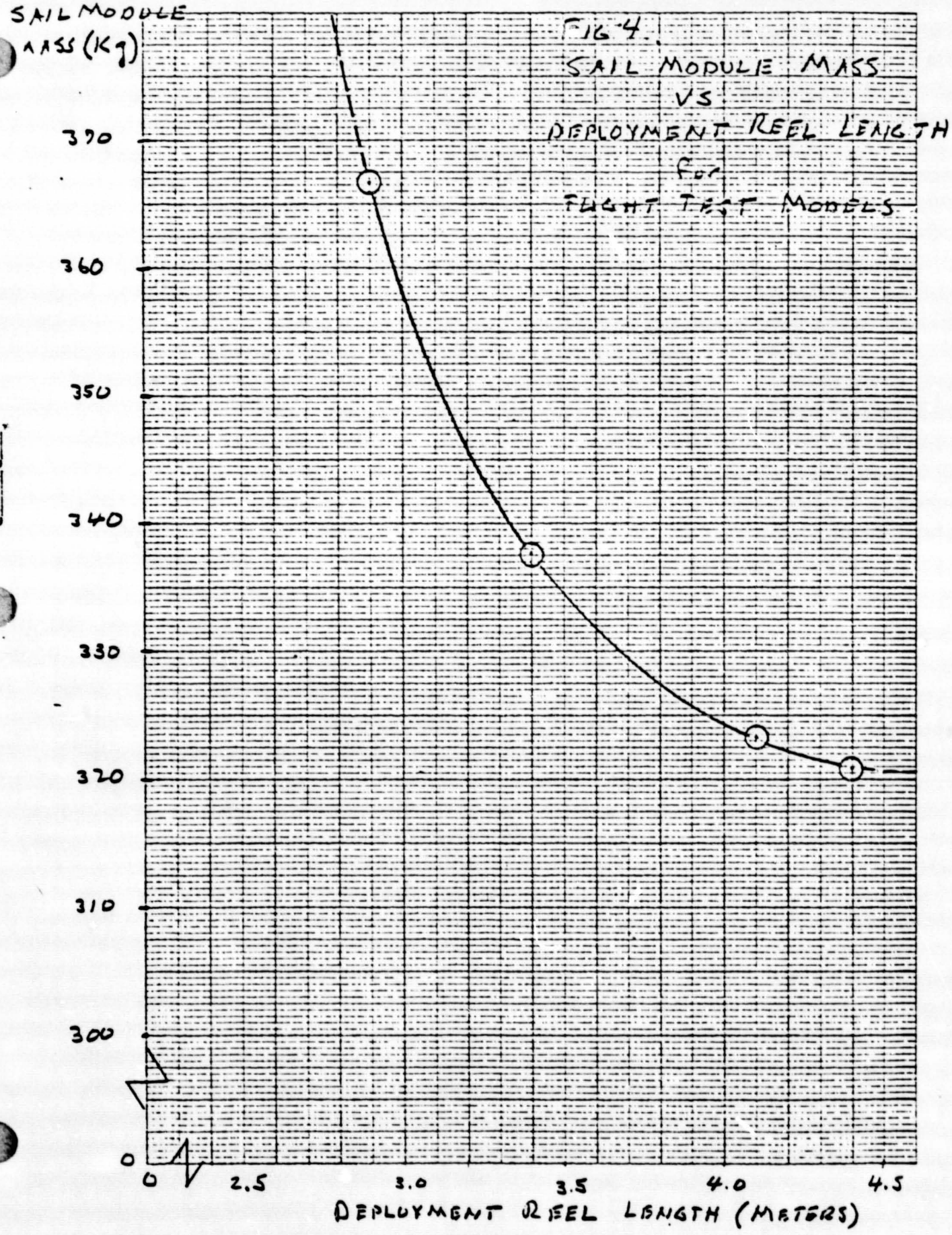

FIG-4.
SAIL MODULE MASS
VS
DEPLOYMENT REEL LENGTH
FOR
FLIGHT TEST MODELS

APPENDIX

DESIGN METHOD

As stated in Section 3 of the main text, certain parameters were taken as given design constraints. These parameters are indicated by asterisks (*) in Table 1. The remaining parameters in Table 1 and also the detailed mass distribution in Table 3 were obtained by application of design principles. The principles and assumptions which were used to obtain each of the parameter and mass values are explained below. Where numbers are quoted, they refer to the 4.1 meter flight test model.

1. Number of Blades

The only number of blades given serious consideration was six. This is the smallest number of blades for which a symmetric (isotropic) rotor can be built which has damping in all modes. It is also attractive from the viewpoint of space utilization in the stowed configuration (see Figure 1).

2. Sheet Width and Blade Radius

The width of the reflective sheet was taken to be 0.4 m less than the deployment reel length in order to allow room for edge tendons and gaps between the tendons and the sheet. The value 0.4 m is arbitrary and will allow for some flexibility in the design of the blade panels. As explained in the main text, the deployment reel length was treated as a free parameter.

The blade radius was calculated as follows:

$$R = \frac{1.05\ A}{n_b \cdot C} \qquad (1)$$

where A = reflective area (60,000 m^2)

n_b = number of blades (6)

C = sheet width (3.7 m)

The factor 1.05 is the allowance for cut-outs.

3. Deployment Reel Diameter

The considerations affecting selection of the inner and outer reel diameters are:

a. Available space in the stowed configuration (see Figure 1)

b. Adequate volume to stow the blade

c. Adequate strength and stiffness

d. Minimum weight

The design formula for adequate volume is

$$\frac{\pi}{4R} (D_o^2 - D_i^2) > t \qquad (2)$$

where D_o = outer diameter (.5 m)

D_i = inner diameter (.35 m)

R = blade radius (2838 m)

t = blade thickness allowance in the stowed configuration (.0283 mm)

The value for t is the value used in the full-scale design. In the case of the 2.9 m design, it was necessary to reduce D_i to 0.3 m in order to satisfy Equation 2.

4. Blade Root Tension

The only consideration used in selecting blade root tension was that the susceptibility to flutter be the same as for the full-scale

vehicle. An approximate design formula for equal flutter susceptibility is

$$T_o\left(\frac{r_s}{R}\right)^{4/3} = \text{constant} \qquad (3)$$

where T_o = the blade root tension

R = the blade radius

r_s = minimum distance from the sun

The value of T_o for the 4.1 meter flight test model (161 Newtons) is obtained from Equation 3 and the parameters listed in Table 1.

5. Edge Tendon Mass

The edge tendons must carry the blade tension while withstanding persistent attack by micrometeoroids. A rational design procedure to meet the micrometeoroid threat was not available during preliminary design of the full-scale vehicle. However, in order to scale the value of edge tendon mass to the flight test model, it will be assumed that the cross-sectional area can be separated into a part required to carry ultimate tensile loads and a part that may be removed by micrometeoroids. It will be further assumed that each tendon consists of two .001 mil graphite polyimide tapes with frequent load transfer points. Under these assumptions, an approximate design formula for the mass of the edge tendons is

$$M_{et} = \rho n_b R\left[\frac{2.4}{\sigma_u}\cdot\frac{2T_o}{3}\left(1+\frac{750}{T_o}\left(\frac{\tau_m}{4\text{ yrs}}\times\frac{n_b R}{90{,}000}\right)^{1/3}\right)\right] \qquad (4)$$

where ρ = density of material (1527.5 kg/m^3)

σ_u = ultimate tensile strength of tapes (8.96×10^8 N/m^2)

τ_m = mission duration (5 years)

and n_b, R and T_o have been defined previously.

When this formula is applied to the full-scale vehicle, it gives a value of M_{et} equal to 367 Kg rather than the value of 514 Kg given in Table 3. The value in Table 3 is considered to be overly conservative.

6. Batten Mass

It is assumed that batten weight is 5.1% of bare film weight, independent of vehicle size.

7. Tip Mass

Tip mass is assumed equal to 0.2 Kg per meter of sheet width, which is consistent with the full-scale design.

8. Blade Hardware

The mass of blade hardware is assumed equal to 4% of bare film weight independent of vehicle size.

9. Mass of Film, Coatings and Seams

The masses of these items are scaled directly from the full-scale design in proportion to reflective area.

10. Spin Rate

An approximate design formula for spin rate is

$$\Omega = \left(\frac{2T_o}{M_b r}\right)^{1/2} \quad (= .0514 \text{ rad/sec}) \qquad (5)$$

where T_o = blade root tension (161 N)

M_b = mass of one blade (42.935 Kg)

R = blade radius (2838 m)

Equation 5 assumes that the blade mass is uniformly distributed along the blade.

11. Relative Maneuver Time

Relative maneuver time is defined as the time required to perform a maneuver with given blade pitch settings, divided by the orbital period around the sun. It can be shown that

$$(\tau_{rm} \cdot C/\Omega r_s^{1/2} M_b) = \text{constant} \qquad (6)$$

where τ_{rm} is the relative maneuver time, Ω is the spin rate, r_s is the distance to the sun, M_b is the mass of a blade, and C is the blade chord.

12. Flap Hinge Offset

Flap hinge offset is calculated to give the same value of blade flapping as the full-scale vehicle for a given error in blade pitch angle. It can be shown that

$$\frac{e}{R} \sim \frac{r_s^2 RC}{T_o} \qquad (7)$$

where e is the flap hinge offset and the other quantities have been previously defined. For the 3.4 m and 2.9 m blades, the value of e/R given by Equation 7 eads to excessively large retention system weight and has been increased as shown in the following table:

Model	e/r	
2.9 m	.006	increased over values given by Eq. 7
3.4 m	.005	
4.1 m	.00587	
4.4 m	.00651	
Full-scale vehicle	.005	

13. Damper Stiffness

The damper is designed to give the same damping coefficient for blade vibration modes as in the full-scale design. The design formula for damper stiffness is

$$K_d = \frac{g_d}{g_1} \cdot \frac{3T_o R}{2} \cdot \left(\frac{e}{R}\right)^2 \quad (= 7086 \text{ Nm/rad}) \qquad (8)$$

where g_d = damping coefficient of damper (0.3)

g_1 = damping of first flapping mode (.001)

14. Flap Hinge Stays

The length of the flap hinge stays is computed by the following formula which maximizes flap hinge brace stiffness for a given mass.

$$S_o = \frac{1.5e}{1 - \frac{eT_o}{K_d}\left(1 + \frac{K_d}{K_b} + \frac{K_d}{K_y}\right)} \quad (= 53.43 \text{ m}) \qquad (9)$$

where K_d = damper stiffness

K_b = boom stiffness (assumed equal to 6.39 K_d)

K_y = yoke stiffness (assumed equal to 4.0 K_d)

The mass of the stays is computed by the formula

$$m_s = \frac{16\rho T_o S_o^3 n_b}{Eh^2} \quad (= 2.57 \text{ Kg}) \qquad (10)$$

where E = modulus of elasticity (1.2065×10^{11} N/m^2)

ρ = density of material (1522.5 Kg/m^3)

h = vertical separation between stays (3.4 m)

In order to minimize weight, the vertical separation was increased for the shorter deployment reels as follows:

Deployment reel length	h
2.9 m	4.0 m
3.4 m	3.6 m
4.1 m	3.4 m
4.4 m	3.3 m

15. Mass of Deployment Reels

The mass fraction of the deployment reels (relative to film mass) was assumed to be proportional to the square root of the deployment reel length. In addition, the masses of the shorter deployment reels were increased arbitrarily to account for increased vertical stay separation (see Section 14 above) and for decreased reel diameter (in the case of the 2.9 meter reel).

16. Booms and Yokes

The booms and yokes are designed by stiffness. The assumed ratio of boom stiffness and yoke stiffness to damper stiffness is given just below Equation 9 above. The cross-sectional area of effective material in the boom and in the yoke to provide the required stiffnesses is given by the design formula

$$A_y = A_b = \frac{4(\ell_y + \ell_b)}{Ew^2} \left[\frac{1}{K_b} + \frac{1}{K_y}\right]^{-1} \qquad (11)$$

where ℓ_y = length of yoke (4.1 m)

ℓ_b = length of boom (2.68 m)

w = width of cross-section (0.3 m)

E = modulus of elasticity (1.2065×10^{11} N/m^2)

The masses of the booms and yokes are computed from

$$M_b = 5n_b \rho \ell_b A_b \quad (= 5.33 \text{ Kg}) \tag{12}$$

$$M_y = 5n_b \rho \ell_y A_y \quad (= 8.15 \text{ Kg}) \tag{13}$$

The factor of 5 is a structural inefficiency factor derived from the full-scale design.

17. Maximum Flapping Moment

The maximum flapwise bending moment is assumed to occur in the maximum precessional maneuver with one blade feathered due to a non-functioning pitch motor. It can be shown that the moment has the following proportion to design parameters:

$$M_{max} \sim \left(\frac{R}{R_s}\right)^2 C \tag{14}$$

Table 1 shows that the value for the full-scale design is 1222 Nm, which gives 56 Nm for the 4.1 meter model.

18. Damper Mass

The design formula for damper mass is

$$m_d = \frac{2n_b \rho M_{max}^2}{\gamma^2 G K_d} \quad (= .269 \text{ Kg}) \tag{15}$$

where n_b = number of blades (6)

ρ = density of damper material (1384 Kg/m^3)

γ = maximum shear strain (0.2)

G = shear modulus (6.894×10^5 N/m^2)

K_d = damper stiffness (7086 Nm/rad)

M_{max} = maximum flapwise bending moment (56 Nm)

19. Pitch Motor Design

The maximum pitch motor torque consists of a part due to the maximum static blade restoring moment and a part due to friction. The design formula is

$$M_\theta = .675 \times \frac{T_o}{750} \times \left(\frac{C}{2.0}\right)^2 \times \left(\frac{7500}{R}\right) + \frac{2C_f r_b M_{max}}{\ell_b} \quad (= .288 \text{ Nm}) \qquad (16)$$

where C_f = coefficient of friction (.01)

r_b = inner radius of bearings (.025 m)

ℓ_b = distance between bearings (.15 m)

M_{max} = maximum flapwise bending moment (56 Nm)

The factor .675 is the maximum blade restoring moment for the full-scale design. The design torque was increased to 0.4 Nm for conservatism.

The maximum shaft power is assumed proportional to ΩM_θ where Ω is the spin rate of the vehicle. With this assumption, the power rating of the pitch motor for the flight-test model is 15.2% as large as that for the full-scale design.

The masses of the pitch motor, of the pitch bearings, and of the pitch axis structure were scaled from full-scale design values by the following assumptions:

$$M \text{ (pitch motors)} \sim (\text{Power})^{2/3} \quad (= 6.84 \text{ Kg total})$$

$$M \text{ (pitch bearings)} \sim (M_{max})^{2/3} \quad (= 1.22 \text{ Kg total})$$

$$M \text{ (pitch axis structure)} \sim (M_{max})^{2/3} \quad (= 7.06 \text{ Kg total})$$

20. Center Truss

The mass of the center truss (5.39 Kg) was scaled from the mass of the hub end assemblies for the full-scale vehicle (90 Kg) by assuming

that the mass is proportional to the film mass multiplied by the two-thirds power of the distance from the centerline to the axis of the deployment reel in the stowed configuration.

21. Deployment Mechanisms

The mass of the deployment mechanisms (6.93 Kg) was assumed equal to 4% of the bare film mass.

22. Control System and Electrical Wiring

The mass of the control system (10 Kg) was assumed equal to two-thirds of the mass of the full-scale control system.

The mass of the electrical wiring (1.25 Kg) was assumed equal to one-eighth of the mass of electrical wiring for the full-scale vehicle. This was done because there are half as many blades, the distances are one-half as large, and the power rating is much smaller.

HELIOGYRO USER'S MANUAL

MS404-4

30 November 1977

MS404-4

HELIOGYRO USER'S MANUAL

by

E. D. Bellinger

for

Jet Propulsion Laboratory

under Contract No. 954709

30 November 1977

THE MACNEAL-SCHWENDLER CORPORATION
7442 North Figueroa Street
Los Angeles, California 90041

TABLE OF CONTENTS

LIST OF APPENDICES

LIST OF APPENDICES

(Continued)

1.0 INTRODUCTION

A rotating elastic body requires a dynamic analysis to determine the presence of dynamic instabilities. As part of the investigation of the Heliogyro blade design studies, a stability analysis was conducted using MSC/NASTRAN. This analysis required the development of solution methods for NASTRAN that included the following items:

1. Centrifugal forces
2. Tennis-racket moments
3. Influence coefficients for blade flutter
4. Structural damping of elastomeric damper
5. Coriolis forces
6. Hub boundary conditions for reactionless, collective and cyclic modes analysis
7. Blade pitch effects
8. Vertical and inplane solar pressure loads
9. Blade fabrication distortion effects

The methods for implementation of the above items and the usage of NASTRAN for the stability analysis are the subjects for this report, including the unusual steps associated with obtaining a NASTRAN solution.

Usage of NASTRAN to simulate the equations of motion for the Heliogyro blades requires the addition of special terms which account for items 1 through 5 above. Section 2.3 of Reference 1 presents a general description of the equations of motion for a rotating blade. That description generally applies to the methods of solution developed for NASTRAN. Items 1, 2, 3 and 4 were included with the stiffness matrix. Item 5 was included in the damping matrix. Item 6 was incorporated with the mass matrix.

Items 7, 8 and 9 were included through redefinition of the geometry of the basic NASTRAN model. Extensive alters to the NASTRAN rigid formats were necessary to generate the sequence of NASTRAN solutions including the effects due to items 1 through 5.

2.0 NASTRAN RUN SEQUENCE DESCRIPTION

This section describes the procedures that were used in the NASTRAN dynamic analysis of the Heliogyro Solar Sail. The intent of this section is to provide the reader (who is a NASTRAN user) with sufficient details to enable him to perform a similar type of analysis. The NASTRAN user is assumed to have some knowledge of the following NASTRAN capabilities and solutions:

1. DMAP and Rigid Format Alters
2. Differential Stiffness Solutions
3. Modes Analysis (Direct and Modal)
   a. Real (SØL 3 or SØL 25)
   b. Complex (SØL 7 and SØL 10)
4. Data Base Operations

All of the above items are described in Reference 2. In addition to the above, it is important to understand the contents of Chapters 1 through 3 in Reference 1. A description of the Heliogyro NASTRAN model and results of the analysis are described in Reference 3.

2.1 Straight Blades

The designation of straight blades means that the blade is a straight line and the blade axis is coincident with the radial line emanating from the center of rotation. Only items which would cause no inplane or vertical

deflections may be analyzed with the following sequence of runs. The items included are centrifugal loads and/or imposed blade pitch. The sequence of NASTRAN runs which are required to obtain straight blade results is described by the following steps:

1. The Differential Stiffness Solution (SØL 4,1) uses RF 4$33A which puts in the centrifugal stiffness terms and the tennis racket effect. The output to be used for the next run is the differential stiffness matrix $[K^d_{gg}]$ which has been stored on a Data Base. When preparing the NASTRAN input, the following details should be considered:

   a. Set parameters MØDEL and THETAZ for storage of $[K^d_{gg}]$ and the geometry data on the Data Base for doing structure plots.

   b. Select the proper set of DMIG data for the ØM2 (Ω^2 data). The 2,2 term of ØM2 should be set to zero, corresponding to a prestretched blade.

   c. Select proper TENPAD data for correct tennis racket moments. See Appendix I for calculation of TENPAD.

   d. Eliminate unnecessary data such as ASET, EIGR, DMIG's for complex constraints.

   e. Select the proper set of SPC's.

   f. If this is the first run and the Data Base has not been created, the following alter is necessary:

```
ALTER    2
DBMGR    //0 $
```

   g. Note the core allocations set with PARAM statements with parameter DØWN.

   h. Note whether EPØINT's or SPØINT's are included for later modes runs for the complex constraints.

i. When design changes for the blade are being made which include chord reductions, be careful with the RBE2's, as they don't have differential stiffness capability.

2. Reactionless Modes Solution (SØL 25) uses the alter RCTMØDE to fetch the differential stiffness matrix $[K^d_{gg}]$ stored on the Data Base during the SØL 4 run. The alter includes the centrifugal force terms and tennis racket moments. The alter also stores the mode shapes for plotting at a later time. When preparing the NASTRAN input, watch for the following:

   a. Set parameters MØDEL and THETAZ for fetching the right $[K^d_{gg}]$ from the Data Base. Set the parameter SØLID to identify the modes to be stored on the Data Base.

   b. Select the ASET for the Reactionless Modes.

   c. Remove the extraneous data used by the differential stiffness such as the SPC and RFØRCE data.

   d. Select the proper ASET, SPC, ØM2, CØUPLX and EIGR data for the type of modes.

3. Collective Modes Solution (SØL 25) uses the alter RCTMØDE to fetch $[K^d_{gg}]$ stored on the Data Base during the differential stiffness solution. This solution is nearly the same as the reactionless modes solution in item 2, except for the following:

   a. Select the proper SPC's

   b. Set parameter SØLID for mode storage on the Data Base.

4. Cyclic (Regressive and Progressive Sequence) Modes (SØL 7,1 or SØL 10,1) use alters NEWCYC or NEWFLUT, respectively, to put in the $[K^d_{gg}]$ from SØL 4,0, the centrifugal force terms, the tennis racket moments and Coriolis force terms. When the "direct" approach is used in NASTRAN, structural damping is automatically included, however, the "modal" approach requires an alter to include the structural damping. The modal method was not the original approach used to solve for cyclic modes. The direct method was first used and only the inplane modes

were obtained because of the core size limitation for the ASET points used in the analysis. Whenever preparing a cyclic modes solution, consider the following:

a. Set parameters MØDEL and THETAZ for fetching the correct $[K^d_{gg}]$ for the run.

b. Remove differential stiffness related data, SPC's and RFØRCE.

c. Put in structural damping on CELAS1's for SØL 7,1 and on CELAS1 and MAT1 cards for SØL 10,1.

d. Select proper ASET, SPC, ØM2 and CØUPLX data. SØL 7,1 uses SPØINTS for CØUPLX while SØL 10,1 uses EPØINTS.

e. If doing a two-bladed model, special temporary storage is required due to the problem size.

2.2 Blades with Inplane and Vertical Deflections

Whenever inplane or vertical blade deflections are included so that the blade axis does not coincide with the y-axis, the blade geometry changes are necessary to calculate the modes. Inplane and vertical blade deflections are caused by solar pressure loads and differential strain (manufacturing deformations) effects. The combined effects of solar pressure loads, differential strain, centrifugal loads and blade pitch may be analyzed in any combination with the following sequence of NASTRAN runs.

1. Differential Stiffness Solution (SØL 4,0) has to be performed to obtain $[K^d_{gg}]$ for the straight blade (see Section 2.1). If this $[K^d_{gg}]$ was already obtained from a previous run, then this step may be omitted.

2. Static Solution (SØL 24,1) uses the $[K^d_{gg}]$ generated in Step 1 and the STATSØL alter. The alter includes the addition of the straight blade $[K^d_{gg}]$ to the conventional stiffness matrix, the

centrifugal force effects and the tennis-racket moments. The solar pressure loads (see Appendix L) are put in to the bulk data by the conventional NASTRAN static solution through FØRCE data cards. Manufacturing deformations are introduced through the DEFØRM bulk data cards. The values put on the DEFØRM cards are 1/20000 times the rod element length on the trailing edge stiffener and +1/20000 for the leading edge. Solar pressure loads which simulate untrimmed collective pitch are shown in Appendix L. When setting up the NASTRAN deck, note the following details.

a. Set the parameters MØDEL and THETAZ to fetch the proper $[K^{d}_{gg}]$ from the Data Base.

b. Select the proper loads, SPC's and ØM2 data (term 2,2 is $-\Omega^2$ now).

c. Remove the data associated with the modes solution for ASET, EIGR, SPC and CØUPLX.

d. Remember to include the differential strains (DEFØRM) or inplane solar pressure loads to simulate untrimmed collective pitch.

3. The Differential Stiffness Solution (SØL 4,0) has to be repeated with the selected effects (centrifugal force, solar pressure loads, differential strain, etc.) included. In addition, the blade geometry has to be modified to include the deflections of the grid points obtained from the static solution (Item 2). Going from the static solution to this second differential stiffness solution has the effect of neglecting any internal element loads introduced by the static solution. To determine how well the solar pressure loads are balanced by the centrifugal loads, vertical SPC's are introduced along the blade in this differential stiffness solution so that forces of single point constraints may be obtained to measure any unbalanced forces. The truss tip usually had significant SPC forces. Since internal loads were lost, primarily in the truss, the DEFØRM capability was used to introduce the internal

loads in the rod elements of the truss. The loads resulting from the DEFØRM cards were spread to the boom, yoke and post elements so that iterations were required to obtain a balance between the solar pressure and centrifugal loads. Details to check while assembling the NASTRAN deck are the same as the straight blade differential stiffness solution.

4. The Modes Solution (SØL 10,1) uses the NEWFLUT alter and the $[K^d_{gg}]$ matrix from the previous solution (Item 3). Since the blade has vertical and inplane displacements, the Coriolis forces must be included in reactionless, collective and cyclic-type modes solutions. The NEWFLUT alter includes the Coriolis forces, the differential stiffness matrix, centrifugal force terms, tennis racket moments and structural damping. Details of the NASTRAN deck to check are:

   a. Set the parameters MØDEL and THETAZ to get the proper $[K^d_{gg}]$ matrix.

   b. Select the proper ASET and SPC data for type of modes, reactionless, collective or cyclic.

   c. Select the proper ØM2 data (term 2,2 is Ω^2).

   d. Remove differential stiffness data, RFØRCE.

   e. Include structural damping on CELAS1 and MAT1 data cards.

   f. If cyclic modes, put in CØUPLX and EPØINT data.

   g. If two-bladed model, special temporary storage is required.

2.3 Flutter Solution

To obtain the aerodynamic force coefficients, calculate off-diagonal stiffness terms as described in Appendix M. The flutter solution is precisely the same as the modes solution (Section 2.2, Item 4) when vertical and inplane deflections are present, except for the addition of the AERØ term to be added to the stiffness matrix.

3.0 REFERENCES

1. MacNeal, R. H., "The Dynamics of Rotating Elastic Bodies," MacNeal-Schwendler Corporation Report MSR-36, August 1973.

2. McCormick, C. W. (Ed.), "MSC/NASTRAN User's Manual," MacNeal-Schwendler Corporation Report MSR-39, January 1977.

3. Bellinger, E. D. "Summary of Heliogyro Preliminary Design Vibration Modes and Flutter Data for the NASTRAN Finite Element Model," MacNeal-Schwendler Corporation Memo EDB-6 (EC-404), July 1977.

APPENDIX A

SØL 4,0 Sample Deck for the Two-Bladed Model

```
$RUN  DBDS2B,228     ,DEAN,25,300/200      . ISD
$SYM  PRINT$,,MNS
$ASG,UPR EB4PRT(+1)
$USE Z,EB4PRT(+1)
$BRKPT PRINT$/Z
$QUAL  ISDMSC
$ASG,A  *NASTRAN.
$HDG   UPDATE RF4$33
$ELT    *RFALTERS,RF4$33,TPF$,RF4$33
$ASG,AX  DEANDB01.
$USE  DB01,DEANDB01
$ASG,AX MIKEDATA.
$HDG  EDIT DATA
$ELT  MIKEDATA,M15BLD1,TPF$,BLADE1
$ELT  MIKEDATA,M15BLD2,TPF$,BLADE2
$ELT  MIKEDATA,M1581T0,TPF$,BLD1T0
$ELT  MIKEDATA,M1582T0,TPF$,BLD2T0
$ELT MIKEDATA,HUBA007,TPF$,HUBDA
-14,39
-48,48
-53,57
$FREE MIKEDATA.
$ADD  MIKEDATA,ASGCRDS
NASTRAN TITLEOPT = 0 , DAYLIMIT = 99, MICORE = 90000
ID HELIOGYRO SOLAR SAILER DIFFERENTIAL STIFFNESS RUN
TIME 6
DIAG 8
DIAG 22
SOL 4,0
ECHOOFF
$ADD  TPF$,RF4$33
$       PUT IN RF ALTER 4$33
ECHOON
CEND
TITLE = HELIOGYRO SOLAR SAILER TWO BLADED MODEL 15, THETAZ = 0
SUBTI = DIF STF WITH CENT FORCE,R=7500M, C=7.63M,OMG=.027RAD/SEC
ECHO = SORT
SPC = 1
  OLOAD = ALL
  DISP = ALL
  SPCF = ALL
  ELFORCE = ALL
  GPFORCE = ALL
SUBCASE 10
  LABEL = STATIC SOLUTION, CUTOUTS AND REDUCED CHORD
  LOAD = 1
SUBCASE 20
  LABEL = DIFFERENTIAL STIFFNESS SOLUTION
  DSCOEF = DEFAULT
```

```
BEGIN BULK
$ADD   TPFS,BLADE1
$ADD   TPFS,BLADE2
$ADD   TPFS,BLD1TO
$ADD   TPFS,BLD2TO
$ADD   TPFS,HUBDA
SPC1,1,123456,900000,900001
SPC1,1,123456,19997,29997
PARAM,MODEL,15
PARAM,THETAZ,0
PARAM,GRDPNT,1
ENDDATA
$BRKPT PRINTS
$FREE,R Z
$SYM EB4PRT,,MNS
$SYM PRINTS,,MNS
```

APPENDIX B

RF4$33A Alter for SØL 4,0

```
$ BEGINNING OF RF ALTER 4533A
$ + + + + + + + + + + + + + + +          23 NOV 1975     + + + + + + + + + + + +
$  GRIDPOINT FORCE BALANCE AND ELEMENT STRAIN ENERGY                          RF1/3
$       04/15/75      R I G I D   F O R M A T   4   /  SERIES M1
$                                                                            RF1/3
$  CASE CONTROL INPUT                                                        RF1/3
$     1.REQUEST FOR GRIDPOINT BALANCE AT GRIDPOINTS SPECIFIED                RF1/3
$       THROUGH SET N=1,2,...-                                               RF1/3
$                                                                            RF1/3
$              GPFORCE=N                                                     RF1/3
$                                                                            RF1/3
$       OR                                                                   RF1/3
$                                                                            RF1/3
$              GPFORCE=ALL                                                   RF1/3
$                                                                            RF1/3
$     2.REQUEST FOR ELEMENT STRAIN ENERGY CALCULATIONS FOR ELEMENTS          RF1/3
$       SPECIFIED THROUGH SET M=5,7,...                                      RF1/3
$                                                                            RF1/3
$              ESE=M                                                         RF1/3
$                                                                            RF1/3
$       OR                                                                   RF1/3
$              ESE=ALL                                                       RF1/3
$                                                                            RF1/3
$--------------                                          --------------RF1/3
ALTER 2
PARAM     //DOWN/25000 $
DBMGR     // $
ALTER 8
DBSTORE SIL,EQEXIN,ECT,CSTM,BGPDT//V,Y,MODEL/V,Y,THETAZ $
ALTER 25,26                                                                  RF1/3
TA1,,ECT,EPT,BGPDT,SIL,GPTT,CSTM/EST,,GEI,GPECT,/V,N,LUSET/C,N,123/          RF1/3
        V,N,NOSIMP/1/V,N,NOGENL/V,N,GENEL $                                  RF1/3
SAVE NOSIMP,NOGENL,GENEL                                                     RF1/3
CHKPNT EST,GEI,GPECT $                                                       RF1/3
PARAM  //ADD/V,N,NOKGGX/1/0 $                                                RF1/3
PARAM  //ADD/V,N,NOMGG/V,N,SKPMGG/1 $                  UNTIL EMG FIX       RF1/3
ALTER 29,29
CHKPNT OGPST $
ALTER 30,35
EMG  EST,CSTM,MPT,DIT,GEOM2,,,/KELM,KDICT,MELM,MDICT,,/V,N,NOKGGX/           RF1/3
        V,N,NOMGG/0///C,Y,COUPMASS $
SAVE NOKGGX,NOMGG  $                                                         RF1/3
CHKPNT KELM,KDICT,MELM,MDICT $
EMA  GPECT,KDICT,KELM,BGPDT,SIL,CSTM/KGGX,GPST $                             RF1/3
CHKPNT KGGX,GPST $
COND     LBL1,SKPMGG $
COND JMPMGG,NOMGG                                                            RF1/3
EMA  GPECT,MDICT,MELM,BGPDT,SIL,CSTM/MGG,/C,N,-1/V,Y,WTMASS = 1.0 $          RF1/3
CHKPNT MGG $
LABEL  JMPMGG $                                                              RF1/3
ALTER 47
SMULTIPLY TIMES MGG, ADD TO KGG
MATMOD    OM2,,,,,/OM2G,/5/V,N,LUSET $
MTRXIN,   ,MATPOOL,EQEXIN,SIL,/TENPAD,,/S,N,LUSET/S,N,NOTH $
DIAGONAL KGG/IGG/SQUARE/0.0 $
ADD       TENPAD,IGG/COS2TH/(-1.0,0.0) $
MPYAD     OM2G,COS2TH,/OMCOS $
```

```
MPYAD     OMCOS,MGG,KGG/KGGQ $
EQUIV     KGGQ,KGG/ALWAYS $
ALTER 102
PARAM     //DOWN/0 $
GPFDR  CASECC,UGV,KELM,KDICT,ECT,EQEXIN,GPECT,PG ,QG,BGPDT,SIL,CSTM/     RF1/3
     ONRGY1,OGPFB1/DS0/C,Y,TINY $
PARAM     //DOWN/25000 $
OFP ONRGY1,OGPFB1,,,,  // $                                              RF1/3
ALTER    103,107
COND      P2,JUMPPLOT $
PLOT  PLTPAR,GPSETS,ELSETS,CASECC,BGPDT,EQEXIN,SIL,PUGV1,,GPECT,OES1/     RF1/3
          PLOTX2/V,N,NSIL/V,N,LUSET/V,N,JUMPPLOT/V,N,PL  T/V,N,PFILE     RF1/3
SAVE      PFILE $
PRTMSG    PLOTX2 // $
LABEL     P2 $
ALTER 108,109
PARAML    CASECC//DTI/1/7//V,N,TSET $
PARAML    CASECC//DTI/1/6//V,N,DEFSET $
EMG    EST,CSTM,MPT,DIT,,UGV,GPTT,EDT/KDELM,KDDICT,,,,,/1/0/0/
          ///V,N,TSET/V,N,DEFSET $
CHKPNT KDELM,KDDICT $
EMA  GPECT,KDDICT,KDELM,BGPDT,SIL,CSTM/KDGG,/-1 $
CHKPNT KDGG $
DBSTORE   KDGG//V,Y,MODEL/V,Y,THETAZ/ $
DBMGR  // $
EXIT $
ALTER    160,164
COND      P3,JUMPPLOT $
PLOT  PLTPAR,GPSETS,ELSETS,CASECC,BGPDT,EQEXIN,SIL,PUBGV1,,GPECT,OESB1/
          PLOTX3/V,N,NSIL/V,N,LUSET/V,N,JUMPPLOT/V,N,PLTFLG/V,N,PFILE    RF1/3
SAVE      PFILE $
PRTMSG    PLOTX3 // $
LABEL     P3 $
$ ITERATED DIFFERENTIAL STIFFNESS                                        RF 4/
$         10/ 1/73          R I G I D   F O R M A T   4    /SERIES M1    RF 4/
$                                                                        RF 4/
$    CASE CONTROL INPUT                                                  RF 4/
$         DSCOEFFICIENT CARD                                             RF 4/
$                                                                        R6 4/
$    BULK DATA INPUT                                                     RF 4/
$         DSFACT CARD                                                    RF 4/
$         PARAMS EPSIO, NT, BETA ARE OPTIONAL                            RF 4/
$                                                                        RF 4/
$  IMPROVES ACCURACY OF DIFFERENTIAL STIFFNESS MATRIX BY ITERATION       RF 4/
$-----------------------------------------------------------------------RF 4/
ALTER     98,98       $ RF4/21                                           RF 4/
SDR1      USET,  ,ULV,UOOV,YS,GO,GM,PS,KFS,KSS,/UGV,PG1,QG/C,N,1/C,N,    RF 4/
          DS0 $                                                          RF 4/
ALTER 99,100                                                             RF 4/
CHKPNT    UGV,QG $                                                       RF 4/
SDR2      CASECC,CSTM,MPT,DIT,EQEXIN,STL,GPTT,EDT,BGPDT,PG,QG,UGV,EST,/  RF 4/
          OPG1,OQG1,OUGV1,OES1,OEF1,PUGV1/C,N,DS0 $                      RF 4/
ALTER  110                                                               RF 4/
PARAM     //C,N,ADD/V,N,SHIFT/C,N,-1/C,N,0 $                            RF 4/
PARAM     //C,N,ADD/V,N,COUNT/V,N,ALWAYS=-1/V,N,NEVER=1 $               RF 4/
PARAMR    //C,N,ADD/V,N,DSEPSI/C,N,0.0/C,N,0.0 $                        RF 4/
PARAML    YS//C,N,NULL/C,N,/C,N,/C,N,/V,N,NOYS $                       RF 4/
```

```
JUMP     OUTLPTOP
LABEL    OUTLPTOP $                                                    RF 4/
EQUIV    PG,PG1/NOYS $                                                 RF 4/
CHKPNT   PG1                                                           RF 4/
PARAM    //C,N,KLOCK/V,N,TO $                                          RF 4/
ALTER    129,136                                                       RF 4/
ADD      KAA,KDAA/KBLL $                                               RF 4/
ADD      KFS,KDFS/KBFS $                                               RF 4/
ADD      KSS,KDSS/KBSS $                                               RF 4/
COND     PGOK,NOYS $                                                   RF 4/
MPYAD    KBSS,YS,/PSS/C,N,0/C,N,1/C,N,1/C,N,1 $                        RF 4/
MPYAD    KBFS,YS,/PFS/C,N,0/C,N,1/C,N,1/C,N,1 $                        RF 4/
UMERGE   USET,PFS,PSS/PN/C,N,N/C,N,F/C,N,S $                           RF 4/
EQUIV    PN,PGX/MPCF1                                                  RF 4/
COND     NOMS,MPCF1                                                    RF 4/
UMERGE   USET,PN,/PGX/C,N,G/C,N,N/C,N,M $                              RF 4/
LABEL    NOMS $                                                        RF 4/
ADD      PGX,PG/PGG/C,N(-1,0,0,0) $                                    RF 4/
EQUIV    PGG,PG1/ALWAYS                                                RF 4/
LABEL    PGOK                                                          RF 4/
ADD      PG1,/PGO/ $                                                   RF 4/
ALTER    141                                                           RF 4/
JUMP     INLPTOP
LABEL    INLPTOP                                                       RF 4/
PARAM    //C,N,KLOCK/V,N,TI $                                          RF 4/
SSG2     USET,GM,YS,KDFS,GO,,PG1/,PBO,PBS,PBL $                        RF 4/
ALTER    148,148                                                       RF 4/
SDR1     USET,,UBLV,,YS,GO,GM,PBS,KBFS,KBSS,/UBGV,,QBG/C,N,1/C,N,DS1 $ RF 4/
ALTER    150,156
ADD      UBGV,UGV/DUGV/C,N,(-1,0,0,0) $                                RF 4/
EMG      EST,CSTM,MPT,DIT,,DUGV,GPTT,EDT/DKDELM,DKDDICT,,,,/1/0/0/
         ///V,N,TSET/V,N,DEFSET $
CHKPNT   DKDELM,DKDDICT $
EMA      GPECT,DKDDICT,DKDELM,BGPDT,SIL,CSTM/DKDGG,/-1 $
CHKPNT   DKDGG $                                                       RF 4/
MPYAD    DKDGG,UBGV,PGO/PGI1/C,N,0/C,N,1/C,N,1/C,N,1 $                 RF 4/
DSCHK    PG1,PGI1,UBGV//C,Y,EPSIO=1.5E-5/V,N,DSEPSI/C,Y,NT=-1/V,N,TO/V,RF 4/
         N, TI/V,N,DONE/V,N,SHIFT/V,N,COUNT/C,Y,BETA=4 $               RF 4/
SAVE     DSEPSI,DONE,SHIFT,COUNT $                                     RF 4/
COND     DONE,DONE                                                     RF 4/
COND     SHIFT,SHIFT $                                                 RF 4/
EQUIV    PG,PG1/NEVER $                                                R6+4/
EQUIV    PGI1,PG1/ALWAYS $                                             RF 4/
EQUIV    PG1,PGI1/NEVER $                                              RF 4/
REPT     INLPTOP,1000 $                                                RF 4/
TABPT    PGI1,PG1,PG,,// $                                             RF 4/
LABEL    SHIFT $                                                       RF 4/
ADD      DKDGG,KDGG/KDGG1/C,N,(-1,0,0,0) $                             RF 4/
CHKPNT   KDGG1 $                                                       RF 4/
EQUIV    UBGV,UGV/ALWAYS/KDGG1,KDGG/ALWAYS $                           RF 4/
CHKPNT   UGV,KDGG $                                                    RF 4/
EQUIV    KDGG,KDGG1/NEVER/UGV,UBGV/NEVER $                             RF 4/
REPT     OUTLPTOP,1000 $                                               RF 4/
TABPT    KDGG1,KDGG,UGV,,// $                                          RF 4/
LABEL    DONE $                                                        RF 4/
ALTER 170,171
ALTER 176,177
$ END OF RF ALTER 4533
```

APPENDIX C

SØL 24,1 Sample Deck for One-Bladed Model

```
$RUN  DBSTAT,228     ,DEAN,06,300/200        , ISD
$SYM  PRINTS,,MNS
$ASG,UPR EB1PRT(+1)
$USE Z,EB1PRT(+1)
$BRKPT PRINTS/Z
$QUAL  ISDMSC
$ASG,AX  DEANDB01,
$USE  DB01,DEANDB01
$ASG,AX MIKEDATA,
$HDG  EDIT DATA
$ELT  MIKEDATA,M14BLD1,TPFS,BLADE1
$ELT  MIKEDATA,M14B1T0,TPFS,BLD1T0
$ELT  MIKEDATA,HUBADDZ,TPFS,HUBDA
-14,39
-49,49
-53,57
-59,73
$ELT  MIKEDATA,SOLPRS,TPFS,SOLPRS
-1,31
$ELT  MIKEDATA,STATSOL,TPFS,STATSOL
$FREE MIKEDATA,
$ADD  MIKEDATA,ASGCRDS
NASTRAN TITLEOPT = 0 , DAYLIMIT = 99
ID HELIOGYRO SOLAR SAILER SOLAR PRESSURE LOADS
TIME 2
DIAG 8
DIAG 22
SOL 24,1
$ADD  TPFS,STATSOL
CEND
TITLE = HELIOGYRO SOLAR SAILER ONE BLADED MODEL 14, THETA0 = 0
SUBTI = SOLAR PRESSURE LOADS AND ONE DEG UNTRIMMED COLL PITCH
LABEL = R=7500M,C=7.63M,OMG=.027RAD/SEC, CUTOUTS AND REDUCED CHORD
ECHO = SORT
SPC = 1
  OLOAD = ALL
  DISP = ALL
  SPCF = ALL
  ELFORCE = ALL
  GPFORCE = ALL
  LOAD = 2
BEGIN BULK
$ADD  TPFS,BLADE1
$ADD  TPFS,BLD1T0
$ADD  TPFS,HUBDA
$ADD  TPFS,SOLPRS
SPC1,1,123456,900000,19997
SPC1,1,,999990
PARAM,MODEL,14
PARAM,THETAZ,0
PARAM,GRDPNT,1
ENDDATA
$BRKPT PRINTS
$FREE,R Z
$SYM EB1PRT,,MNS
$SYM PRINTS,,MNS
```

APPENDIX D

STATSØL Alter for SØL 24,1

```
$       BEGINNING OF    ALTER TO GET DEFLECTIONS OF ROTATING BLADE
$       WITH SOLAR PRESSURE
ALTER 93
DBFETCH   /KDGG,,,,/V,Y,MODEL/V,Y,THETAZ/ $
ADD       KGG,KDGG/KGGDS/ $
MATMOD    OM2,,,,,/OM2G,/5/V,N,LUSET $
MTRXIN,   ,MATPOOL,EQEXIN,SIL,/TENPAD,,/S,N,LUSET/S,N,NOTH $
DIAGONAL  KGG/IGG/SQUARE/0,0 $
ADD       TENPAD,IGG/COS2TH/(-1.0,0,0) $
MPYAD     OM2G,COS2TH,/OMCOS $
MPYAD     OMCOS,MGG,KGGDS/KGGQ $
EQUIV     KGGQ,KGG/ALWAYS $
ALTER 104,105
$       END OF ALTER
```

APPENDIX E

SØL 25,1 Sample Deck for Two-Bladed Model

```
$RUN  DBMD2B,228     ,DEAN,25,300/200       , ISD
$SYM  PRINTS,,MNS
$ASG,UPR EBSPRT(+1)
$USE Z,EBSPRT(+1)
$BRKPT PRINTS/Z
$QUAL  ISDMSC
$ASG,A  *NASTRAN,
$ASG,AX  DEANDB01,
$USE  DB01,DEANDB01
$ASG,AX MIKEDATA,
$HDG  EDIT DATA
$ELT  MIKEDATA,M15BLD1,TPFS,BLADE1
$ELT  MIKEDATA,M15BLD2,TPFS,BLADE2
$ELT  MIKEDATA,M15B1T0,TPFS,BLD1T0
$ELT  MIKEDATA,M15B2T0,TPFS,BLD2T0
$ELT  MIKEDATA,HUBAOD7,TPFS,HUBDA
-9,16
-28,39
-49,49
-53,57
$ELT  MIKEDATA,RCTMODE,TPFS,RCTMODE
$FREE MIKEDATA,
$DELETE,C M15CMDDICT,
$ASG,UP M15CMDDICT,F///50
$BRKPT PUNCHS/M15CMDDICT
$DELETE,C M15CMDNPTP,
$ASG,UP M15CMDNPTP,F///500
$USE NPTP,M15CMDNPTP
$ADD  MIKEDATA,ASGCRDS
NASTRAN TITLEOPT = 0 , DAYLIMIT = 99 , MICORE = 82000
ID HELIOGYRO SOLAR SAILER VIBRATION MODES RUN
CHKPNT YES
TIME 10
DIAG 8
SOL 25,1
$ADD  TPFS,RCTMODE
CEND
TITLE = HELIOGYRO SOLAR SAILER TWO BLADED MODEL 15, THETAZ = 0
SUBTI = MODES WITH CENT FORCE, R=7500M, C=7.63M, OMG=.027RAD/SEC
LABEL = REDUCED CHORD AND CUTOUTS, COLLECTIVE MODES
ECHO = SORT
SPC = 1
METHOD = 2
  DISP = ALL
BEGIN BULK
$ADD  TPFS,BLADE1
$ADD  TPFS,BLADE2
$ADD  TPFS,BLD1T0
$ADD  TPFS,BLD2T0
$ADD  TPFS,HUBDA
ASET1,36,900000,900001
EIGR,2,MGIV,0.,,,02,34,34,,1,-9,+EIGR2
PARAM,SOLID,3
SPC1,1,1245,900000,900001
SPC1,1,12456,19997,29997
```

```
PARAM,MODEL,15
PARAM,THETAZ,0
PARAM,GRDPNT,1
ENDDATA
$BRKPT PRINTS
$FREE,R Z
$SYM EBSPRT,,MNS
$SYM PRINTS,,MNS
```

APPENDIX F

RCTMØDE Alter for SØL 25,1

```
$        BEGINNING OF ALTER
$        RIGID FORMAT 25 ALTER TO GET REACTIONLESS MODES FOR
$        A STRAIGHT BLADE WITH A CENTRIFUGAL LOADING
ALTER 92 $ DIFF. STIFF., CENT. FORCE AND TENNIS RACKET MOMENT
DBFETCH  /KDGG,,,,/0,Y,MODEL/V,Y,THETAZ/ $
ADD      KGG,KDGG/KGGDS/ $
MATMOD   OM2,,,,,/OM2G,/5/V,N,LUSET $
MTRXIN,  ,MATPOOL,EQEXIN,SIL,/TENPAD,,/S,N,LUSET/S,N,NOTH $
DIAGONAL KGG/IGG/SQUARE/0,0 $
ADD      TENPAD,IGG/COS2TH/(-1.0,0.0) $
MPYAD    OM2G,COS2TH,/OMCOS $
MPYAD    OMCOS,MGG,KGGDS/KGGQ $
EQUIV    KGGQ,KGG/ALWAYS $
ALTER 102,103 $ AVOID SOL 25 ERROR
ALTER 154 $ SAVE BLADE MODE SHAPES FOR PLOTTING
DBSTORE  PHIG,LAMA//V,Y,MODEL/V,Y,SOLID $
DBMGR    ///7/V,Y,MODEL/V,Y,SOLID/V,Y,MODEL/V,Y,SOLID/0/PHIG/UGV/ $
DBMGR    // $
$        END OF ALTER
```

APPENDIX G

SØL 7,1 Sample Deck for One-Bladed Model

```
$RUN,N  CYCMOD,228    ,DEAN,23,400/200      . ISD
$SYM  PRINTS,,MNS
$ASG,UPR EB3PRT(+1)
$USE Z,EB3PRT(+1)
$BRKPT PRINTS/Z
$QUAL  ISDMSC
$ASG,A  *NASTRAN,
$ASG,AX MIKEDATA,
$ASG,AX DEANDB01,
$USE  DB01,DEANDB01
$HDG  EDIT DATA
$ELT  MIKEDATA,M14BLD1,TPFS,BLADE1
=281,282
$ELT  MIKEDATA,M14B1T0,TPFS,BLD1T0
$ELT  MIKEDATA,HUBAOD7,TPFS,HUBDA
=10,27
=49,49
$ELT  MIKEDATA,NEWCYC,TPFS,NEWCYC
$FREE  MIKEDATA,
$DELETE,C M14B1CYDICT,
$ASG,UP   M14B1CYDICT,F///100
$BRKPT   PUNCHS/M14B1CYDICT
$DELETE,C M14B1CYNPTP,
$ASG,UP   M14B1CYNPTP,F///1000
$USE NPTP,M14B1CYNPTP
$ADD  MIKEDATA,ASGCRDS
NASTRAN TITLEOPT = 0 , DAYLIMIT = 99
±± H±LIOGYRO SOLAR SAILER CYCLIC MODES RUN
TIME 7
CHKPNT YES
DIAG 7
DIAG 8
DIAG 13
DIAG 20
SOL 7,1
$ADD  TPFS,NEWCYC
CEND
TITLE = HELIOGYRO SOLAR SAILER ONE BLADED MODEL 14, THETAZ = 0
SUBTI = CYC MDS WITH CENT. LOADS, R=7500M, C=7.63M, OMG=.027RAD/SEC
LABEL = C=6M AT (.49=.61R,CUTOUT AT (.9=.95)R
ECHO = SORT
SPC = 1
CMETHOD = 3
DISP = ALL
BEGIN BULK
$ADD  TPFS,BLADE1
$ADD  TPFS,BLD1T0
$ADD  TPFS,HUBDA
ASET,999990,0,900000,12
PARAM,MODEL,14
PARAM,THETAZ,0
CELAS1,19992,19992,19996,5,19997,5
PELAS,19992,100,,,3
MAT1,11,120,65+9,,,3,,,,,3
ENDDATA
$BRKPT PRINTS
$FREE,R Z
$SYM EB3PRT,,MNS
$SYM PRINTS,,MNS
```

APPENDIX H

NEWCYC Alter for SØL 7,1

```
$
$       RIGID FORMAT ALTER TO INCLUDE THE EFFECTS OF -
$
$          1.  CENTRIFUGAL FORCES
$          2. CORIOLIS EFFECTS
$          3. TENNIS RACKET EFFECTS
$          4. COMPLEX CONSTRAINTS AT THE CENTER OF ROTATION
$
$       ON ROTATING BODIES.
$
$
ALTER 33 $
SETVAL   //V,N,NOBGG/0 $ OVER-RULE SMA2
ALTER 47 $
MATMOD   OM2,SIL,,,,/OM2G,/5/ $
DBFETCH  /KDGG,,,,/V,Y,MODEL/V,Y,THETAZ $
ADD      KGG,KDGG/KGGA $
EQUIV    KGGA,KGG/ALWAYS $          PAD
MTRXIN,  ,MATPOOL,EQEXIN,SIL,/TENRAC,COUPLX,/S,N,LUSET/S,N,NOTH $
DIAGONAL KGG/IGG/SQUARE/0,0 $
ADD      TENRAC,IGG/COS2TH/(-1.0,0.0) $
MPYAD    OM2G,COS2TH,/OMCOS $
MPYAD    OMCOS,MGG,/OMMGG $
ADD      OMMGG,/KCENT/ $
MATMOD   OM1,SIL,,,,/OM1G,/5/ $
MPYAD    OM1G,MGG,/BCOR $
ADD      BCOR,BGG/BGGQ/ $
EQUIV    BGGQ,BGG/ALWAYS $
ALTER 136 $
UPARTN   USETD,COUPLX/COUPLXD,,,/P/D/0 $
MATREDU  KCENT,USET,GM,GO/KAAQ/S,N,NOKCENT $
ADD      KDD,KAAQ/KDDQQ $
EQUIV    KDDQQ,KDD/ALWAYS $
ADD      MDD,COUPLXD/MDDQ $
EQUIV    MDDQ,MDD/ALWAYS $
ALTER 142 $ GENERALIZED MASS CALCULATION
MPYAD    MDD,PHID,/MPHI $
MATMOD   PHID,,,,,/PHIDCNJ,/10 $
MPYAD    PHIDCNJ,MPHI,/GMCX/1 $
MATMOD   GMCX,,,,,/GMCXF,/2////1.-5 $
MATPRN   GMCXF // $
$
$
$       END OF RIGID FORMAT ALTER
```

APPENDIX I

SØL 10,1 Sample Deck for Two-Bladed Model

```
$RUN,N/T   DBCM28,228     ,DEAN,75,2500/400       , ISD
$SYM  PRINT$,,MNS
$ASG,UPR EB6PRT(+1),F///5000
$USE Z,EB6PRT(+1)
$BRKPT PRINT$/Z .
$QUAL  ISDMSC
$ASG,A  *NASTRAN,
$ASG,AX MIKEDATA,
$ASG,AX DEANDB01,
$USE  DB01,DEANDB01
$HDG  EDIT DATA
$ELT  MIKEDATA,M15BLD1,TPF$,BLADE1
-281,282
$ELT  MIKEDATA,M15BLD2,TPF$,BLADE2.
-278,278
$ELT  MIKEDATA,M15B1T0,TPF$,BLD1T0
$ELT  MIKEDATA,M15B2T0,TPF$,BLD2T0
$ELT  MIKEDATA,HUBAOD7,TPF$,HUBDA
-9,16
-28,31
-49,49
-59,59
EPOINT,999990
-73,73
EPOINT,999991
$ELT  MIKEDATA,NEWFLUT,TPF$,CPLXMD
$FREE MIKEDATA,
$DELETE,C M15B1CPDICT,
$ASG,UP   M15B1CPDICT,F///300
$BRKPT    PUNCH$/M15B1CPDICT
$SAVETAPE  NPTP,
 M15=2BLD CM NPTP
$ADD MIKEDATA,SECONDS
$ADD  MIKEDATA,ASGCRDS
NASTRAN TITLEOPT = 0 , DAYLIMIT = 99 , HICORE = 127000
ID HELIOGYRO SOLAR SAILER COMPLEX MODES RUN
TIME 21
CHKPNT YES
DIAG 14
DIAG 7
DIAG 8
DIAG 13
DIAG 20
SOL 10,1
$ADD TPF$,CPLXMD
CEND
TITLE = HELIOGYRO SOLAR SAILER TWO BLADED MODEL 15, THETAZ = 0
SUBTI = R=7500M, C=7.63M, OMG=.027RAD/SEC
LABEL = REDUCED CHORD AND CUTOUTS, CYCLIC MODES
ECHO = SORT
SPC = 1
METHOD = 2
```

```
SET 100 = 1,-7,2,-7,3,-7,4,-7,5,-7,6,-7,7,-7,8,-7,9,-7,10,-7,
          11,-7,12,-7,13,-7,14,-7,15,-7,16,-7,17,-7,18,-7,19,-7,20,-7,
          21,-7,22,-7,23,-7,24,-7,25,-7,26,-7,27,-7,28,-7,29,-7,30,-7,
          31,-7,32,-7,33,-7,34,-7,35,-7,36,-7,38,-7,39,-7,40,-7
SFREQ = 100
  DISP = ALL
BEGIN BULK
$ADD  TPFS.BLADE1
$ADD  TPFS.BLADE2
$ADD  TPFS.BLD1TO
$ADD  TPFS.BLD2TO
$ADD  TPFS.HUBDA
ASET1,0,999990,999991
ASET1,12,900000,900001
CELAS1,19992,19992,19996,5,19997,5
CELAS1,29992,19992,29996,5,29997,5
PELAS,19992,100,,,3
MAT1,11,120,65+9,,,.3,,,,.3
EIGR,2,MGIV,0,,,.02,40,40,,1,-9,+EIGR2
PARAM,LMODES,40
PARAM,MODEL,IS
PARAM,THETAZ,0
PARAM,GRDPNT,1
ENDDATA
$BRKPT PRINTS
$FREE,R Z
$SYM EB6PRT,,MNS
$SYM PRINTS,,MNS
```

APPENDIX J

NEWFLUT Alter for SØL 10,1

```
$        BEGINNING OF ALTER FOR COMPLEX MODES
$         R.F. 10 ALTER FOR COMPLEX MODES
$  MODIFIED FOR FLUTTER MG  18 MAY 77
$  INPUT AERO FACTORS IN DMIG AERO, AND SCALAR FACTOR IN
$  PARAM ACOEF, COMPLEX
ALTER 2 $
PARAM    //DOWN/55000 $
ALTER 21,21 $              EMG AND EMA FOR R.F. 10
TA1,     ,ECT,EPT,BGPDT,SIL,GPTT,CSTM/FST,,GEI,GPECT,/V,N,LUSET/123/
         V,N,NOSIMP/1/V,N,NOGENL/V,N,GENEL $
ALTER 25,25 $
CHKPNT   EST,GEI,GPECT,OGPST $
SETVAL   //V,N,NOKGGX/1 $
SETVAL   //V,N,NOMGG/1 $
SETVAL   //V,N,NOBGG/1 $
SETVAL   //V,N,NOK4GG/1 $
EMG      EST,CSTM,MPT,DIT,GEOM2,,,/KELM,KDICT,MELM,MDICT,BELM,
         BDICT/S,N,NOKGGX/S,N,NOMGG/S,N,NOBGG/S,N,NOK4GG//C,Y,
         COUPMASS $
CHKPNT   KELM,KDICT,MELM,MDICT,BELM,BDICT $
ALTER 26,26 $
EMA      GPECT,KDICT,KELM,BGPDT,SIL,CSTM/KGGX,GPST $
ALTER 28,30 $
COND     ERROR1,NOMGG $
EMA      GPECT,MDICT,MELM,BGPDT,SIL,CSTM/MGG,/-1/V,Y,WTMASS=1.0 $
ALTER 31 $
PURGE    BGG/NOBGG $
COND     LEMAB,NOBGG $
EMA      GPECT,BDICT,BELM,BGPDT,SIL,CSTM/BGG,/S,N,NOBGG $
LABEL    LEMAB $
CHKPNT   BGG $
PURGE    K4GG/NOK4GG $
COND     LEMAK4,NOK4GG $
EMA      GPECT,KDICT,KELM,BGPDT,SIL,CSTM/K4GG,/S,N,NOK4GG $
CHKPNT K4GG $
LABEL    LEMAK4 $
ALTER   42 $ CENT. AND CORIOLIS FORCES
MATMOD   OM2,,,,,/OM2G,/S/V,N,LUSET $
DBFETCH /KDGG,,,,,/V,Y,MODEL/V,Y,THETAZ  $
ADD      KGG,KDGG/KGGA $
CHKPNT KGGA $
EQUIV    KGGA,KGG/ALWAYS $
CHKPNT KGG $
MTRXIN,, MATPOOL,EQEXIN,SIL,/TENPAD,,/S,N,LUSET/S,N,NOTH $
DIAGONAL KGG/IGG/SQUARE/0.0
ADD TENPAD,IGG/COS2TH/(-1.0,0.0) $
MPYAD    OM2G,COS2TH,/OMCOS       $
MPYAD    OMCOS,MGG,/OMMGG         $
ADD      OMMGG,/KCENT/S
CHKPNT KCENT $
MATMOD   OM1,,,,,/OM1G,/S/V,N,LUSET $
MPYAD    OM1G,MGG,/BCOR  $
CHKPNT BCOR $
$        1.
$        2.      SMP1- TYPE OPERATIONS
ALTER 94 $ PRINT REAL MODES
MATGPR   GPL,USET,SIL,PHIA//H/A $
```

```
ALTER 105 $
MTRXIN,,MATPOOL,EQDYN,,/COUPLX,AERO,/V,N,LUSETD/S,N,NOCOUPLX/S,N,
        NOAERO $ P-SIZE MATRICES
EQUIV K4GG,K4PP/NOUE/KCENT,KCPP/NOUE/BGG,BPP/NOUE
EQUIV BCOR,BCPP/NOUE/KGG,KPP/NOUE $
CHKPNT K4PP,KCPP,BPP,BCPP,KPP $
COND LNOPSET,NOUE $
VEC USETD/VPGE/P/G/E $
MERGE K4GG,,,,VPGE,/K4PP $
MERGE KGG,,,,VPGE,/KPP $
MERGE KCENT,,,,VPGE,/KCPP $
MERGE BGG,,,,VPGE,/BPP $
MERGE BCOR,,,,VPGE,/BCPP $
LABEL LNOPSET $
PARAMR //DIV/V,N,RGOW3/C,Y,G=0.0/C,Y,W3=0.0 $
PARAMR  //COMPLEX//RGOW3//V,N,GOW3 $
PARAMR //DIV/V,N,ROOW4/1.0/C,Y,W4=0.0 $
PARAMR  //COMPLEX//ROOW4//V,N,OOW4 $
ADD B2PP,BPP/BX1 $
ADD KPP,BX1/BX2 /GOW3 $
ADD K4PP,BX2/BX3/OOW4 $
ADD BCPP,BX3/BX4 $
CHKPNT BX4 $
EQUIV BX4,B2PP/ALWAYS $
CHKPNT B2PP $
PARAML B2PP//PRESENCE////V,N,NOB2PP $
$ GENERATE STIFFNESS TERMS
ADD K2PP,K4PP/KX1/(1.,0.)/(0.,1.) $
ADD KCPP,KX1/KX2 $
ADD KX2,AERO/KX3//C,Y,MAERO=(1.,0.) $
CHKPNT KX3 $
EQUIV KX3,K2PP/ALWAYS $
CHKPNT K2PP $
PARAML K2PP//PRESENCE////V,N,NOK2PP $
ADD COUPLX,M2PP/M2PPX $
CHKPNT M2PPX $
EQUIV M2PPX,M2PP/ALWAYS $
CHKPNT M2PP $
PARAML M2PP//PRESENCE////V,N,NOM2PP $
ALTER 106 $
CHKPNT M2PP,B2PP,K2PP $
ALTER 108,108 $
CHKPNT M2DD,B2DD,K2DD $
ALTER 109,109 $
GKAD USETD,GM,GO,  ,  ,  ,  ,K2PP,M2PP,B2PP/KDD,BDD,MDD,GMD,
     GOD,K2DD,M2DD,B2DD/C,N,CMPLEV/C,N,DISP/C,N,DIRECT/C,Y,G=0.0/C,
     N,0.0/0.0/V,N,NOK2PP/V,N,NOM2PP/V,N,NOB2PP/V,N,MPCF1/V,
N,SINGLE/V,N,OMIT/V,N,NOUE/V,N,NOK4GG/V,N,NOBGG/-1/-1 $
ALTER 110,110 $
CHKPNT KDD,BDD,MDD,GMD,GOD,K2DD,M2DD,B2DD $
ALTER 113
ADD      KHH,/KHHX/(54154,208.0,) $
ADD      BHH,/BHHX/(232,71057,0,) $
ALTER 114,115
PARAM    //DOWN/0 $
CEAD     KHHX,BHHX,MHH,EED,CASEXX/PHIH,CLAMA,OCEIGS/S,N,EIGVS $
PARAM    //DOWN/55000 $
```

```
ALTER 118 $  GENERALIZED MASS CALCULATIONS
MPYAD MHH,PHIH,/MPHI $
MATMOD PHIH,,,,,/PHIHCNJ,/10 $
MPYAD PHIHCNJ,MPHI,/GMCX/1 $
MATMOD GMCX,,,,,/GMCXF,/2////1.-2 $
MATPRN GMCXF // $
ALTER 126 $
PURGE     QPC/ALWAYS $
MODACC    CASEXX,CLAMA,PHIH,,,/CLAMAX,PHIHX,CASEZZ,,/CEIG $
CHKPNT    CLAMAX,PHIHX $
EQUIV     PHIHX,PHIH/ALWAYS/CLAMAX,CLAMA/ALWAYS $
CHKPNT PHIH,CLAMA,CASEZZ $
EQUIV     CASEZZ,CASEXX/ALWAYS $
CHKPNT CASEXX $
ALTER 133 $ STRAIN ENERGY DATA RECOVERY
GPFDR     CASEXX,CPHIP,KELM,KDICT,ECT,EQEXIN,GPECT,CLAMA,QPC,
          BGPDT,SIL,CSTM/ONRGYR,OGPFBR/REIG/C,Y,TINY $
OFP       ONRGYR,OGPFBR//S,N,CARDNO $
ADD       CPHIP,/CPHIPI/(0.,-1.) $
GPFDR     CASEXX,CPHIPI,KELM,KDICT,ECT,EQEXIN,GPECT,CLAMA,QPC,
          BGPDT,SIL,CSTM/ONRGYI,OGPFBI/REIG/C,Y,TINY $
OFP       ONRGYI,OGPFBI//S,N,CARDNO $
$         END OF ALTER FOR COMPLEX MODES
```

APPENDIX K

Blade Pitch Distribution

1. Static Torsional Deflection of the Heliogyro Blade

Whenever the Heliogyro blade root is set at a prescribed angle, the torsional deflection (twist distribution) of the blade involves the numerical solution of the nonlinear differential equation:

$$-\frac{\partial}{\partial y}\left[\left(\frac{c}{2}\right)^2 T \frac{\partial\theta}{\partial y}\right] + \frac{1}{2}(I'_\theta \Omega^2)\sin 2\theta = m_\theta$$

where c = blade chord

T = centrifugal tension load

I'_θ = distributed blade pitch inertia

m_θ = applied blade pitching moment

θ = blade pitch angle

Ω = rotational speed

y = radial coordinate

The difference equation used to obtain the solution of Table 1 is:

$$\theta_n = \theta_{n+1} + \frac{M_{n+1} - M_i + \frac{45}{\pi}\Omega^2(I_{\theta_n} + I_{\theta_{n+1}})\sin 2\theta_{n+1}}{T_n\left(\frac{(c/2)^2}{\Delta y}\right)}$$

where $M_i = \frac{90}{\pi}\Omega^2 I_{\theta_{tip}} \sin 2\theta_{tip}$

$$(M_{n+1})_{tip} = 0$$

APPENDIX K

Table 1. Static Torsional Deflection of Heliogyro Blade for R = 6250 m.

y/R	$(c/2)^2$ (m^2)	T (Nt)	I_θ (kg-m^2)	Δy (m)	θ_n (deg)	TENPAD $=1-\cos 2\theta_n$
1.0		12.337	21.33	0	30.00	.500000
.9875	16	29.271	29.85	78.125	30.15	.504483
.95	16	79.109	61.63	234.375	30.52	.515816
.90	16	143.630	64.09	312.5	31.01	.530695
.85	16	205.474	66.41	312.5	31.50	.545986
.80	16	250.827	39.08	312.5	32.01	.561857
.75	16	280.432	41.14	312.5	32.53	.578415
.70	16	320.648	70.59	312.5	33.08	.596796
.65	16	370.500	74.38	312.5	33.65	.614138
.60	16	417.065	76.04	312.5	34.25	.633543
.55	16	460.246	77.79	312.5	34.88	.654078
.50	16	499.979	78.96	312.5	35.54	.675809
.45	16	536.188	80.22	312.5	36.24	.698808
.40	16	568.783	81.35	312.5	36.96	.723159
.35	16	597.693	82.35	312.5	37.73	.748953
.30	16	622.859	83.21	312.5	38.54	.776291
.25	16	644.237	83.94	312.5	39.39	.805280
.20	12.5	660.934	61.89	312.5	40.52	.844322
.15	9	672.486	39.51	312.5	42.15	.900538
.10	9	679.535	31.76	281.25	43.64	.952490
.07	9	583.279	23.86	218.75	44.82	.993747
.04	9	685.086	16.79	159.64	45.70	1.024306
.02783	9	686.169	54.80	84.910	46.18	1.041012
.01896	9		0	48.005	46.45	1.050662
.01010	9		0	57.97	46.79	1.062309
.0012336	9	686.812	206.5	57.97	47.15	1.074887

APPENDIX L

Solar Pressure Calculation and Other Static Deformations

1. Solar pressure at 0.25 A.U. with inertia relief for calculation of the blade vertical deflection in SØL 24,1:

$$p = p_o(1 - \mu)$$

where $\mu = \dfrac{\text{Mass of Center Body + Flap Hinge Brace}}{\text{Total Vehicle Mass}}$

$p_o = \left(\frac{1}{.25}\right)^2$ (perfect reflector pressure)(reflective coefficient)

Typical values of μ and p_o are

$$\mu = \frac{117.041 + 32.961}{404.391} = 0.370933$$

$$p_o = (16)(0.9026 \times 10^{-5})(0.9136 - 0.0049)$$
$$= 1.3123 \times 10^{-4} \text{ Nt/m}^2$$

Values for the vertical loads are shown in Table 1.

$$p_3 = p\Delta yc$$

Note: No solar pressure loads should be applied to the cutouts and reduced loads applied to reduced chord regions.

2. Differential Chordwise Strain resulting from manufacturing deformations (5 x the design limit):

Leading Edge Strain: 5×10^{-5}

Trailing Edge Strain: -5×10^{-5}

3. Inplane Solar Pressure Loads due to 1° of untrimmed collective pitch at 0.25 A.U.

$$p_1 = (p_o \sin \theta_o \cos \theta_o)\Delta yc$$

The inplane loads are shown in Table 2.

APPENDIX L

Table 1. Vertical Solar Pressure Loads at 0.25 A.U.

y/R		Δy (m)	c (m)	P_3 (Nt)
Tip	1.0	0	7.6289	0.
	.9875	187.5	7.6289	.118085
	.95	187.5	7.6289	.118085
	.90	187.5	7.6289	.118085
	.85	375.0	7.6289	.236169
	.80	375.0	7.6289	.236169
	.75	375.0	7.6289	.236169
	.70	375.0	7.6289	.236169
	.65	375.0	7.6289	.236169
	.60	375.0	6.8145	.210958
	.55	375.0	6.0	.185743
	.50	375.0	6.0	.185743
	.45	375.0	6.8145	.210958
	.40	375.0	7.6289	.236169
	.35	375.0	7.6289	.236169
	.30	375.0	7.6289	.236169
	.25	375.0	7.6289	.236169
	.20	375.0	7.6289	.236169
	.15	375.0	7.6289	.236169
	.10	300.0	7.6289	.188935
	.07	225.0	7.6289	.141702
	.04	175.54	7.6289	.110552
True Apex	.023188	63.04	7.6289	.039702

APPENDIX L

Table 2. Inplane Solar Pressure Loads at 0.25 A.U.

y/R	Δy (m)	c (m)	θ_o (deg)	p_l (Nt)
Tip 1.0	0.	7.6289	.627	0
.9875	187.5	7.6289	.630	.002064
.95	187.5	7.6289	.639	.002093
.90	187.5	7.6289	.652	.002136
.85	375.0	7.6289	.665	.004357
.80	375.0	7.6289	.678	.004442
.75	375.0	7.6289	.693	.004540
.70	375.0	7.6289	.708	.004639
.65	375.0	7.6289	.723	.004737
.60	375.0	6.8145	.738	.004319
.55	375.0	6.0	.755	.003890
.50	375.0	6.0	.773	.003983
.45	375.0	6.8145	.790	.004623
.40	375.0	7.6289	.808	.005294
.35	375.0	7.6289	.829	.005431
.30	375.0	7.6289	.851	.005575
.25	375.0	7.6289	.873	.005719
.20	375.0	7.6289	.894	.005857
.15	375.0	7.6289	.920	.006027
.10	300.0	7.6289	.947	.004963
.07	225.0	7.6289	.962	.003781
.04	175.54	7.6289	.978	.002999
Truss Apex .023188	63.04	7.6289	.987	.001087

Table 3. NASTRAN Solar Pressure Loads at 0.25 A.U. (SØLPRS)

```
FORCE   2       10120   1       1.      0.      0.      .118085
FORCE   2       10500   1       1.      0.      0.      .118085
FORCE   2       11000   1       1.      0.      0.      .118085
FORCE   2       11500   1       1.      0.      0.      .236169
FORCE   2       12000   1       1.      0.      0.      .236169
FORCE   2       12500   1       1.      0.      0.      .236169
FORCE   2       13000   1       1.      0.      0.      .236169
FORCE   2       13500   1       1.      0.      0.      .236169
FORCE   2       14000   1       1.      0.      0.      .210958
FORCE   2       14500   1       1.      0.      0.      .185743
FORCE   2       15000   1       1.      0.      0.      .185743
FORCE   2       15500   1       1.      0.      0.      .210958
FORCE   2       16000   1       1.      0.      0.      .236169
FORCE   2       16500   1       1.      0.      0.      .236169
FORCE   2       17000   1       1.      0.      0.      .236169
FORCE   2       17500   1       1.      0.      0.      .236169
FORCE   2       18000   1       1.      0.      0.      .236169
FORCE   2       18500   1       1.      0.      0.      .236169
FORCE   2       19000   1       1.      0.      0.      .188935
FORCE   2       19300   1       1.      0.      0.      .141702
FORCE   2       19600   1       1.      0.      0.      .110552
FORCE   2       19700   1       1.      0.      0.      .039702
DEFORM  5       1001    -.0046881002    +.004688
DEFORM  5       1013    -.0140621014    +.014062
DEFORM  5       1051    -.01875 1052    +.01875
=,      =,      *(50),  =,      *(50),  =,      =,      == $
=(15)
$       GENERATE DEFORMS ON TF AND LE
DEFORM  5       1901    -.01125 1902    +.01125
DEFORM  5       1931    -.01125 1932    +.01125
DEFORM  5       1961    -.0063041962    +.006304
FORCE   2       10120   1       1.      .002064 0.      .118085
FORCE   2       10500   1       1.      .002093 0.      .118085
FORCE   2       11000   1       1.      .002136 0.      .118085
FORCE   2       11500   1       1.      .004357 0.      .236169
FORCE   2       12000   1       1.      .004442 0.      .236169
FORCE   2       12500   1       1.      .004540 0.      .236169
FORCE   2       13000   1       1.      .004639 0.      .236169
FORCE   2       13500   1       1.      .004737 0.      .236169
FORCE   2       14000   1       1.      .004319 0.      .210958
FORCE   2       14500   1       1.      .003890 0.      .185743
FORCE   2       15000   1       1.      .003983 0.      .185743
FORCE   2       15500   1       1.      .004623 0.      .210958
FORCE   2       16000   1       1.      .005294 0.      .236169
FORCE   2       16500   1       1.      .005431 0.      .236169
FORCE   2       17000   1       1.      .005575 0.      .236169
FORCE   2       17500   1       1.      .005719 0.      .236169
FORCE   2       18000   1       1.      .005857 0.      .236169
FORCE   2       18500   1       1.      .006027 0.      .236169
FORCE   2       19000   1       1.      .004963 0.      .188935
FORCE   2       19300   1       1.      .003781 0.      .141702
FORCE   2       19600   1       1.      .002999 0.      .110552
FORCE   2       19700   1       1.      .001087 0.      .039702
```

APPENDIX M

Aerodynamic Force Coefficients

1. Inplane aerodynamic force coefficients for 30° of half-P pitch and at zero sun angle are calculated from the following equation:

$$K_{15} = -\frac{dp_x}{d\theta} c \Delta y$$

where

$$\frac{dp_x}{d\theta} = -\frac{7}{4} p_o a_{\frac{1}{2}}^2$$

$$a_{\frac{1}{2}}^2 = \left(\frac{\pi}{6}\right)^2 K$$

K = washout of $a_{\frac{1}{2}}^2$

Table 1 lists the inplane aerodynamic force coefficients for $a_{\frac{1}{2}} = 30°$ at 0.7R and $\gamma = 0°$ at 0.25 A.U.

2. Inplane and vertical aerodynamic force coefficients for 5° collective pitch and zero sun angle at 0.25 A.U.:

$$K_{15} = \frac{dp_x}{d\theta} c \Delta y$$

$$K_{35} = \frac{dp_z}{d\theta} c \Delta y$$

where

$$\frac{dp_x}{d\theta} = p_o$$

$$\frac{dp_z}{d\theta} = -3p_o \sin\theta_o \cos^2\theta_o (\theta_c/\theta_o)$$

Table 2 shows inplane and vertical aerodynamic force coefficients $\theta_c = 5°$ at 0.7R and $\gamma = 0°$ at 0.25 A.U.

APPENDIX M

Table 1. Inplane Aerodynamic Force Coefficients for $a_{\frac{1}{2}} = 30°$ and $\gamma = 0°$

y/R	Δy (m)	c (m)	K	K_{15} (m/rad)
1.0	0	7.6289	.833	0
.9875	187.5	7.6289	.839	.07556
.95	187.5	7.6289	.859	.07736
.90	187.5	7.6289	.884	.07961
.85	375.0	7.6289	.911	.16409
.80	375.0	7.6289	.937	.16877
.75	375.0	7.6289	.969	.17454
.70	375.0	7.6289	1.000	.18012
.65	375.0	7.6289	1.032	.18588
.60	375.0	6.8145	1.065	.17135
.55	375.0	6.0	1.105	.15654
.50	375.0	6.0	1.144	.16206
.45	375.0	6.8145	1.185	.19066
.40	375.0	7.6289	1.226	.22083
.35	375.0	7.6289	1.277	.23001
.30	375.0	7.6289	1.328	.23920
.25	375.0	7.6289	1.381	.24875
.20	375.0	7.6289	1.434	.25829
.15	375.0	7.6289	1.502	.27054
.10	300.0	7.6289	1.570	.22623
.07	225.0	7.6289	1.612	.17421
.04	175.54	7.6289	1.655	.13954
.023188	63.04	7.6289	1.672	.05063

APPENDIX M

Table 2. Inplane and Vertical Aerodynamic Force Coefficients for $\theta_c = 5°$, $\gamma = 0°$ at 0.25 A.U.

y/R	Δy (m)	c (m)	θ_c/θ_o	K_{15} (m/rad)	K_{35} (m/rad)
1.0	0	7.6289	.886	0	0
.9875	187.5	7.6289	.890	.187714	.043183
.95	187.5	7.6289	.903	.187714	.043813
.90	187.5	7.6289	.921	.187714	.044687
.85	375.0	7.6289	.939	.375428	.091120
.80	375.0	7.6289	.958	.375428	.092964
.75	375.0	7.6289	.979	.375428	.095002
.70	375.0	7.6289	1.000	.375428	.097040
.65	375.0	7.6289	1.020	.375428	.099078
.60	375.0	6.8145	1.042	.335350	.090321
.55	375.0	6.0	1.067	.295268	.081433
.50	375.0	6.0	1.092	.295268	.083341
.45	375.0	6.8145	1.116	.335350	.096735
.40	375.0	7.6289	1.141	.375428	.110722
.35	375.0	7.6289	1.171	.375428	.113633
.30	375.0	7.6289	1.202	.375428	.116642
.25	375.0	7.6289	1.233	.375428	.119650
.20	375.0	7.6289	1.263	.375428	.122561
.15	375.0	7.6289	1.300	.375428	.126152
.10	300.0	7.6289	1.338	.300342	.103871
.07	225.0	7.6289	1.359	.225256	.079126
.04	175.54	7.6289	1.382	.175741	.062777
.023188	63.04	7.6289	1.394	.063112	.022741

APPENDIX M

Table 3. NASTRAN Inplane Aerodynamic Force Coefficients (AERØCØEF)

```
DMIG     AERO    0       1       1       0
$        $       $       $       $       $       $               $       $
DMIG     AERO    10120   5               10120   1       .07556
DMIG     AERO    10500   5               10500   1       .07736
DMIG     AERO    11000   5               11000   1       .07961
DMIG     AERO    11500   5               11500   1       .16409
DMIG     AERO    12000   5               12000   1       .16877
DMIG     AERO    12500   5               12500   1       .17454
DMIG     AERO    13000   5               13000   1       .18012
DMIG     AERO    13500   5               13500   1       .18588
DMIG     AERO    14000   5               14000   1       .17135
DMIG     AERO    14500   5               14500   1       .15654
DMIG     AERO    15000   5               15000   1       .16206
DMIG     AERO    15500   5               15500   1       .19066
DMIG     AERO    16000   5               16000   1       .22083
DMIG     AERO    16500   5               16500   1       .23001
DMIG     AERO    17000   5               17000   1       .23920
DMIG     AERO    17500   5               17500   1       .24875
DMIG     AERO    18000   5               18000   1       .25829
DMIG     AERO    18500   5               18500   1       .27054
DMIG     AERO    19000   5               19000   1       .22623
DMIG     AERO    19300   5               19300   1       .17421
DMIG     AERO    19600   5               19600   1       .13954
DMIG     AERO    19700   5               19700   1       .05063
```

APPENDIX M

Table 4. NASTRAN Inplane and Vertical Aerodynamic Force Coefficients (AERØCØEF)

DMIG	AERO	0	1	1	0		
DMIG	AERO	10120	5		10120	1	-.18771
DMIG	AERO	10500	5		10500	1	-.18771
DMIG	AERO	11000	5		11000	1	-.18771
DMIG	AERO	11500	5		11500	1	-.37543
DMIG	AERO	12000	5		12000	1	-.37543
DMIG	AERO	12500	5		12500	1	-.37543
DMIG	AERO	13000	5		13000	1	-.37543
DMIG	AERO	13500	5		13500	1	-.37543
DMIG	AERO	14000	5		14000	1	-.33535
DMIG	AERO	14500	5		14500	1	-.29527
DMIG	AERO	15000	5		15000	1	-.29527
DMIG	AERO	15500	5		15500	1	-.33535
DMIG	AERO	16000	5		16000	1	-.37543
DMIG	AERO	16500	5		16500	1	-.37543
DMIG	AERO	17000	5		17000	1	-.37543
DMIG	AERO	17500	5		17500	1	-.37543
DMIG	AERO	18000	5		18000	1	-.37543
DMIG	AERO	18500	5		18500	1	-.37543
DMIG	AERO	19000	5		19000	1	-.30034
DMIG	AERO	19300	5		19300	1	-.22526
DMIG	AERO	19600	5		19600	1	-.17574
DMIG	AERO	19700	5		19700	1	-.06311
DMIG	AERO	10120	5		10120	3	.04318
DMIG	AERO	10500	5		10500	3	.04381
DMIG	AERO	11000	5		11000	3	.04469
DMIG	AERO	11500	5		11500	3	.09112
DMIG	AERO	12000	5		12000	3	.09296
DMIG	AERO	12500	5		12500	3	.09500
DMIG	AERO	13000	5		13000	3	.09704
DMIG	AERO	13500	5		13500	3	.09908
DMIG	AERO	14000	5		14000	3	.09032
DMIG	AERO	14500	5		14500	3	.08143
DMIG	AERO	15000	5		15000	3	.08334
DMIG	AERO	15500	5		15500	3	.09673
DMIG	AERO	16000	5		16000	3	.11072
DMIG	AERO	16500	5		16500	3	.11363
DMIG	AERO	17000	5		17000	3	.11664
DMIG	AERO	17500	5		17500	3	.11965
DMIG	AERO	18000	5		18000	3	.12256
DMIG	AERO	18500	5		18500	3	.12615
DMIG	AERO	19000	5		19000	3	.10387
DMIG	AERO	19300	5		19300	3	.07913
DMIG	AERO	19600	5		19600	3	.06278
DMIG	AERO	19700	5		19700	3	.02274

APPENDIX N

MIKEDATA.M15BLD1

```
$ HELIOGYRO BLADE GRIDS
$
$       BLADE CENTER LINE GRIDS
GRID    10000   100     0.      0.      0.      1
GRID    10120   101     0.      0.      0.      1
GRID    10500   105     0.      0.      0.      1
=,      *(500), *(5),   =,      == $
=(16)
$       GENERATES GRIDS 11000 THRU 19000
GRID    19300   193     0.      0.      0.      1
GRID    19600   196     0.      0.      0.      1
$       BLADE TRAILING EDGE GRIDS
GRID    10001   100     3.81445 0.      0.      1
GRID    10121   101     3.81445 0.      0.      1
GRID    10501   105     3.81445 0.      0.      1
=,      *(500), *(5),   == $
=(6)
$       GENERATES GRIDS 11001 THRU 14001
GRID    14003   140     3.      0.      0.      1
GRID    14501   145     3.      0.      0.      1
GRID    15001   150     3.      0.      0.      1
GRID    15503   155     3.      0.      0.      1
GRID    15501   155     3.81445 0.      0.      1
=,      *(500), *(5),   == $
=(6)
$       GENERATES GRIDS 16001 THRU 19001
GRID    19301   193     3.81445 0.      0.      1
GRID    19601   196     3.81445 0.      0.      1
$       BLADE LEADING EDGE GRIDS
GRID    10002   100     -3.814450.      0.      1
GRID    10122   101     -3.814450.      0.      1
GRID    10502   105     -3.814450.      0.      1
=,      *(500), *(5),   == $
=(6)
$       GENERATES GRIDS 11002 THRU 14002
GRID    14004   140     -3.     0.      0.      1
GRID    14502   145     -3.     0.      0.      1
GRID    15002   150     -3.     0.      0.      1
GRID    15504   155     -3.     0.      0.      1
GRID    15502   155     -3.814450.      0.      1
=,      *(500), *(5),   == $
=(6)
$       GENERATES GRIDS 16002 THRU 19002
GRID    19302   193     -3.814450.      0.      1
GRID    19602   196     -3.814450.      0.      1
$ HELIOGYRO BLADE TRUSS FLAP HINGE POST AND BOOM GRIDS
GRID    19700   199     0.      173.91  0.      1
GRID    19701   199     3.81445 173.91  0.      1
GRID    19702   199     -3.81445173.91  0.      1
GRID    19751   199     3.81445 118.51  -1.108  1
GRID    19752   199     -3.81445118.51  -1.108  1
GRID    19753   199     3.81445 118.51  1.108   1
GRID    19754   199     -3.81445118.51  1.108   1
GRID    19801   199     3.81445 63.11   -2.217  1
GRID    19802   199     -3.8144563.11   -2.217  1
GRID    19803   199     3.81445 63.11   2.217   1
```

```
GRID     19804    199      -3.8144563.11    2.217    1
GRID     19851    199      3.81445 7.71     -3.325   1
GRID     19852    199      -3.814457.71     -3.325   1
GRID     19853    199      4.       7.71    0.       1
GRID     19854    199      0.       7.71    0.       1
GRID     19855    199      -4.      7.71    0.       1
GRID     19856    199      3.81445 7.71     3.325    1
GRID     19857    199      -3.814457.71     3.325    1
$        BLADE ATTACHMENT AND HUB GRIDS
GRID     19990    199      0.       2.15    0.       1
GRID     19996    199      0.       0.      0.       1
GRID     19997    199      0.       0.      0.       1
GRID     19998    199      0.       0.      0.       1
$        BLADE ELEMENTS
BARDR             1001                      0.       0.       1000.    1
CBAR     1000     1000     10120    10000
CBAR     1012              10500    10120
CBAR     1050              11000    10500
=,       *(50),   =,       *(500),  *(500),  == $
=(15)
$        GENERATES BARS 1100 THRU 1850
CBAR     1900              19300    19000
CBAR     1930              19600    19300
CBAR     1960              19700    19600
$        TRAILING EDGE RODS
CONROD   1001     10121    10001    10       .2229-6
CONROD   1013     10501    10121    10       .2229-6
CONROD   1051     11001    10501    10       .2229-6
CONROD   1101     11501    11001    10       .2742-6
CONROD   1151     12001    11501    10       .3739-6
CONROD   1201     12501    12001    10       .4678-6
CONROD   1251     13001    12501    10       .5557-6
CONROD   1301     13501    13001    10       .6378-6
CONROD   1351     14001    13501    10       .7141-6
CONROD   1401     14501    14003    10       .7845-6
CONROD   1451     15001    14501    10       .8490-6
CONROD   1501     15503    15001    10       .9076-6
CONROD   1551     16001    15501    10       .9604-6
CONROD   1601     16501    16001    10       1.007-6
CONROD   1651     17001    16501    10       1.048-6
CONROD   1701     17501    17001    10       1.084-6
CONROD   1751     18001    17501    10       1.113-6
CONROD   1801     18501    18001    10       1.136-6
CONROD   1851     19001    18501    10       1.154-6
CONROD   1901     19301    19001    10       1.164-6
CONROD   1931     19601    19301    10       1.169-6
CONROD   1961     19701    19601    10       1.172-6
$        LEADING EDGE RODS
CONROD   1002     10122    10002    10       .2229-6
CONROD   1014     10502    10122    10       .2229-6
CONROD   1052     11002    10502    10       .2229-6
CONROD   1102     11502    11002    10       .2742-6
CONROD   1152     12002    11502    10       .3739-6
CONROD   1202     12502    12002    10       .4678-6
CONROD   1252     13002    12502    10       .5557-6
```

```
CONROD  1302    13502   13002   10      .6378-6
CONROD  1352    14002   13502   10      .7141-6
CONROD  1402    14502   14004   10      .7845-6
CONROD  1452    15002   14502   10      .8490-6
CONROD  1502    15504   15002   10      .9076-6
CONROD  1552    16002   15502   10      .9604-6
CONROD  1602    16502   16002   10      1.007-6
CONROD  1652    17002   16502   10      1.048-6
CONROD  1702    17502   17002   10      1.084-6
CONROD  1752    18002   17502   10      1.113-6
CONROD  1802    18502   18002   10      1.136-6
CONROD  1852    19002   18502   10      1.154-6
CONROD  1902    19302   19002   10      1.164-6
CONROD  1932    19602   19302   10      1.169-6
CONROD  1962    19702   19602   10      1.172-6
$       SHEAR PANELS
CSHEAR  1009    1009    10001   10002   10122   10121
CSHEAR  1019    1009    10121   10122   10502   10501
CSHEAR  1109    1009    11001   11002   11502   11501
=,      *(50),  =,      *(500), *(500), *(500), *(500), == $
=(4)
$       GENERATE SHEAR PANELS 1159 THRU 1359
CSHEAR  1409    1009    14003   14004   14502   14501
CSHEAR  1459    1009    14501   14502   15002   15001
CSHEAR  1509    1009    15001   15002   15504   15503
CSHEAR  1559    1009    15501   15502   16002   16001
=,      *(50),  =,      *(500), *(500), *(500), *(500), == $
=(5)
$       GENERATES SHEAR PANELS 1609 THRU 1859
CSHEAR  1909    1009    19001   19002   19302   19301
CSHEAR  1939    1009    19301   19302   19602   19601
CSHEAR  1969    1009    19601   19602   19702   19701
$       TRUSS AND BOOM ELEMENTS
CBAR    1970    1970    19700   19701   19854                   2
CBAR    1975    1970    19702   19700   19854                   2
CBAR    1993    1993    19855   19854   30                      2
CBAR    1994    1993    19854   19853   30                      2
CBAR    1995    1995    19851   19853   19854                   2
CBAR    1996    1995    19852   19855   19854                   2
CBAR    1997    1995    19853   19856   19854                   2
CBAR    1998    1995    19855   19857   19854                   2
CBAR    1999    1999    19990   19854   31                      2
CONROD  1971    19701   19751   10      4.7154-6
CONROD  1972    19702   19752   10      4.7154-6
CONROD  1973    19701   19753   10      4.7154-6
CONROD  1974    19702   19754   10      4.7154-6
CONROD  1976    19751   19801   10      4.7154-6
CONROD  1977    19752   19802   10      4.7154-6
CONROD  1978    19753   19803   10      4.7154-6
CONROD  1979    19754   19804   10      4.7154-6
CONROD  1981    19801   19851   10      4.7154-6
CONROD  1982    19802   19852   10      4.7154-6
```

```
CONROD  1983    19803   19856   10      4.7154-6
CONROD  1984    19804   19857   10      4.7154-6
CONROD  1986    19751   19752   10      4.7154-6
CONROD  1987    19753   19754   10      4.7154-6
CONROD  1988    19801   19802   10      4.7154-6
CONROD  1989    19803   19804   10      4.7154-6
CSHEAR  19708   19708   19701   19702   19752   19751
CSHEAR  19709   19708   19701   19702   19754   19753
CSHEAR  19758   19708   19751   19752   19802   19801
CSHEAR  19759   19708   19753   19754   19804   19803
CSHEAR  19808   19708   19801   19802   19852   19851
CSHEAR  19809   19708   19803   19804   19857   19856
RBAR    2000    19996   19998   5       12346   12346
RBAR    2001    19998   900000          123456  123456
$       ELEMENT PROPERTIES
PBAR    1000    10              1.-9    1.-9
PBAR    1001    10              1.-8    1.-8
PBAR    1970    10      4.14-4  2.589-5 2.589-5 2.589-5
PBAR    1993    10      4.1475-52.589-6 2.589-6 9.309-6                 +PB199
+PB1993                                                                 +PB199
+PB1993A.9      .9
PBAR    1995    10      7.52-5  4.73-7  4.73-7  4.73-7
PBAR    1999    10      2.291-4 1.5926-51.0193-51.977-7                 +PB199
+PB1999                                                                 +PB199
+PB1999A.3      .3
PBAR    19991   11      2.291-4 9.567-7 9.567-7 1.-6                    +B1999
+B19991                                                                 +B1999
+B19991A.3      .3
PSHEAR  1009    30      2.54-6
PSHEAR  19708   20      2.54-6
$       LUMPED MASSES
CONM2   100     10000   100     2.                                      +CM100
CONM2   101     10120   101     6.476                                   +CM101
CONM2   105     10500   105     6.667                                   +CM105
CONM2   110     11000   110     6.667                                   +CM110
CONM2   115     11500   115     13.129                                  +CM115
CONM2   120     12000   120     13.294                                  +CM120
CONM2   125     12500   125     13.458                                  +CM125
CONM2   130     13000   130     13.596                                  +CM130
CONM2   135     13500   135     13.731                                  +CM135
CONM2   140     14000   140     12.285                                  +CM140
CONM2   145     14500   145     10.830                                  +CM145
CONM2   150     15000   150     10.935                                  +CM150
CONM2   155     15500   155     12.602                                  +CM155
CONM2   160     16000   160     14.259                                  +CM160
CONM2   165     16500   165     14.334                                  +CM165
CONM2   170     17000   170     14.399                                  +CM170
CONM2   175     17500   175     14.455                                  +CM175
CONM2   180     18000   180     14.500                                  +CM180
CONM2   185     18500   185     14.535                                  +CM185
CONM2   190     19000   190     11.648                                  +CM190
CONM2   193     19300   193     8.742                                   +CM193
CONM2   196     19600   196     6.824                                   +CM196
CONM2   197     19700   199     5.076                                   +CM197
CONM2   198     19854   199     32.916                                  +CM198
```

```
CONM2   199     19997   199     32.041                                  +CM199
+CM100  .1              21.33                   .1
+CM101  .1              34.333                  .1
+CM105  .1              37.112                  .1
+CM110  .1              37.112                  .1
+CM115  .1              71.225                  .1
+CM120  .1              73.638                  .1
+CM125  .1              75.905                  .1
+CM130  .1              78.026                  .1
+CM135  .1              80.000                  .1
+CM140  .1              59.492                  .1
+CM145  .1              38.100                  .1
+CM150  .1              38.964                  .1
+CM155  .1              63.091                  .1
+CM160  .1              87.679                  .1
+CM165  .1              88.776                  .1
+CM170  .1              89.726                  .1
+CM175  .1              90.531                  .1
+CM180  .1              91.189                  .1
+CM185  .1              91.701                  .1
+CM190  .1              73.653                  .1
+CM193  .1              55.329                  .1
+CM196  .1              43.212                  .1
+CM197  .1              53.740                  .1
+CM198  .1              219.801                 .1
+CM199  .1              .1                      .1
$       BLADE COORDINATE SYSTEM
CORD2R  1       9000    0.      0.      0.      0.      0.      1.      +CR1
+CR1    1.      0.      0.
$       CBARS TO REMOVE SINGULARITIES ON TRUSS
CBAR    19751   19751   19751   19701   19856                           2
CBAR    19752   19751   19752   19702   19857                           2
CBAR    19753   19751   19753   19701   19851                           2
CBAR    19754   19751   19754   19702   19852                           2
CBAR    19801   19751   19801   19751   19856                           2
CBAR    19802   19751   19802   19752   19857                           2
CBAR    19803   19751   19803   19753   19851                           2
CBAR    19804   19751   19804   19754   19852                           2
CBAR    19851   19751   19851   19801   19856                           2
CBAR    19852   19751   19852   19802   19857                           2
CBAR    19856   19751   19856   19803   19851                           2
CBAR    19857   19751   19857   19804   19852                           2
PBAR    19751   10              1.-8
$       RBE2S TO GET MOTIONS ON CENTERLINE OF BLADE
RBE2    1003    10000   123     10001   10002
RBE2    1015    10120   123     10121   10122
RBE2    1053    10500   123     10501   10502
=,      *(50),  *(500), =,      *(500), *(500), == $
=(5)
$       GENERATES RBE2 1103 THRU 1403
RBE2    1403    14000   123     14001   14002   14003   14004
RBE2    1453    14500   123     14501   14502
RBE2    1503    15000   123     15001   15002
RBE2    1553    15500   123     15501   15502   15503   15504
RBE2    1603    16000   123     16001   16002
=,      *(50),  *(500), =,      *(500), *(500), == $
=(5)
$       GENERATES RBE2 1653 THRU 1903
```

```
RBE2    1933    19300   123     19301   19302
RBE2    1963    19600   123     19601   19602
$       ELASTOMERIC BEARING STIFFNESS
CBAR    19991   19991   19996   19990   32                                      2
CELAS2  19992   100.    19996   5       19997   5
MAT1    11      120.65+9        .3
$       ELEMENTS FOR CENTER BODY INERTIA
CELAS2  19994   140.    19996   1       19997   1
CELAS2  19995   140.    19996   2       19997   2
CELAS2  19996   140.    19996   3       19997   3
$       CONSTRAINTS TO REMOVE SINGULAR DEGREES OF FREEDOM
$       ON TRUSS AND BLADE
SPC1    1       456     14003   14004   15503   15504
SPC1    1       456     19751   19752   19753   19754
SPC1    1       456     19801   19802   19803   19804
SPC1    1       456     10001   10002   10121   10122
SPC1    1       456     10501   10502   11001   11002
=,      =,      =,      *(1000),*(1000),*(1000),*(1000),== $
=(7)
$       GENERATES SPCS ON LE AND TE OF BLADE
SPC1    1       456     19301   19302   19601   19602
```

APPENDIX C

MIKEDATA.M15BLD2

```
$ HELIOGYRO BLADE GRIDS
$
$       BLADE CENTER LINE GRIDS
GRID    20000   200     0.      0.      0.      2
GRID    20120   201     0.      0.      0.      2
GRID    20500   205     0.      0.      0.      2
=,      *(500), *(5),   =,      == $
=(16)
$       GENERATES GRIDS 21000 THRU 29000
GRID    29300   293     0.      0.      0.      2
GRID    29600   296     0.      0.      0.      2
$       BLADE TRAILING EDGE GRIDS
GRID    20001   200     3.81445 0.      0.      2
GRID    20121   201     3.81445 0.      0.      2
GRID    20501   205     3.81445 0.      0.      2
=,.     *(500), *(5),   == $
=(7)
$       GENERATES GRIDS 21001 THRU 24501
GRID    24503   245     3.      0.      0.      2
GRID    25001   250     3.      0.      0.      2
GRID    25503   255     3.      0.      0.      2
GRID    25501   255     3.81445 0.      0.      2
=,      *(500), *(5),   == $
=(6)
$       GENERATES GRIDS 26001 THRU 29001
GRID    29301   293     3.81445 0.      0.      2
GRID    29601   296     3.81445 0.      0.      2
$       BLADE LEADING EDGE GRIDS
GRID    20002   200     -3.814450.      0.      2
GRID    20122   201     -3.814450.      0.      2
GRID    20502   205     -3.814450.      0.      2
=,      *(500), *(5),   == $
=(7)
$       GENERATES GRIDS 21002 THRU 24502
GRID    24504   245     -3.     0.      0.      2
GRID    25002   250     -3.     0.      0.      2
GRID    25504   255     -3.     0.      0.      2
GRID    25502   255     -3.814450.      0.      2
=,      *(500), *(5),   == $
=(6)
$       GENERATES GRIDS 26002 THRU 29002
GRID    29302   293     -3.814450.      0.      2
GRID    29602   296     -3.814450.      0.      2
$ HELIOGYRO BLADE TRUSS FLAP HINGE POST AND BOOM GRIDS
GRID    29700   299     0.      173.91  0.      2
GRID    29701   299     3.81445 173.91  0.      2
GRID    29702   299     -3.81445173.91  0.      2
GRID    29751   299     3.81445 118.51  -1.108  2
GRID    29752   299     -3.81445118.51  -1.108  2
GRID    29753   299     3.81445 118.51  1.108   2
GRID    29754   299     -3.81445118.51  1.108   2
GRID    29801   299     3.81445 63.11   -2.217  2
GRID    29802   299     -3.81445 63.11  -2.217  2
```

```
GRID    29803   299     3.81445 63.11   2.217   2
GRID    29804   299     -3.8144563.11   2.217   2
GRID    29851   299     3.81445 7.71    -3.325  2
GRID    29852   299     -3.814457.71    -3.325  2
GRID    29853   299     4.      7.71    0.      2
GRID    29854   299     0.      7.71    0.      2
GRID    29855   299     -4.     7.71    0.      2
GRID    29856   299     3.81445 7.71    3.325   2
GRID    29857   299     -3.814457.71    3.325   2
$       BLADE ATTACHMENT AND HUB GRIDS
GRID    29990   299     0.      2.15    0.      2
GRID    29996   299     0.      0.      0.      2
GRID    29997   299     0.      0.      0.      2
GRID    29998   299     0.      0.      0.      2
$       BLADE ELEMENTS
CBAR    2000    1000    20120   20000
CBAR    2012            20500   20120
CBAR    2050            21000   20500
=,      *(50),  =,      *(500), *(500), == $
=(15)
$       GENERATES BARS 2100 THRU 2850
CBAR    2900            29300   29000
CBAR    2930            29600   29300
CBAR    2960            29700   29600
$       TRAILING EDGE RODS
CONROD  2001    20121   20001   10      .2229-6
CONROD  2013    20501   20121   10      .2229-6
CONROD  2051    21001   20501   10      .2229-6
CONROD  2101    21501   21001   10      .2742-6
CONROD  2151    22001   21501   10      .3739-6
CONROD  2201    22501   22001   10      .4678-6
CONROD  2251    23001   22501   10      .5557-6
CONROD  2301    23501   23001   10      .6378-6
CONROD  2351    24001   23501   10      .7141-6
CONROD  2401    24501   24001   10      .7845-6
CONROD  2451    25001   24503   10      .8490-6
CONROD  2501    25503   25001   10      .9076-6
CONROD  2551    26001   25501   10      .9604-6
CONROD  2601    26501   26001   10      1.007-6
CONROD  2651    27001   26501   10      1.048-6
CONROD  2701    27501   27001   10      1.084-6
CONROD  2751    28001   27501   10      1.113-6
CONROD  2801    28501   28001   10      1.136-6
CONROD  2851    29001   28501   10      1.154-6
  29001   10      1.164-6
CONROD  2931    29601   29301   10      1.169-6
CONROD  2961    29701   29601   10      1.172-6
$       LEADING EDGE RODS
CONROD  2002    20122   20002   10      .2229-6
CONROD  2014    20502   20122   10      .2229-6
CONROD  2052    21002   20502   10      .2229-6
CONROD  2102    21502   21002   10      .2742-6
CONROD  2152    22002   21502   10      .3739-6
```

```
CONROD  2202    22502   22002   10      .4678-6
CONROD  2252    23002   22502   10      .5557-6
CONROD  2302    23502   23002   10      .6378-6
CONROD  2352    24002   23502   10      .7141-6
CONROD  2402    24502   24002   10      .7845-6
CONROD  2452    25002   24504   10      .8490-6
CONROD  2502    25504   25002   10      .9076-6
CONROD  2552    26002   25502   10      .9604-6
CONROD  2602    26502   26002   10      1.007-6
CONROD  2652    27002   26502   10      1.048-6
CONROD  2702    27502   27002   10      1.084-6
CONROD  2752    28002   27502   10      1.113-6
CONROD  2802    28502   28002   10      1.136-6
CONROD  2852    29002   28502   10      1.154-6
CONROD  2902    29302   29002   10      1.164-6
CONROD  2932    29602   29302   10      1.169-6
CONROD  2962    29702   29602   10      1.172-6
$       SHEAR PANELS
CSHEAR  2009    2009    20001   20002   20122   20121
CSHEAR  2019    2009    20121   20122   20502   20501
CSHEAR  2109    2109    21001   21002   21502   21501
PSHEAR  2109    30      1.27-6
CSHEAR  2159    2009    21501   21502   22002   22001
=,      *(50),  =,      *(500), *(500), *(500), *(500), == $
=(4)
$       GENERATE SHEAR PANELS 2159 THRU 2409
$       GENERATE SHEAR PANELS 2159 THRU 2409
CSHEAR  2459    2009    24503   24504   25002   25001
CSHEAR  2509    2009    25001   25002   25504   25503
CSHEAR  2559    2009    25501   25502   26002   26001
=,      *(50),  =,      *(500), *(500), *(500), *(500), == $
=(5)
$       GENERATES SHEAR PANELS 2609 THRU 2859
CSHEAR  2909    2009    29001   29002   29302   29301
CSHEAR  2939    2009    29301   29302   29602   29601
CSHEAR  2969    2009    29601   29602   29702   29701
$       TRUSS AND BOOM ELEMENTS
CBAR    2970    2970    29700   29701   29854                   2
CBAR    2975    2970    29702   29700   29854                   2
CBAR    2993    2993    29855   29854   40                      2
CBAR    2994    2993    29854   29853   40                      2
CBAR    2995    2995    29851   29853   29854                   2
CBAR    2996    2995    29852   29855   29854                   2
CBAR    2997    2995    29853   29856   29854                   2
CBAR    2998    2995    29855   29857   29854                   2
CBAR    2999    2999    29990   29854   41                      2
CONROD  2971    29701   29751   10      4.7154-6
CONROD  2972    29702   29752   10      4.7154-6
CONROD  2973    29701   29753   10      4.7154-6
CONROD  2974    29702   29754   10      4.7154-6
CONROD  2976    29751   29801   10      4.7154-6
CONROD  2977    29752   29802   10      4.7154-6
CONROD  2978    29753   29803   10      4.7154-6
CONROD  2979    29754   29804   10      4.7154-6
```

```
CONROD  2981    29801   29851   10      4.7154-6
CONROD  2982    29802   29852   10      4.7154-6
CONROD  2983    29803   29856   10      4.7154-6
CONROD  2984    29804   29857   10      4.7154-6
CONROD  2986    29751   29752   10      4.7154-6
CONROD  2987    29753   29754   10      4.7154-6
CONROD  2988    29801   29802   10      4.7154-6
CONROD  2989    29803   29804   10      4.7154-6
CSHEAR  29708   29708   29701   29702   29752   29751
CSHEAR  29709   29708   29701   29702   29754   29753
CSHEAR  29758   29708   29751   29752   29802   29801
CSHEAR  29759   29708   29753   29754   29804   29803
CSHEAR  29808   29708   29801   29802   29852   29851
CSHEAR  29809   29708   29803   29804   29857   29856
RBAR    3000    29996   29998   5       12346   12346
RBAR    3001    29998   900001          123456  123456
$       ELEMENT PROPERTIES
PBAR    2970    10      4.14-4  2.589-5 2.589-5 2.589-5
PBAR    2993    10      4.1475-52.589-6 2.589-6 9.309-6                 +PB29
+PB2993                                                                 +PB29
+PB2993A.9      .9
PBAR    2995    10      7.52-5  4.73-7  4.73-7  4.73-7
PBAR    2999    10      2.291-4 1.5926-51.0193-51.977-7                 +PB29
+PB2999                                                                 +PB29
+PB2999A.3      .3
PBAR    29991   11      2.291-4 9.567-7 9.567-7 1.-6                    +B299
+B29991                                                                 +B299
+B29991A.3      .3
PSHEAR  2009    30      2.54-6
PSHEAR  29708   20      2.54-6
$       LUMPED MASSES
CONM2   200     20000   200     2.                                      +CM20
CONM2   201     20120   201     6.476                                   +CM20
CONM2   205     20500   205     6.667                                   +CM20
CONM2   210     21000   210     0.382                                   +CM21
CONM2   215     21500   215     13.129                                  +CM21
CONM2   220     22000   220     13.294                                  +CM22
CONM2   225     22500   225     13.450                                  +CM22
CONM2   230     23000   230     13.596                                  +CM23
CONM2   235     23500   235     13.731                                  +CM23
CONM2   240     24000   240     13.856                                  +CM24
CONM2   245     24500   245     12.401                                  +CM24
CONM2   250     25000   250     10.935                                  +CM25
CONM2   255     25500   255     12.602                                  +CM25
CONM2   260     26000   260     14.259                                  +CM26
CONM2   265     26500   265     14.334                                  +CM26
CONM2   270     27000   270     14.399                                  +CM27
CONM2   275     27500   275     14.455                                  +CM27
CONM2   280     28000   280     14.500                                  +CM28
CONM2   285     28500   285     14.535                                  +CM28
CONM2   290     29000   290     11.648                                  +CM29
CONM2   293     29300   293     8.742                                   +CM29
CONM2   296     29600   296     6.824                                   +CM29
CONM2   297     29700   299     5.076                                   +CM29
```

```
CONM2   298     29854   299     32.916                                  +CM29
CONM2   299     29997   299     202.041                                 +CM29
+CM200  .1              21.33           .1
+CM201  .1              34.333          .1
+CM205  .1              37.112          .1
+CM210  .1              5.558           .1
+CM215  .1              71.225          .1
+CM220  .1              73.638          .1
+CM225  .1              75.905          .1
+CM230  .1              78.026          .1
+CM235  .1              80.000          .1
+CM240  .1              81.829          .1
+CM245  .1              60.806          .1
+CM250  .1              38.964          .1
+CM255  .1              63.091          .1
+CM260  .1              87.679          .1
+CM265  .1              88.776          .1
+CM270  .1              89.726          .1
+CM275  .1              90.531          .1
+CM280  .1              91.189          .1
+CM285  .1              91.701          .1
+CM290  .1              73.653          .1
+CM293  .1              55.329          .1
+CM296  .1              43.212          .1
+CM297  .1              53.740          .1
+CM298  .1              219.801         .1
+CM299  .1              .1              .1
$       BLADE COORDINATE SYSTEM
CORD2R  2       9000    0.      0.      -9.     0.      0.      1.      +CR2
+CR2    1.7320511.      0.
$       CBARS TO REMOVE VERTICAL SINGULARITIES ON TRUSS
CBAR    29751   29751   29751   29701   29856                           2
CBAR    29752   29751   29752   29702   29857                           2
CBAR    29753   29751   29753   29701   29851                           2
CBAR    29754   29751   29754   29702   29852                           2
CBAR    29801   29751   29801   29751   29856                           2
CBAR    29802   29751   29802   29752   29857                           2
CBAR    29803   29751   29803   29753   29851                           2
CBAR    29804   29751   29804   29754   29852                           2
CBAR    29851   29751   29851   29801   29856                           2
CBAR    29852   29751   29852   29802   29857                           2
CBAR    29856   29751   29856   29803   29851                           2
CBAR    29857   29751   29857   29804   29852                           2
PBAR    29751   10              1.-8
$       RBE2S TO GET MOTIONS ON CENTERLINE OF BLADE
RBE2    2003    20000   123     20001   20002
RBE2    2015    20120   123     20121   20122
RBE2    2053    20500   123     20501   20502
=,      *(50),  *(500), =,      *(500), *(500), == $
=(5)
$       GENERATES RBE2 2103 THRU 2403
RBE2    2403    24000   123     24001   24002
RBE2    2453    24500   123     24501   24502   24503   24504
RBE2    2503    25000   123     25001   25002
RBE2    2553    25500   123     25501   25502   25503   25504
```

```
RBE2    2603    26000   123     26001   26002
=,      *(50),  *(500), =,      *(500), *(500), == $
=(5)
$       GENERATES RBE2 2653 THRU 2903
RBE2    2933    29300   123     29301   29302
RBE2    2963    29600   123     29601   29602
$       ELASTOMERIC BEARING STIFFNESS
CBAR    29991   29991   29996   29990   42                              2
CELAS2  29992   100.    29996   5       29997   5
MAT2    11      120.65+9        .3
$       ELEMENTS FOR CENTER BODY INERTIA
CELAS2  29994   140.    29996   1       29997   1
CELAS2  29995   140.    29996   2       29997   2
CELAS2  29996   140.    29996   3       29997   3
$       CONSTRAINTS TO REMOVE SINGULAR DEGREES OF FREEDOM
$       ON TRUSS AND BLADE
SPC1    1       456     24503   24504   25503   25504
SPC1    1       456     29751   29752   29753   29754
SPC1    1       456     29801   29802   29803   29804
SPC1    1       456     20001   20002   20121   20122
SPC1    1       456     20501   20502   21001   21002
=,      =,      =,      *(1000),*(1000),*(1000),*(1000),== $
=(7)
$       GENERATES SPCS ON LE AND TE OF BLADE
SPC1    1       456     29301   29302   29601   29602
```

APPENDIX P

MIKEDATA.M15B1T0

```
CORD2R  100     1       0.      7500.   0.      0.      7500.   1000.   +CR1
CORD2R  101     1       0.      7406.25 0.      0.      7406.25 1000.   +CR1
CORD2R  105     1       0.      7125.   0.      0.      7125.   1000.   +CR1
CORD2R  110     1       0.      6750.   0.      0.      6750.   1000.   +CR1
CORD2R  115     1       0.      6375.   0.      0.      6375.   1000.   +CR1
CORD2R  120     1       0.      6000.   0.      0.      6000.   1000.   +CR1
CORD2R  125     1       0.      5625.   0.      0.      5625.   1000.   +CR1
CORD2R  130     1       0.      5250.   0.      0.      5250.   1000.   +CR1
CORD2R  135     1       0.      4875.   0.      0.      4875.   1000.   +CR1
CORD2R  140     1       0.      4500.   0.      0.      4500.   1000.   +CR1
CORD2R  145     1       0.      4125.   0.      0.      4125.   1000.   +CR1
CORD2R  150     1       0.      3750.   0.      0.      3750.   1000.   +CR1
CORD2R  155     1       0.      3375.   0.      0.      3375.   1000.   +CR1
CORD2R  160     1       0.      3000.   0.      0.      3000.   1000.   +CR1
CORD2R  165     1       0.      2625.   0.      0.      2625.   1000.   +CR1
CORD2R  170     1       0.      2250.   0.      0.      2250.   1000.   +CR1
CORD2R  175     1       0.      1875.   0.      0.      1875.   1000.   +CR1
CORD2R  180     1       0.      1500.   0.      0.      1500.   1000.   +CR1
CORD2R  185     1       0.      1125.   0.      0.      1125.   1000.   +CR1
CORD2R  190     1       0.      750.    0.      0.      750.    1000.   +CR1
CORD2R  193     1       0.      525.    0.      0.      525.    1000.   +CR1
CORD2R  196     1       0.      300.    0.      0.      300.    1000.   +CR1
CORD2R  199     1       0.      0.      0.      0.      0.      1000.   +CR1
+CR100  300.    7500.   +400.
+CR101  300.    7406.25 +400.
+CR105  300.    7125.   +400.
+CR110  300.    6750.   +400.
+CR115  300.    6375.   +400.
+CR120  300.    6000.   +400.
+CR125  300.    5625.   +400.
+CR130  300.    5250.   +400.
+CR135  300.    4875.   +400.
+CR140  300.    4500.   +400.
+CR145  300.    4125.   +400.
+CR150  300.    3750.   +400.
+CR155  300.    3375.   +400.
+CR160  300.    3000.   +400.
+CR165  300.    2625.   +400.
+CR170  300.    2250.   +400.
+CR175  300.    1875.   +400.
+CR180  300.    1500.   +400.
+CR185  300.    1125.   +400.
+CR190  300.    750.    +400.
+CR193  300.    525.    +400.
+CR196  300.    300.    +400.
+CR199  300.    0.      +400.
GRID    30      199     0.      7.71    1000.           123456
GRID    31      199     0.      2.15    1000.           123456
GRID    32      199     0.      0.      1000.           123456
DMIG    TENPAD  10000   5                       10000   5       0.
DMIG    TENPAD  10120   5                       10120   5       0.
DMIG    TENPAD  10500   5                       10500   5       0.
DMIG    TENPAD  11000   5                       11000   5       0.
DMIG    TENPAD  11500   5                       11500   5       0.
DMIG    TENPAD  12000   5                       12000   5       0.
```

```
DMIG    TENPAD  12500   5               12500   5       0.
DMIG    TENPAD  13000   5               13000   5       0.
DMIG    TENPAD  13500   5               13500   5       0.
DMIG    TENPAD  14000   5               14000   5       0.
DMIG    TENPAD  14500   5               14500   5       0.
DMIG    TENPAD  15000   5               15000   5       0.
DMIG    TENPAD  15500   5               15500   5       0.
DMIG    TENPAD  16000   5               16000   5       0.
DMIG    TENPAD  16500   5               16500   5       0.
DMIG    TENPAD  17000   5               17000   5       0.
DMIG    TENPAD  17500   5               17500   5       0.
DMIG    TENPAD  18000   5               18000   5       0.
DMIG    TENPAD  18500   5               18500   5       0.
DMIG    TENPAD  19000   5               19000   5       0.
DMIG    TENPAD  19300   5               19300   5       0.
DMIG    TENPAD  19600   5               19600   5       0.
DMIG    TENPAD  19700   5               19700   5       0.
DMIG    TENPAD  19854   5               19854   5       0.
```

APPENDIX Q

MIKEDATA.M15B2T0

```
CORD2R  200     2       0.      7500.   0.      0.      7500.   1000.   +CR20(
CORD2R  201     2       0.      7406.25 0.      0.      7406.25 1000.   +CR20'
CORD2R  205     2       0.      7125.   0.      0.      7125.   1000.   +CR20!
CORD2R  210     2       0.      6750.   0.      0.      6750.   1000.   +CR21(
CORD2R  215     2       0.      6375.   0.      0.      6375.   1000.   +CR21!
CORD2R  220     2       0.      6000.   0.      0.      6000.   1000.   +CR22(
CORD2R  225     2       0.      5625.   0.      0.      5625.   1000.   +CR22!
CORD2R  230     2       0.      5250.   0.      0.      5250.   1000.   +CR23(
CORD2R  235     2       0.      4875.   0.      0.      4875.   1000.   +CR23!
CORD2R  240     2       0.      4500.   0.      0.      4500.   1000.   +CR24(
CORD2R  245     2       0.      4125.   0.      0.      4125.   1000.   +CR24!
CORD2R  250     2       0.      3750.   0.      0.      3750.   1000.   +CR25(
CORD2R  255     2       0.      3375.   0.      0.      3375.   1000.   +CR25!
CORD2R  260     2       0.      3000.   0.      0.      3000.   1000.   +CR26(
CORD2R  265     2       0.      2625.   0.      0.      2625.   1000.   +CR26!
CORD2R  270     2       0.      2250.   0.      0.      2250.   1000.   +CR27(
CORD2R  275     2       0.      1875.   0.      0.      1875.   1000.   +CR27!
CORD2R  280     2       0.      1500.   0.      0.      1500.   1000.   +CR28(
CORD2R  285     2       0.      1125.   0.      0.      1125.   1000.   +CR28!
CORD2R  290     2       0.      750.    0.      0.      750.    1000.   +CR29(
CORD2R  293     2       0.      525.    0.      0.      525.    1000.   +CR29'
CORD2R  296     2       0.      300.    0.      0.      300.    1000.   +CR29(
CORD2R  299     2       0.      0.      0.      0.      0.      1000.   +CR29!
+CR200  300.    7500.   +400.
+CR201  300.    7406.25 +400.
+CR205  300.    7125.   +400.
+CR210  300.    6750.   +400.
+CR215  300.    6375.   +400.
+CR220  300.    6000.   +400.
+CR225  300.    5625.   +400.
+CR230  300.    5250.   +400.
+CR235  300.    4875.   +400.
+CR240  300.    4500.   +400.
+CR245  300.    4125.   +400.
+CR250  300.    3750.   +400.
+CR255  300.    3375.   +400.
+CR260  300.    3000.   +400.
+CR265  300.    2625.   +400.
+CR270  300.    2250.   +400.
+CR275  300.    1875.   +400.
+CR280  300.    1500.   +400.
+CR285  300.    1125.   +400.
+CR290  300.    750.    +400.
+CR293  300.    525.    +400.
+CR296  300.    300.    +400.
+CR299  300.    0.      +400.
GRID    40      299     0.      7.71    1000.           123456
GRID    41      299     0.      2.15    1000.           123456
GRID    42      299     0.      0.      1000.           123456
DMIG    TENPAD  20000   5                       20000   5       0.
DMIG    TENPAD  20120   5                       20120   5       0.
DMIG    TENPAD  20500   5                       20500   5       0.
DMIG    TENPAD  21000   5                       21000   5       0.
DMIG    TENPAD  21500   5                       21500   5       0.
DMIG    TENPAD  22000   5                       22000   5       0.
DMIG    TENPAD  22500   5                       22500   5       0.
```

```
DMIG    TENPAD  23000   5               23000   5       0.
DMIG    TENPAD  23500   5               23500   5       0.
DMIG    TENPAD  24000   5               24000   5       0.
DMIG    TENPAD  24500   5               24500   5       0.
DMIG    TENPAD  25000   5               25000   5       0.
DMIG    TENPAD  25500   5               25500   5       0.
DMIG    TENPAD  26000   5               26000   5       0.
DMIG    TENPAD  26500   5               26500   5       0.
DMIG    TENPAD  27000   5               27000   5       0.
DMIG    TENPAD  27500   5               27500   5       0.
DMIG    TENPAD  28000   5               28000   5       0.
DMIG    TENPAD  28500   5               28500   5       0.
DMIG    TENPAD  29000   5               29000   5       0.
DMIG    TENPAD  29300   5               29300   5       0.
DMIG    TENPAD  29600   5               29600   5       0.
DMIG    TENPAD  29700   5               29700   5       0.
DMIG    TENPAD  29854   5               29854   5       0.
```

APPENDIX R

MIKEDATA.HUBAØD7

```
$       COORDINATE TRANSFORMATIONS
CORD2R  9000            0.      0.      0.      0.      0.      1.      +CR900
+CR9000 1.      0.      0.
GRID    900000  9000    0.      0.      0.      9000
$       MATERIAL CONSTANTS
MAT1    10      120.65+9                .3
MAT1    20              .4309+9
MAT1    30              .984+6
$
$       CENTRIFUGAL LOAD DATA
$
RFORCE* 1               900000          9000            .4297183463E-2  +RFOR1
*RFOR1  0.E0            0.E0            1.E0            1
$       MODES TYPE BULK DATA
$
EIGR    2       MGIV    0.      .02     17      17              1.-9    +EIGR2
+EIGR2  MASS
ASET1   2       10000   12500   15000   19700
ASET1   135     10000   10120   10500   11000   11500   12000   12500
ASET1   135     13000   13500   14000   14500   15000   15500   16000
ASET1   135     16500   17000   17500   18000   18500   19000   19300
ASET1   135     19600   19700   19854
ASET1   2       20000   22500   25000   29700
ASET1   135     20000   20120   20500   21000   21500   22000   22500
ASET1   135     23000   23500   24000   24500   25000   25500   26000
ASET1   135     26500   27000   27500   28000   28500   29000   29300
ASET1   135     29600   29700   29854
$       CYCLIC MODES TYPE DATA
ASET1   1       10000   10500   11500   12500   13500   14500   15500
ASET1   1       16500   17500   18500   19300   19700   19997
ASET1   2       10000   15500   19997
EIGC    3       HESS    MAX                             1.-8                    +EIGC
+EIGC                                                   9999
EIGC    4       DET     MAX                             1.-3                    +EIGCD
+EIGCD  0.      .02     0.      .04     .002    3       4
SPC1    1       456     19997
SPC1    1       456     29997
SPC1    1       356     900000
SPC1    1       356     900001
DMI     OM1     0       1       2       2               6       6
DMI*    OM1             1               2               -.54000000000D-1 +D1
+D1
DMI*    OM1             2               1               +.54000000000D-1 +D2
+D2
DMI     OM2     0       6       2       2               6       6
DMI*    OM2             1               1               -.72900000000D-3 +M1
+M1
DMI*    OM2             2               2               -.72900000000D-3 +M2
DMI*    OM2             2               2               0.D0             +M2
+M2
DMI*    OM2             5               5               +.72900000000D-3 +M3
+M3
DMIG    COUPLx  0       1       3       0
```

```
DMIG     COUPLX  900000  1                   999990  0       0.      1.
DMIG     COUPLX  900000  2                   999990  0       1.      0.
DMIG     COUPLX  999990  0                   900000  1       0.      -1.     +COUPL
+COUPLX  900000  2       +1.     0.
DMIG     TENPAD  0       6       1       0
SPOINT   999990
$
$         TWO BLADED MODEL DATA
$
$        LOWER HUB GRID
GRID     900001  9000    0.      0.      -9.     9000
$        STRUCTURE BETWEEN THE TWO HUBS
CBAR     90000   90000   900001  900000  1000.   0.      0.      1
PBAR     90000   10      3.177-4 .893-4  .893-4  .893-4
$        CYCLIC MODES DATA FOR TWO BLADED MODELS
DMIG     COUPLX  900001  1                   999991  0       0.      1.
DMIG     COUPLX  900001  2                   999991  0       1.      0.
DMIG     COUPLX  999991  0                   900001  1       0.      -1.     +COUPL
```